CANINE BLADDER CANCER AS A MODEL FOR TARGETED RADIOTHERAPEUTIC DEVELOPMENT

By

Isabelle Lynch

A THESIS

Submitted to
Michigan State University
in partial fulfillment of the requirements
for the degree of

Comparative Medicine and Integrative Biology - Master of Science

2025

ABSTRACT

The more advanced form of bladder cancer (BC), muscle-invasive bladder cancer (MIBC), remains a significant clinical challenge in both canine and human patients afflicted with the disease. Although non-muscle invasive bladder cancer is the more dominant subtype, cases often reccur or progress, even after treatment. Despite current treatment options like chemotherapy, cystectomy, and external beam radiation, invasive bladder cancers have poor prognosis, with a 50% mortality rate in humans, and dogs are rarely cured. Dogs naturally develop bladder cancer in the presence of a complete immune system, making them an ideal preclinical model for studying human bladder cancer and developing novel targeted therapies as opposed to current available murine models. This study investigated the potential of radiolabeled FDA-approved monoclonal antibodies dual-targeting EGFR1 and EGFR2 biomarkers for treating canine bladder cancer and the possibility of eventually translating these findings into human treatment.

This thesis project aimed to characterize EGFR1 and EGFR2 expression in five different canine bladder cancer cell lines using technetium-99m binding assays, and confirming the binding affinities of monoclonal antibodies cetuximab and trastuzumab for these receptors. Colony formation assays were conducted to assess the impact of radiation therapy using beta-particle therapy (Lu-177-[cetuximab/trastuzumab]) and were compared with results from studies performed without radiation. Findings suggested that the antibodies alone do not have an inhibitory or proliferative effect on the canine bladder cancer and that any theraputic effects may be attributed to that of the radiation alone. Additionally, this study supports the use of targeting radiation therapy as a more promising treatment for both canine and human bladder cancer, with the potential for reduced off-target effects when compared to traditional radiation therapies, like external beam radiation therapy.

The utilization of pet dogs as a model for MIBC is particularly advantageous, given that canine bladder cancer closely resembles the disease in humans. Overall, this approach could accelerate the development of targeted radiotherapies and improve treatment outcomes for both veterinary and human patients. Leveraging similarities between canine and human bladder cancer should allow for enhanced therapeutic strategies that expedite the translation of novel therapeutics into clinical practice, a win-win scenario for canine and human patients alike.

This thesis is dedicated to my family. To my grandmother Maria Ross, the matriarch of our family, whose strength and bravery I will look up to for the rest of my life. To my father, Kevin Lynch, who always reminded me growing up that I could be anyone and do anything, and who has been my biggest supporter since I was a little girl. With your unwavering support and belief in me, Dad, I can do amazing things! To my mother, Johanna Lynch, who is never, ever lacking in unconditional love and support. To my four younger siblings, Alexander, Sophia, Maxwell and Evelyn, who are my built-in best friends for life…words simply cannot explain how much I love you all with my whole entire heart. I would not have been able to do this without you.

AKNOWLEDGEMENTS

I could not have completed this thesis project without support from my mentors, collegues, family and friends.

My first and most humble thank yous are alloted to my advisors, Dr. Kurt Zinn and Dr. Jinda Fan. Thank you both for your unwavering support and mentorship, and for always being there to guide my research endeavors and for answering my many questions. I am so grateful to have had your support over the course of my thesis research, and for our many conversations that have molded me into the researcher I am able to be today.

To my labmates, specifically Lucy Xu, Dr. Kylie Smith, and Chelsea Nayback, thank you all for always being there to lend an ear and for providing me with support and friendship. To Lucy, for being my biggest supporter and friend, and always making time for me regardless of how busy you were day or night. To Kylie and Chelsea, for being such strong role-models who I strive to be like in years to come. To Marayam Sabbaghan, you were such a figure of comfort during my hardest times, and I am so grateful I had the opportunity of getting to know you. You were the one who was my caretaker, always checking in on me, and offering warmth even on the most diffucult of days. To Katie Buelow of Corewell Hospital, our days working together were some of my favorite, you showed me how fun science can be, and what opportunities are out there for me. Thank you for your unwavering support and mentorship, even cities away.

Thank you to the rest of my committee members, Dr. Colleen Hegg, and Dr. Alison Masyr for guiding me through my thesis reasearch and for helping to strenghten my abilities as a researcher and scientific writer.

Thank you to my family, I could not have done this without your unwavering support. And to my life-long best friends Chase Rodriquez and Sydney Boresma. Although you both are now states and countries away from me, pursuing your own amazing academic endeavors, our late-night calls, texts, and unwavering friendship have supported me through this journey.

So, one last thank you to everyone mentioned here… I could not have done this without you!

TABLE OF CONTENTS

1. INTRODUCTION

1.1. Background

1.1.1. Human Bladder Cancer

In the 21st century, cancer is projected to be the leading cause of mortality and the leading barrier to increasing life expectancy in humans globally (1). Bladder cancer (BC), alternatively named urological cancer or urinary bladder cancer, ranks as the 6th most diagnosed cancer in men worldwide, with the majority (~95%) of cases occurring in older populations (aged 55 or older) (2,3). The bladder is a hollow organ located in the peritoneal space of the lower abdomen and is both the receptacle and excretory site for urine. It is lined with large, round transitional epithelium (also called urothelium) cells that can flatten to accommodate urine as the bladder fills (4). Almost all bladder cancers (90%) are urothelial carcinomas, and though patients with non-invasive forms have optimistic prognosis rates, it's once the tumor has invaded the smooth muscle of the bladder wall that survival outlook decreases drastically (2,5). Bladder cancer has two main forms: non-muscle invasive bladder cancer (NMIBC) and muscle-invasive bladder cancer (MIBC), each distinct in clinical behavior, biology, prognosis, and treatment approaches. Therefore, stage is a key factor in determining treatment approaches and potential success of treatment (6). The most common form of bladder cancer in humans is NMIBC, where cancer cells are confined to the inner lining of the bladder, or mucosa. There are three tumor (T) stages for NMIBC; Tis (or CIS; also called carcinoma *in situ*), where cancer cells are confined to the inner layer of the bladder, Ta – where the tumor is only in the innermost layer of the bladder, and T1 – when the cancer has spread to the connective tissue beneath the bladder lining (7). Most human patients (75%) diagnosed with bladder cancer have NMIBC (stages Ta, CIS, or T1), and diagnosis is typically followed by standard treatments; Bacillus Calmette-Guerin (BCG) intravesical immunotherapy, transurethral resection of bladder tumor (TURBT), instillations of chemotherapy (1-year maximum) or partial or radical cystectomy (RC), all with excellent survival rates (8). The remaining cases with muscle-invasive bladder cancer (stage T3 or greater), however, present with a high risk of death unless high-cost and radical treatments, like chemotherapy, radical cystectomy, or radical radiotherapy, are performed (9). Current therapies are often not effective enough and are associated with significant negative side effects (9). Even with radical treatment of the bladder, the cancer has likely metastasized to other organs (lymph nodes, lungs, liver, bones) and approximately half of human patients diagnosed with MIBC will eventually die of bladder cancer within 5-years (9).

Tobacco smoking and occupational exposures are the most well-documented risk factors for bladder cancer while emerging evidence suggests the role of additional risk factors like diet and genetic predisposition (3,10–12)

1.1.2. Canine Bladder Cancer

Bladder cancer is naturally occurring in pet dogs and is often muscle-invasive at the time of diagnosis. Invasive urothelial carcinoma (InvUC) is estimated at 60,000 cases in canine patients each year (13). Bladder cancer is typically diagnosed in older dogs with the average age at diagnosis reported as being between 9-11 years old (13). In dogs, InvUC usually arises in the trigone region of the bladder that oftentimes (56% of dogs) extends into the urethra, obstructing urination (14). The most common type of bladder tumor found in dogs is InvUC, and in most cases involves high-grade papillary infiltrative tumors that have invaded into surrounding bladder muscle (15). Survival time is dependent on the location of the tumor in the bladder, whether the tumor has yet metastasized to other organs, and the tumor's rate of growth. According to a review by Fulkerson and Knapp on the management of InvUC, symptoms noticeable to pet owners are more obvious once tumor cells have invaded the dog's bladder wall or metastasized to other organs, which occurs in over 50% of cases (16). Dogs diagnosed with InvUC can receive treatment but are rarely cured of the disease, even with treatments options like those offered to human patients – surgery, radiation therapy, and chemotherapy (13). Radical cystectomy is uncommon in pet dogs due to the high cost, risks of significant morbidity from the surgery, the tumor's tendency to extend into the urethra of the bladder, and the presence of metastasis at diagnosis in some cases (16,17). InvUC in pet dogs is influenced by risk factors like breed association, environmental exposures such as lawn chemicals, dated flea control products, obesity, and female sex (15,18,19). For breed-associated risk, Scottish terriers have a 16-fold to 20-fold increased risk, as well as a lesser increased risk in West Highland white terriers, Shetland sheepdogs, beagles, wire hair fox terriers, American eskimos, Keeshonds, and Samoyeds when compared to risk association in mixed-breeds (15,16).

1.1.3. Origin of Canine Companions

It is important to acknowledge the origin of canine companions in society, who 150 centuries ago were bred first from wolves to help humans survive as fierce protectors, and as dedicated hunters, a role that has since evolved simultaneous to evolution of human societies (20). As time progresses, and society continues to industrialize, humans have maintained a co-dependent relationship with

pet dogs, now breeding them not only for function but also for form, with emphasis on desirable traits and selective characteristics (21). Purebred dogs have limited genetic variability from strict trait selection in specific breeds, which is why one breed is more predisposed to inheriting a certain disease over another (22,23). Cancers, although more complex to consider in terms of inheritance patterns than other diseases, exhibit a higher risk in certain purebreds due to limited genetic variability that result from centuries of selective breeding (21). Restricted gene variation in purebred dogs also gives an opportunity for researchers to more easily identify the genetic basis of cancers, and because bladder cancer in dogs is primarily due to genetic predisposition, breeds more susceptible to BC will be important for studies involving cancer prevention and development of therapeutics (21,24).

1.1.4. Translational Research and Bridging Models for Impact

Improving health outcomes for both human and canine patients with urothelial carcinoma remains a significant need and emphasizes how research incorporating preclinical animal models is important for bringing scientific discoveries into clinical practice (15,25). There has been an increase in the argument for integrating veterinary species into the oncology drug development pipeline, since they spontaneously develop tumors in the presence of a complete immune system (26). Rodent models, although more common, widely available, and vital to preliminary findings in cancer research, are often immunodeficient and do not fully embody the intricacies of human cancer, such as the complexity of driver mutations or tumor-host microenvironments (25). Given that UTC in dogs closely resembles the disease in humans, canines would make a valuable and more comprehensive model for understanding and developing of novel therapies (13). Studying corresponding cancer in both humans and canines, coined the term canine/human comparative oncology, is increasingly being regarded as a better modeling system than murine models for advancing research for all cancers, including bladder cancer (21,27).

1.1.5. Limitations of Murine Models for Bladder Cancer Research

Small rodents like mice are often used as preclinical *in vivo* models for developing new therapies for human diseases. Due to considerations like ethics and logistical practicality, rodents have become the standard model for mammalian systems in human biology research (28). A range of different murine models are available for studying cancer, each with their strengths and weaknesses and while these models are continually being improved to enhance their accuracy and relevance, they are limited in many ways (29). Studies incorporating murine models can be

credited for having provided a wealth of biological insights, however there are still limitations to certain aspects of human biology that are not accounted for in mouse studies, especially the immune system (30). For example, Toll-like receptors (TLRs) – a class of pattern recognition receptors that activate the innate immune system in the presence of pathogens or damaged host tissues – are different between species; human innate immune systems include a functional TLR10, which is absent in mice, and mice express TLR11, TLR12, and TLR13, receptors not found in humans (30). Additionally, many pathogens and drugs are species-specific, and their effect or infectivity is often species-dependent (31). There could be significant differences in the nature and pathogenesis in immune responses against pathogens that only infect human cells, and murine infectious agents, or murine-adapted pathogens (28,31). Rodents are resistant to several infections that affect humans, and modern therapeutic and immunomodulatory agents are often designed to target human biology (32). Limitations also include an inability to precisely mimic critical cellular interactions, for example between tumor cells, stromal cells, and immune components – which are fundamental in the pursuit of a complete understanding of cancer biology and treatment responses (33). Given that bladder cancer in humans is primarily seen in older men, studies using young, immunodeficient, usually female mice, fail to accurately represent these populations of humans that are most likely to be afflicted with the disease (34,35). These contrasts are important to acknowledge, especially since only 11% of oncology drugs that show success in mice ultimately receive approval for use in humans (36,37). Though there has been a notable expansion in the development of murine models for various types of tumors, bladder cancer, in comparison to others, remains lacking in accurate mouse models (38).

1.1.6. Options for Mouse Models for Bladder Cancer

There are different mouse models for bladder cancer, depending on how they are established in the mouse – carcinogen-induced models, engraftment models, and the genetically engineered mouse (GEM). Carcinogen models involve treating mice with carcinogens to induce tumors, while GEM models involve manipulating certain genes in the bladder to promote tumor development. Both carcinogen and GEM models are autochthonous, meaning they originate directly within the bladder. Disadvantages to carcinogen treatment are that it is difficult to limit carcinogenic agents to other tissues near the bladder, and GEM models for bladder cancer are primarily for non-invasive phenotypes and not MIBC/InvUC. Another murine model for bladder cancer is the engraftment model, which is non-autochthonous, meaning that they do not originate directly within

the bladder. Engraftment involves implanting bladder cancer cells or tissues directly into a recipient mouse, and this method for model establishment can be quick and straightforward (38). Recipient mice are often immunodeficient, and this is important to emphasize since the immune system plays a critical role in cancer progression and metastasis (39). It has also been suggested that urothelium in mice may be inherently resistant to developing bladder cancer due to the urothelium's slow turnover and limited proliferation, which could make it more resistant to genetic damage (40,41).

1.1.7. Modeling Non-Invasive Versus Invasive Bladder Cancer

'Bladder cancer' refers to a heterogenous set of diseases (38). Past studies have supported the notion that low-grade, non-invasive and high-grade, invasive bladder tumors are molecularly distinct, and this is upheld by gene expression profiling (42–47) and genomic alterations (38,45,48–51). In contrast, meta-analysis of expression profiling data does not identify specific molecular subtypes that distinctly correspond to a single pathological state of bladder cancer (52). Considering this, researchers have had trouble fully accepting the idea that there exist completely mutually exclusive models for non-invasive and muscle invasive bladder cancer, especially since superficial tumors are known to progress into MIBC (38). The distinction between non-muscle invasive and muscle invasive bladder cancer is thought to not be a rigid one, and the progression of NMIBC to MIBC is suggested to exist on a range of disease progression (38). Although NMIBC and MIBC are categorized as different forms of bladder cancer, molecular and biological overlaps make it challenging to model them in isolation without considering the possibility of progression and shared pathways (53). These overlaps make it difficult to model bladder cancer in mice. Current murine models have failed to capture the full complexities of human bladder cancer especially when considering challenges in establishing specific molecular heterogeneity and tumor plasticity (54).

1.1.8. The Need for a More Relevant Model

There is a great need for a more relevant, biologically accurate animal model that better recapitulates the conditions of human bladder cancer. Given that most bladder cancer-related deaths in pet dogs and humans are due to primary tumors and muscle invasion of urothelial transitional carcinomas (UTC), respectively, the use of a more comprehensive model may improve preclinical research and drive the development of novel therapeutics to combat poor prognosis rates in some human cases and in pet dogs (15,55). Current murine models for bladder cancer, both

autochthonous and non-autochthonous, often fail to replicate with accuracy the complexities of the disease, like dynamic tumor heterogenicities (56). Limitations of murine models available for researching bladder cancer emphasize the need for a better translational *in vivo* model that can better mimic the complexities of human bladder cancer.

1.1.9. Canine Bladder Cancer as a Model

Since the first targeted therapeutic antibodies (Abs) were evaluated and approved by the FDA, the field of oncology has continued making advancements in novel targeted pharmaceuticals with radiation, immunotherapy, and chemotherapy (57). The swift progress in the pursuit of new effective therapies for humans with bladder cancer cannot be supported by murine models alone, and additional animal models addressing the limitations of current models are needed (57). To more accurately predict health outcomes of novel therapies, dogs who spontaneously develop bladder tumors are increasingly being recognized as a valuable model due to their clinical and biological similarities to human bladder cancer (58,59). Pet dogs who are exposed to risk factors present in their normal daily environments are inclined to develop cancer exhibiting tumor heterogeneity like human patients (26). Importantly, pet dogs can spontaneously develop tumors in the presence of an intact immune system, which, as a model, would address barriers in the development of novel immune therapies for cancer (26). Tumors that develop naturally in the presence of an intact immune system will evade and manipulate normal immune responses by generating an environment that stifles innate immune cells, promotes tumor formation, and prevents tumor eradication by suppressing immune responses (60–62). Animal models with intact immune systems grant the opportunity to be able to develop novel immune therapies for cancer, overcoming the barriers posed by murine models, which lack a fully functional immune system for studying tumorigenesis in the presence of immune response (63). Additionally, adverse side effects often associated with clinical management in oncology are more likely to be mimicked in canine models than in murine models allowing for more accurate assessments of the safety and efficacy of novel therapies (64). The larger size of the dog makes them better than rodents for imaging studies, and serial specimen collection, improving chances for detecting potential side effects (26). There has been an uptick in veterinary clinical trials to meet the growing demand for more advanced options that treat companion animals with cancer. Trials in pet dogs provide a unique opportunity to address their medical needs while simultaneously assessing the safety and efficacy of novel cancer therapies that can be translated to human medicine (26).

1.1.10. Similarity to Human MIBC

Canine and human BC exhibit many of the same characteristics and share overlapping pathology and metastatic trends (15,65). Microscopically, canine bladder cancer is like human bladder cancer, with urothelial carcinoma being the most common type of tumor in both species (14,66). There are common sites of metastatic spread in both species which includes the lymph nodes, lungs, liver, and bones (67,68). Findings from a necroscopy study of 137 dogs with bladder cancer at Purdue University showed that 67% of dogs had metastasis, 9% had nodal metastasis alone, 25% with distant metastasis alone, and 33% with a combination of distant and nodal metastasis and these findings closely mirror human metastatic disease trends (15). Several genes that when mutated initiate the progression to muscle invasion that are common in both species including EGFR, CDKN2B, PIK3CA, BRCA2, NFkB, ARHGEF4, XPA, RB1CC1, RPS6, MITF, and WT1 (27,69–71). RNA-seq analysis demonstrated a shared genetic response related to bladder cancer in both species, where among 2,911 pairs of orthologous genes analyzed, 1,589 were found to be differentially expressed between normal bladder tissue and bladder cancer tissue samples from both dogs and humans, suggesting a correlation between gene mutations and their expression levels in bladder cancer, and remarkable similarities between species (27). Molecular markers like cyclooxygenase-2 (Cox-2) which is involved in tumor growth, and apoptosis-inhibiting protein, survivin, are overexpressed in both canine and human invasive urothelial carcinomas (72–75). Telomerase activity, which prevents telomere shortening and allows cancer cells to achieve replicative immortality, was detected in about 90% of human cases of UTC with similar levels reported in canine UTC cell lines and urine samples from canine patients (76). Epidermal growth factor receptors, EGFR1 and EGFR2 (also known as HER-2, ERBB2, NEU), have also been found to be significantly overexpressed in BC samples from both species (77–80). In addition to molecular parallels in human and canine BC, both species have comparable clinical presentations and responses to therapy (15). In both dogs and humans, urothelial carcinoma is typically diagnosed in older individuals, with the median age at diagnosis being 11 years in dogs (equivalent to ~60 human years) and ranging from early 60s to early 70s in humans (14,81,82). Common symptoms observed as UTC progresses in both dogs and humans include hematuria, frequent urination, stranguria, and recurrent urinary tract infections (UTIs), with pain related to bone metastasis being rare, though this has been reported in some cases (15). Both species also demonstrate similarities in their response to medical therapies. Agents such as vinblastine,

gemcitabine, and platinum-based drugs like cisplatin, carboplatin, and mitoxantrone have shown efficacy in treating urothelial carcinoma in both dogs and humans (14,83–86). Alignments in clinical features and response to therapies further emphasize the value of comparative studies that contribute to an overall understanding of urothelial carcinoma across the two species.

1.1.11. Differences in Bladder Cancer Between Species

While there are many similarities between canine and human bladder cancers, it is also important to acknowledge the differences. For example, in humans, most UTC cases (~75%) are low-grade, superficial tumors whereas canine UTC is typically diagnosed after the cancer has become invasive making non-invasive cases in dogs uncommon (14). Considering this, most pet dogs with spontaneous tumors may be more valuable in studying invasive UTC mechanisms than non-invasive UTC (15). The anatomic distribution of tumors differs between species; dogs more frequently develop tumors in the trigone region of the bladder with extension into the urethra in many cases, whereas humans present with a more scattered tumor distribution across the bladder region (16,87). There are also differences in predisposition of sex: male humans are disproportionately affected compared to female humans, whereas female dogs are at higher risk than male dogs (3,88). Despite these differences, the canine model remains advantageous due to its ability to naturally develop invasive and metastatic forms of urothelial carcinoma more accurately than murine models, and in the presence of a complete immune system.

1.1.12. Advantages Over Murine Models – Bridging the Gap from Murine to Human

The translational value of studying naturally occurring cancers in dogs compared to induced murine models is undeniable. Canine models offer an opportunity for studying the effectiveness of novel therapies that can benefit both species… a potential breakthrough treatment for beloved pets and, eventually, translation to novel therapies for humans (26). The trajectory of the development of new cancer therapies relies on the outcomes of studies in preclinical murine models that often poorly predict efficacy and toxicity levels, and as a result, most (59%) anti-cancer drugs that enter Phase III clinical trials fail due to toxicity and other factors (26,89). Roughly $60 billion is spent on unsuccessful human cancer drug trials each year, however, the cost of comparable veterinary oncology trials in dogs is only 10-20% of that (90,91). Research involving tumor-bearing dogs, while more expensive than mouse models, is similar in expense to studies including other large animals typically used for toxicity research. Dog owners who choose to enroll their pets in clinical studies are usually not responsible for covering the cost of treatment,

and expenses are often covered by a sponsoring company (92). Overall, pet dogs with naturally occurring tumors provide a solution for bridging the gap between preclinical and human clinical trials, improving cancer drug development, and providing treatment options for both canines and humans (92).

1.2. Project and Scientific Basis

1.2.1. Targeted Radiation Therapy

Targeted radionuclide therapy (TRT) has advanced rapidly, both for use in the clinic as well as in research (93). It works by selectively delivering cytotoxic radiation directly to tumor cells, and targets are based on some biological feature unique to cancer (93). With this approach, there is potential for maximizing therapeutic effects while eliminating nonspecific toxicity to healthy tissues (94). Radiopharmaceuticals used in TRT generally consists of three functional components: (1) a vector or carrier molecule that selectively binds to cancer associated biomolecules, (2) a radionuclide that emits therapeutic radiation, and (3) a linker or chelator that stably connects the vector to the radionuclide (95–97). A schematic made using Biorender of these components relevant to this thesis project can be seen in Figure 1. With this targeted mechanism, the therapeutic effects can be localized primarily to malignant tissue while also sparing surrounding normal cells. Two main types of particle emission are used in TRT: beta and alpha emission (98). Beta-emitting radionuclides are the most widely used and include isotopes like lutetium-177 (Lu-177), which is the current standard in many clinical applications. Copper-67 (Cu-67) and terbium-161 (Tb-161) are other examples of beta-emitting radionuclides and are currently under clinical evaluation (98). Beta emitters can enhance the cytotoxicity of targeted tumors cells, and its emission can travel a longer range through multiple tumor cells at a time, making them useful for treatment of heterogeneously expressed tumors and entire tumor masses (95). In contrast, alpha-emitting radionuclides have gained increasing attention due to their higher linear energy transfer (LET, the amount of energy deposited per unit length), shorter pathlength, and greater biological effectiveness, relative to beta-emission (98,99). Radium-223 (Ra-223) is already approved for treatment of bone metastasis in prostate cancer, and other alpha-emitters like actinium-225 (Ac-225) and lead-212 (Pb-212) are under clinical trial (100–103). There are currently no targeted radiopharmaceuticals that are approved for use for treatment of bladder cancer in both canine and human patients. There are several factors to consider related to the development of novel targeted radiotherapeutics for cancer. Off target uptake and collateral damage, specifically in the liver,

kidneys, and bone marrow, raises concerns about toxicity and dose limitations(95). Factors related to radiochemistry, like labeling efficiency, radionuclide availability, or relative stability of chelator complexes can enhance or reduce the effectiveness and reproducibility of targeted radiation therapy(104). For these reasons among others, addressing these barriers and furthering research efforts is important for expanding the clinical impact of targeted radiation therapies.

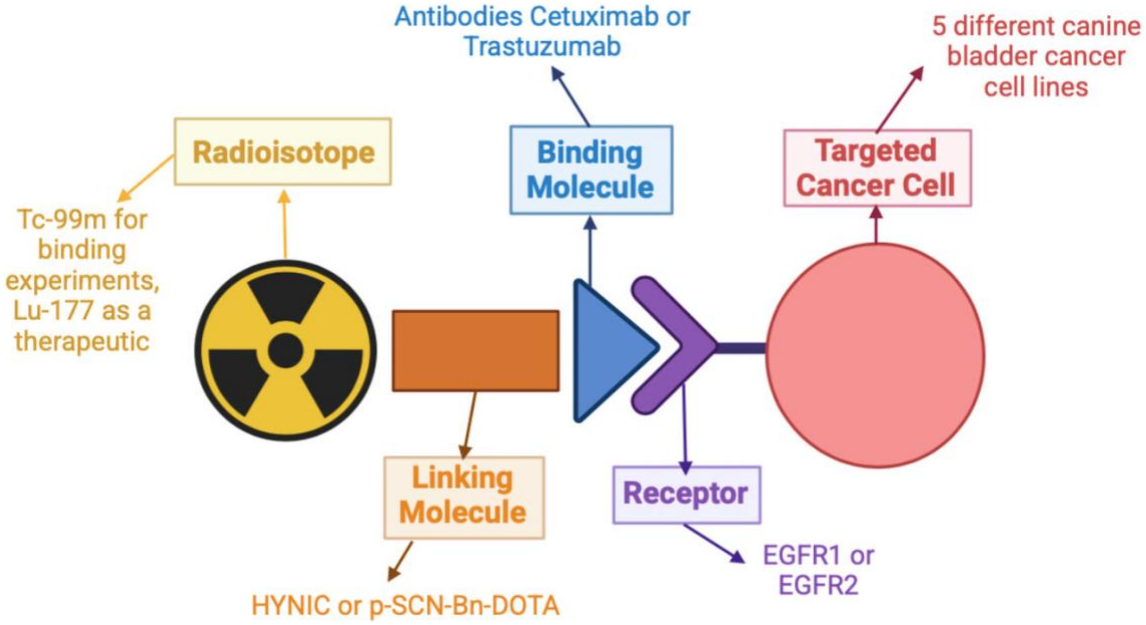

Figure 1. Targeted radiation schematic with relevant components labeled for this project.

1.2.2. Biomarker Validation for Novel Radiotherapeutic Development

Given the epidemiological importance of bladder cancer, both in canines and humans, there is a great need for novel therapeutic options that address the limitations of current therapy options (105). Pet dogs with naturally-occurring bladder cancer present as a more relevant model of the disease. Their similar characteristics and behaviors to high-grade human bladder cancers make canines a great *in vivo* model for pre-clinical trials assessing novel therapies that could benefit both dogs and humans (13). This study began with validating and quantifying specific cell receptors that are overexpressed in both canine and human bladder cancer cells, EGFR1 and EGFR2, with specific binding experiments using technetium-99m (Tc-99m) (106). Common molecular features between species, like EGFR1 and EGFR2 receptors, offer a promising foundation for the development of translational targeted therapies (69,107).

TRT has become increasingly popular among investigators who are developing new cancer therapies, and radioisotopes that emit alpha and beta particles are of the greatest interest for

targeted radiotherapeutic development (93). This research aims to explore the possibility of targeted radiotherapy as an option for treating canine and human bladder cancer, with emphasis on the potential of dual-targeting EGFR1 and EGFR2 receptors simultaneously. Canine studies conducted to assess the efficacy of targeting overexpressed molecular markers would allow for a better understanding of tumor biology of UTC and additionally support the development of targeted therapeutic strategies (13). By utilizing FDA-approved monoclonal antibodies like cetuximab and trastuzumab, labeled with a therapeutic radioisotope, this project aims to contribute to the development of novel targeted radiotherapies that would minimize off-target effects – which is a concern of current radiation treatment options (108). Veterinary clinical trials in bladder tumor-bearing dogs are anticipated to provide essential preliminary data that supports translation of targeted radiotherapies to human clinical applications (109).

1.2.3. Relevance and Significance

Invasive urothelial carcinoma remains a very challenging cancer to treat, with both human and canine patients facing poor prognosis due to disease progression and late-stage diagnoses (110). Current options for radiotherapy, like external beam radiation, present considerable risk of damaging healthy tissues and organs by off-target emission (108). This emphasizes the need for novel TRTs, which, by linking radioisotopes to monoclonal antibodies, will specifically deliver treatment to biomarkers overexpressed on cancer cells (while also minimizing harm to surrounding healthy cells and tissues) (111). EGFR1 and EGFR2 expression is amplified in many cancer types compared to expression in healthy cells, and this overexpression supports tumorigenesis (111). TRT has already shown promise in other applications, like Lu-177 targeted radiotherapy that is already being used to treat neuroendocrine and prostate cancers (112,113). Additionally, EGFR-targeted therapies have been used and are successful for treatment of veterinary species (114).

1.2.4. Project Contribution

This project will contribute to the development of a more effective form of radiotherapy by using monoclonal antibodies (cetuximab and trastuzumab) conjugated with radioisotopes to target specific receptors like EGFR1 and EGFR2 that are overexpressed on cancer cells. The results from this research project will be used as preliminary data to support a future phase I clinical trial for safety and tolerability of this treatment in canine patients with bladder cancer. If successful, this therapeutic strategy has the potential to benefit pet dogs with bladder tumors that are resistant to traditional therapies. Importantly, demonstrating the safety and efficacy of this approach in canine

trials would provide data supporting future human clinical applications, thus bridging the gap between veterinary and human cancer research (107).

1.2.5. Focus Areas

This thesis project focused on testing the practicality of developing novel targeted radiotherapeutics for canine bladder cancer, with the first aim being to validate the expression of key biomarkers EGFR1 and EGFR2 on five different canine bladder cancer cells lines with Tc-99m specific binding assays to confirm the possibility of employing a targeted approach. In addition to validating EGFR1/EGFR2 expression, binding affinity of monoclonal antibodies, cetuximab (chimeric (mouse/human)) and trastuzumab (humanized), to the canine cell lines was also assessed. Figure 2 (created using Biorender) illustrates how total and nonspecific binding are distinguished in the binding experiments: in the blocked condition, receptors were blocked with an excess of unlabeled antibody before adding the radioligand, so any signal reflects non-specific binding, in the unblocked condition, radioligand binds to all available receptors, giving total binding values. Expression level and binding affinity data allow for the selection of candidate cell lines (cell lines that have reasonable receptor expression and affinity) to carry forward for targeted radiation *in vitro* assays.

The hypothesis for this thesis is that dual-targeted alpha therapy will effectively treat canine bladder cancer cell lines *in* vitro, however given the inability to source an alpha-emitting isotope for experimentation, this exact hypothesis could not be tested, and this thesis project is looking at the effects of targeted beta therapy for now using colony formation experiments that evaluate the ability of single cells to proliferate into colonies after incubation with treatment. The methods discussed in this study will include the quantification of EGFR1 and EGFR2 expression in five different canine bladder cancer cell lines, followed by targeted colony formation assays *in vitro* with the antibodies alone as a control as well as TRT studies. The efficacy of targeted radiotherapy will be evaluated using varying concentrations of antibodies alone, and radioisotope-conjugated antibodies. The data from this research project will be used to support a future phase I clinical trial for the safety and efficacy of novel targeted radiotherapeutics *in vivo* in canine patients with naturally occurring bladder cancer.

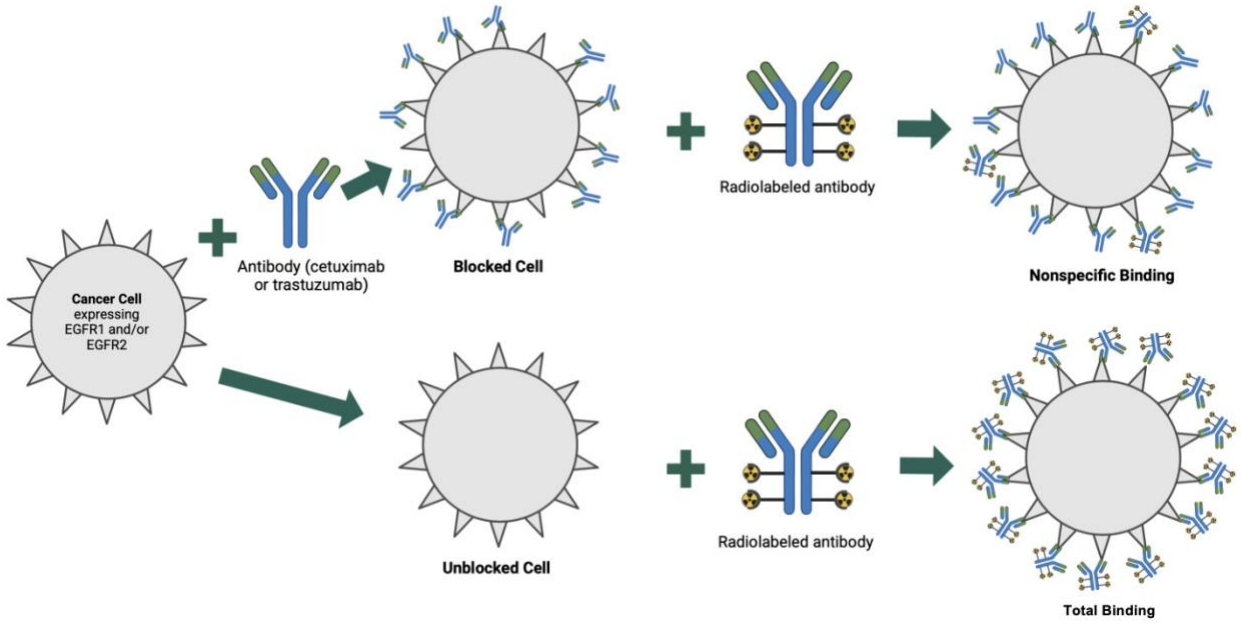

Figure 2. Schematic of total and non-specific binding conditions in the Tc-99m binding experiments.

2. MATERIALS AND METHODS

2.1. Cell Lines

Dr. Deborah Knapp and her research group at Purdue University provided canine urothelial carcinoma (K9UTC AxA, AxC, Nk, Sh, and Org) cell lines that they established for the purpose of *in vitro* comparative bladder cancer research (115). All K9UTC cell lines were established from tumor samples from dogs with histopathologically diagnosed grade 2 or 3 UTC during cystoscopy or surgery. Two of the cell lines, AxA and AxC, were established from the same tumor from the same dog, and the other three cell lines are from different individual dogs. All K9UTC cell lines were grown in DMEM/F12 Media + 10% Fetal Bovine Serum (FBS) and without additional antibiotics. Prior to the characterization performed during this thesis, the EGFR-specific antigen-binding site of cetuximab was previously evaluated for three of the five cell lines (UTC AxA, UTC Org, and UTC Sh) by flow cytometry using the canine antibody can225IgG, known to have the same antigen binding site as cetuximab (116,117). Nagaya et al. suggested that K9UTC Org had minimal EGFR1 expression, K9UTC AxA lower expression, and K9UTC Sh intermediate expression (116). A mouse fibroblast cell line (3T3/NIH) that was purchased from ATCC (Manassas, VA, USA). This cell line, previously shown in the Zinn Lab to have non-detectable EGFR1 and EGFR2 receptor expression, was included in some studies as a negative control for binding. The 3T3 cells were grown in Dulbecco's Modified Eagle Media + 10% FBS + 1% Pen-Strep + 1% L-Glutamine (118). All cell lines were incubated at 37°C, and 5% CO_2.

2.2. Antibodies

Erbitux® (cetuximab) was purchased from the Michigan State University pharmacy and is a chimeric (mouse/human) monoclonal antibody that specifically binds to EGFR1 receptors (https://uspl.lilly.com/erbitux/erbitux.html#pi). Kanjinti® (trastuzumab-anns), a biosimilar to trastuzumab, is a recombinant DNA-derived humanized immunoglobulin G1 kappa antibody specific to EGFR2 receptors (https://www.kanjinti.com/hcp/biosimilar-expertise) and was purchased from the McLaren Health Care pharmacy. Both cetuximab and trastuzumab are approved by the FDA for use in humans. Human IgG1 Kappa-UNLB was purchased from Southern Biotech (Birmingham, AL, USA). IgG1, an isotype-match for cetuximab and trastuzumab, does not specifically bind EGFR1 or EGFR2 and served as a non-specific negative control in colony formation experiments.

2.3. Radioactive Materials

Tc-99m was purchased from Cardinal Health's Flint Pharmacy and delivered to the radiopharmacy at Michigan State University. Doses of 50 mCi were received in approximately 0.5 mL of saline for each shipment. Lutecium-177 was ordered and received from SHINE Technologies, LLC (Janesville, WI, USA). Doses of 100-200 mCi were received in 2 mL V-vials at a concentration of 1.0 Ci/mL the same week experiments were performed. Chelators HYNIC and p-SCN-Bn-DOTA were conjugated to the antibodies at a 6:1 molar ratio for HYNIC, and a 2:1 molar ratio for p-SCN-Bn-DOTA (chelator:Ab) and were needed to radiolabel Tc-99m (HYNIC) and Lu-177 (p-SCN-Bn-DOTA) to antibodies cetuximab and trastuzumab. Lyophilized kits for both HYNIC and p-SCN-Bn-DOTA were prepared in advance for convenient availability on the day of experiments. Glass vials (kits) containing the appropriate amounts of chelators were vacuum dried with a Benchtop Freeze Dryer/ Lyophilizer (SP Scientific VirTis AdVantage Pro Stoppering Tray Freeze Dryer; SP Scientific/VirTis, Warminster, PA, USA) and stored at -20 °C capped under vacuum. Tricine and tin chloride ($SnCl_2$) kits were prepared similarly and had 36.7 mg of Tricine and 51 μg of $SnCl_2$ per kit. The tricine solution (100 mL of MilliQ water with 3.67 g tricine) was adjusted to a pH of 7.0 and degassed (vacuum and ultrasonic bath) before the addition of the $SnCl_2$ (50 mg/mL in ethanol). A total of 1.0 mL of the tricine/ $SnCl_2$ solution was added to each vial followed by freeze-drying.

2.4. Overall Order of Experiments

2.4.1. Specific Binding Assays

For each experiment, for each K9UTC cell line, the cells were detached, counted, and 30,000 cells per well were added a 96-well plate, four columns per each antibody with 8 serial dilutions. Seeded plates were left to incubate overnight to allow cells to reattach to wells of the plate. Antibodies were conjugated to HYNIC (6:1 molar ratio) and a 30k MWCO spin concentrator was used to remove unconjugated chelator by centrifugation. The Tc-99m was always received on the day of experiments, and the entire volume was injected into a Tricine/$SnCl_2$ kit and incubated for 15-30 minutes. The solution containing Tc-99m/Tricine/$SnCl_2$ (~0.5 mL) was then transferred to and incubated with each of the conjugated antibodies for 1 hour to allow Tc-99m to bind with HYNIC. Pre-packed G-25 Sephadex Resin columns were used for purification to remove unbound Tc-99m, and the fraction with the highest activity was selected to be tested for purity by instant thin layer chromatography (iTLC) and protein concentration using Bradford Protein Assay (absorbance =

595nm). Once purity and required concentration for the dilution series were confirmed, the selected fraction was used to prepare the dilution plate (4 replicates for each antibody) with a previously determined highest concentration (40 nM) and diluted 1:2 down the rows. The 96-well plate mentioned previously was removed from incubation, liquid removed, and all wells were washed with PBS. Blocked columns received a molar excess of the respective antibodies (unlabeled, and unblocked triplicates received media only). After 15 minutes of incubation and blocking, Tc-99m labeled antibodies from the dilution plate were transferred to the plate with cells and incubated for 1 hour. After incubation, wells were aspirated, and cells were washed three times with PBS (1X) to remove unbound radiation. All wells then received media prior to the ATPlite protocol that measured the number of cells/well, and lysates were collected into polymerase chain reaction (PCR) vials to measure the radioactivity from each well. Data was analyzed to quantify receptor numbers per cell (Bmax) and to quantify specific binding affinity (Kd).

2.4.2. Flow Cytometry (Aurora Cytek) Experiments

Cetuximab, trastuzumab and IgG were conjugated separately in the lab with IR680 dye. Titration experiments were completed first to determine the concentration of dye-conjugated antibody with the most optimal staining index for flow cytometry. Two cell lines were selected for titration experiments: one canine cell line confirmed to express both receptors of interest, and the 3T3 cell line that does not express either receptor, according to previously performed binding experiments. Cells were dissociated, washed, counted, and then seeded into a 96-well u-bottom plate. Samples were first stained with Live/Dead Blue dye, followed by an apoptosis tracking fluorochrome (Apo-tracker Green), Fc blocking, and finally a titration of the labeled antibodies. After incubation, cells were washed, fixed, resuspended, and filtered before being stored at 4 °C in the dark until analysis. Data were analyzed for all experiments using FCS Express to assess antibody binding by fluorescence.

2.4.3. Colony Formation Assay as Controls without Lu-177

The morning before experiments, media was pipetted to 6-well plates and placed in the incubator to allow media warm for at least two hours. On the afternoon before experiments, each cell line was seeded in low density with more media for a triplicate 1:2 dilution of the treatment conditions with 1) 137 nM of cetuximab and trastuzumab combined as the highest concentration; 2) a no treatment control; and 3) 100 μM of cisplatin as the highest concentration. Cells were left to adhere during overnight incubation. Antibodies were sterile-filtered using a syringe filter before dilution

plate preparation. A dilution series was prepared in a separate 96-well plate, with 8 total dilutions of treatment in a 1:2 ratio. After overnight incubation, cells received their respective treatment conditions, negative control cells received only fresh media, and the positive control cells received a dilution series of cisplatin. To mimic urination of the bladder, after one hour of incubation, wells were washed with PBS two times and then replenished with fresh media, although this is not standard for *in vitro* bladder cell culture work. All plates were put back into the incubator and were checked regularly over a week to assess colony growth. Once colonies had formed (groups of 50 or more cells), plates were removed from the incubator. All media was aspirated, and the crystal violet staining protocol was followed. Stained plates were then imaged, and colonies were counted using ImageJ.

2.4.4. Initial Lu-177 Colony Formation Assay

On the day prior to the experiment, media was pipetted into the plates in the morning and put into the incubator to warm for at least 2 hours. On the afternoon of the day before the experiment, cells were seeded for three triplicate treatment conditions: (1) Higher molarity (7 nM) of cetuximab and trastuzumab combined; (2) Lower molarity (0.5 nM) of cetuximab and trastuzumab combined; (3) Higher molarity (8 nM) of IgG isotype control; (4) Lower molarity (0.5 nM) IgG isotype control; and (5) a no treatment control and left to incubate overnight. On the day of the experiment, antibodies were conjugated to p-SCN-Bn-DOTA at a molar ratio of 2:1 (DOTA: Ab) and a spin concentrator was used to remove unconjugated DOTA by centrifugation. The dose of Lu-177 was received at a concentration of 1 Ci/mL on the week of the experiment and was used to radiolabel the conjugated antibodies. The volume taken from the source vial (usually 10-20 μl) depended on the radioactivity on the day of the experiment, accounting for time since shipment and radioactive decay. After radiolabeling, G-25 resin columns were used to remove free radiation. Purity was assessed by instant thin layer chromatography (iTLC) and protein concentration was measured using Bradford (absorbance = 595nm). Once purity and concentration were determined, the radiolabeled antibodies were diluted to prepare the treatment conditions for radiolabeled cetuximab + trastuzumab and IgG. Stock solutions were prepared for each antibody by diluting the radiolabeled product with media. Cells that were incubating overnight were removed from the incubator and received their respective treatments from the stock vials. The negative control condition received the same volume of fresh media only. After one hour of incubation with the treatment condition, all wells were washed with sterile PBS (1X) and replenished with fresh media.

Plates are checked regularly over the course of a week to assess colony growth. After about a week of incubation, plates were removed from the incubator. All media was aspirated, and the crystal violet staining protocol was followed. Stained plates were then imaged, and colonies were counted using ImageJ.

2.4.5. Additional Lu-177 Colony Formation Assay

For the second Lu-177 experiment, a single canine bladder cancer cell line was selected for treatment. Three treatment conditions were tested: (1) Lu-177-labeled cetuximab and trastuzumab at a high concentration; (2) Lu-177-labeled IgG at the same high concentration; and (3) a no-treatment control. Each condition was assessed at three different time points: 1 hour, 12 hours, and 24 hours. The overall protocol remained the same, with some modifications. Instead of G-25 resin columns, spin concentrators were used this time to remove free Lu-177 and chelator after radiolabeling. Cells were seeded the day before treatment and allowed to incubate overnight. On the day of the experiment, radiolabeling was performed as previously described, and stock solutions were prepared by diluting the radiolabeled product with media. Cells received their respective treatments from the stock vials, while the negative control received an equal volume of fresh media. After incubation over three different time points, all wells were washed with sterile PBS (1X) and replenished with fresh media. Plates were checked regularly over the course of a week to assess colony growth. Then, all media was aspirated, and the crystal violet staining protocol was followed. Stained plates were imaged, and colonies were counted using ImageJ software to quantify clonogenic ability for each treatment condition.

2.5. Detailed Protocols

2.5.1. Canine Cell Line Tc-99m Specific Binding Assays

2.5.1.1. Seeding Cells

Cells were washed with 1X PBS (ThermoScientific; Whaltham, MA, USA) and were detached from the cell culture flasks with 1X TrypLE Express (gibco; Waltham, MA, USA). Live cell count was measured using an Eve Automated Cell Counter (NanoEnTek; Seoul, South Korea) and cells were seeded at 30,000 cells/well with 150 µL of their respective media into the wells of a 96-well clear bottom black plate (ThermoScientific; Whaltham, MA, USA) and placed into the incubator overnight at 37°C, and 5% CO_2. For the specific binding experiments, two antibodies (cetuximab and trastuzumab) per cell line were tested each with a blocked and an unblocked condition. The unblocked condition was plated in triplicate with eight 1:2 dilutions of the Tc-99m labeled

antibody. There was also a single replicate blocked condition, where wells received molar excess of unlabelled antibody (relative to the highest condition of radiolabeled antibody) before the radiolabelled dilution series was added. A total of 1.94e+06 cells was needed for the binding experiments, and 4.78e+06 cells for establishment of the ATPlite standard curve.

2.5.1.2. Conjugation of antibodies with hydrazine nicotinate (HYNIC)

Frozen lyophilized HYNIC kits that had been prepared before the day of the experiment were retrieved from -20°C freezer and allowed to thaw to room temperature. Kits were resuspended to 1 mg antibody per 2 mL of buffer using 0.15 M Na_2HPO_4 buffer (pH=7.4). After dissolving the lyophilized HYNIC, the desired concentration of antibody was added, an additional 100 µL of 0.15 M Na_2HPO_4 for pH maintenance was added, and the solution was mixed by vortexing. Each antibody had its own individual conjugation reaction tube. Tubes were incubated at room temperature for one hour with gentle mixing on a rocker and covered with aluminum foil to protect the reaction from light. After incubation, the conjugated antibodies were purified using a spin concentrator with 1X PBS (pH=7.4) as the buffer.

2.5.1.3. Spin Concentration

Two Vivaspin™ PES ultrafiltration spin column, 30,000 kDa molecular weight cutoff (MWCO), 2 mL - 6 mL capacity (Cytiva; Marlborough, MA, USA) was labeled for each individual conjugated antibody. The entire volume of the previously prepared conjugated antibody was pipetted into the bottom of the sample reservoir of their respectively labeled spin concentrators, and an additional 2 mL of 1x PBS (pH=7.4) was pipetted into the same sample reservoirs on top of the conjugated antibody. The spin concentrators were then centrifuged at 3200 rpm for 8-10 minutes, and the flow through was discarded after each spin. An additional 2 mL of 1X PBS (pH=7.4) was pipetted into the sample reservoir, and centrifuged again at 3200 rpm for 8-10 minutes, and the flow through was discarded. This step was repeated two more times to remove unbound chelator. Final products were retrieved from the sample reservoir by pipetting and transferred into new labeled tubes for storage. Antibody-HYNIC was stored at 4 °C until use.

2.5.1.4. Column Preparation

25 grams of Sephadex™ G-25 Superfine resin (GE Healthcare; Chicago, IL, USA) was added to 100 mL of MilliQ water in a 300 mL glass beaker to swell. When separation of the swelled resin (bottom) and MilliQ water (top) was established, the MilliQ water from the top was aspirated and 100 mL more of MilliQ water was added to the glass beaker with the swollen resin. The previously

described step was repeated three times. After the final wash with MilliQ water, it was aspirated once more to be replaced by 1X PBS for two more washes and then left to swell overnight at 4 °C. Swelled G-25 resin was packed into disposable 10 mL polypropylene columns (Thermo-Scientific; Waltham, MA, USA) and were left to settle at 4°C.

2.5.1.5. Tc-99m Radiolabeling

Tc-99m doses were ordered from and delivered by Cardinal Health, typically ~50 mCi of activity in 0.5 mL of saline in a 1 mL syringe. Once the dose was received, the dose in mCi was measured using a dose calibrator (Model #CRC-25R, Capintec, Florham Park, NJ, USA) and was recorded, and volume was estimated by pipetting, and recorded. The entire volume of the Tc-99m dose was expressed into the previously prepared Tricine/SnCl2 kits and allowed to incubate for 15 minutes at room temperature. After incubation, the Tc-99m/tricine/SnCl2 was divided equally into the already-prepared HYNIC-conjugated antibodies tubes, and was incubated at 37 °C, shaking at 500 rpm, for 30-45 minutes.

2.5.1.6. Column Purification

Simultaneous to the Tc-99m radiolabeling incubation period, the prepared columns packed with the G-25 resin were resuspended and equilibrated with PBS (1X). After the radiolabeling incubation period, purification was achieved by pipetting the entire volume of the radiolabeled antibody (Tc-99m mixed with HYNIC-conjugated antibody) to the top of resin of the packed column, with 1mL of 1X PBS added for every fraction collected. Around 8 fractions were collected, and measurements of activity and time were recorded with the dose calibrator. Fractions with the highest levels of activity following were selected for further analysis by iTLC and the Bradford Protein Assay.

2.5.1.7. iTLC (instant Thin Layer Chromatography)

The solvent used was PBS (1X), and 400 μL was added into 10 mL microcentrifuge tubes with caps (Model#WBB3087927, Globe Scientific; Mahwah, NJ). 2 μL of the selected fraction was pipetted near the bottom of a strip cut from iTLC-SG-Glass microfiber chromatography paper impregnated with silica gel, (Cat. No SGI0001, Agilent Technologies, Folsom, CA). Strips were placed into 10 mL tubes for about 5 minutes, or until it appeared that the solvent had migrated to the top of the strip. Strips were cut into halves, and these pieces were then measured individually on a gamma counter (Wizard2 Gamma Counter, Model#2480-0010, Perkin Elmer; Singapore) to

quantify purity. Purity was calculated with the equation; '[bound/(bound free)]x100,' or '[bottom half / (top half + bottom half)] x 100, and a purity of 95% or above was considered as acceptable.

2.5.1.8. Bradford Protein Assay

The selected fractions with 95% purity or above were measured by Bradford Protein Concentration Assay to measure protein concentration. For this, 5 µL of a standard dilution ladder and 5 µL of each sample were pipetted in duplicate into a clear 96-well plate, followed by the addition of 250 µL of Bradford reagent (#5000201EDU, Bio-Rad Laboratories, Inc; Hercules, CA, USA) into each well containing the ladder or samples of radiolabeled compound. After gentle mixing of the samples with the reagent, the plate was incubated at room temperature for 5-10 minutes in the dark. Absorbance was measured and analyzed with SoftMax Pro Software. A standard curve was generated using the known protein standard ladder, allowing for the calculation of protein concentration of radiolabeled samples. This also allowed for the calculation of the specific activity of the radiolabeled antibody (mCi/mg).

2.5.1.9. Dilution Plate Preparation

The dilution series was prepared at a 1:2 ratio, with 40 nM has the highest condition of Tc-99m radiolabeled antibody. Individual stock tubes were prepared per radiolabeled antibody with 40 nM as the highest concentration. 150 µL of radiolabeled antibody was pipetted into the top wells (four for each radiolabeled antibody) and 75 µL of media was pipetted in the rest of the bottom 7 wells. 75 µL of the radiolabeled antibodies were then pipetted and mixed with the media in the next well down the column, and this process was repeated down each well of the column to create the 1:2 dilution series.

2.5.1.10. Dilution Application

The original media from the cells in the 96-well plates was aspirated, and wells were washed with 200 µL 1X PBS twice. After washing, the blocked condition received 50 µL of unlabeled antibody stock that was prepared at 20x the highest concentration of the dilution series. Unblocked condition was given 50 µL of fresh media, and the plate was placed on a rocker 5% CO_2, 37 °C incubator for 15 minutes. After incubation, wells receive 50 µL of the dilution series of Tc-99m labeled antibody by directly transferring the dilution series into the wells of the plate with cells with a multichannel pipette. The plate was placed on a rocker 5% CO_2, 37 °C incubator for and allowed

to incubate for 1 hour. After incubation, all wells were aspirated, washed 2x with 250 µL PBS (1X), and then aspirated again. All wells were then given 100 µL of fresh media.

2.5.1.11. ATPlite Assay

Revvity Health Sciences Inc. ATPlite 1-step Luminescence Assay System, ATP Assay Kit was used to perform the ATPlite assay. All wells were given 50 µL of mammalian cell lysis solution, and the plate was shaken for 5 minutes at 700 rpm. Next, 50 µL of an ATPlite buffer and lyophilized substrate solution mixture was added to all wells, and the plate was shaken again for 5 minutes at 700 rpm. The 96-well plate was then dark-adapted for 10 minutes, and luminescence was measured with an IVIS Lumina LT Series III machine with Living Image Software 4.7.2 (PerkinElmer; Waltham, MA, USA). The results were later analyzed to determine cell number from a previously created standard curve that correlated photon flux (photon/sec) to the number of cells for each cell line in Microsoft Excel.

2.5.1.12. ATPlite Standards Curve Creation for Cell Count Estimates

For the ATP-lite standard curves for cell count estimates, cells were seeded into black, clear-bottom 96-well plates in a serial dilution format to establish luminescence readings correlating to specific cell counts for each canine bladder cancer cell line. Each row of the plate was seeded identically, beginning with 300,000 cells in column 1. Serial dilutions were performed at a 1:2 ratio across the plate, reducing the cell count by half for each subsequent column. The final column (column 8) contained approximately 2,344 cells per well. This standard curve allowed for the expression of luminescence values to be correlated with cell counts and provided a reference for binding experiments.

2.5.1.13. Measurement of Radioactivity with the gamma counter

After the ATPlite assay was complete, each well (containing 200 µL volumes) was collected into PCR vials with one individual vial dedicated for each well. Radioactivity for each well was measured by the gamma counter (CPM) for 30 seconds per sample, or until 10,000 total counts were recorded. Correction calculations for the decay of Tc-99m and conversions from CPM to mCi were done manually in Microsoft Excel. The absolute efficiency of the gamma counter was 1.42 x 10^6 CPM/µCi based on prior calibrations.

2.5.1.14. Analysis of Data

Recordings from the dose calibrator for the selected fraction and the Bradford protein value for the selected fraction were used to calculate the specific activity after the initial purification step.

ATPlite data was analyzed by standards for cell count and was converted into the total number of cells from the IVIS photon/sec values in Microsoft Excel via linear fit analysis. Triplicates for the different conditions were used to generate standard errors. GraphPad Prism (Dotmatics; Boston, MA, USA) was used to calculate specific binding values. Baseline analysis was carried out with the equation 'Specific Binding = Total Binding (unblocked triplicate condition) – Blocked (single replicate condition). Prism generates a specific binding value (Bmax) to be converted into the total number of receptors by multiplying the specific binding value (in nM) * Avogadro's ($6.023*10^{23}$). The calculated total number of receptors was then divided by the average number of cells per well that was quantified previously by Living Image Software from bioluminescence data, to obtain the number of total receptors (EGFR1 or EGFR2)/cell values. R^2 values were obtained by analyzing the baseline-corrected Specific Binding data to adjust Total and Non-Specific Binding values, followed by One-Site Specific Binding Non-Linear Fit analysis in GraphPad Prism. R^2 reflects the goodness of fit for the theoretical saturation curve, which was generated based on the Kd and Bmax values calculated by GraphPad Prism.

2.5.2. Flow Cytometry Experiments

2.5.2.1. Labeling Antibodies with IR680 Fluorochrome

2.5.2.1.1. Preparation of Antibodies for Labeling

Before labeling, antibodies cetuximab, trastuzumab, and IgG were buffer exchanged in PBS (1X) using two 30K MWCO spin concentrators (one for each antibody). The sample of antibody was placed into the reservoir of the concentrator with 2 mL of PBS and then spun at 3200 x g for 10-15 minutes and this step was repeated three times. Antibodies were also pH balanced using 1 M potassium phosphate (pH=9) until the pH reached 8.5-9 for labeling. Final protein concentrations after buffer exchange were measured on the Nanodrop instrument and antibodies were diluted so that each tube contained a final concentration of 1 mg/mL.

2.5.2.1.2. Labeling with IR680 Dye

Antibodies were labeled using an IRDye® 680D Protein Labeling Kit – High Molecular Weight (P/N: 928-38072; Li-Cor Bio; Lincoln, NE, USA). IR680 dye was removed from the freezer and allowed to warm to room temperature, then 25 µL of ultra-pure water was added, and the tube was vortexed until the dye was completely dissolved. The appropriate amount of dye required for the reaction was calculated based on the molecular weight of the antibody to be labeled. The appropriate amount of dye was added to two tubes each containing 1 mg/mL of the buffer

exchanged/ pH balanced cetuximab and trastuzumab. Tubes were gently mixed by inversion and placed in the dark at room temperature for two hours.

2.5.2.1.3. Removal of Unreacted Dye

Following the incubation period for the labeling reaction, free IR680 dye was separated from the protein conjugate using Zeba™ Spin Desalting Columns (5mL) (Thermo-Scientific; Waltham, MA, USA). Columns were equilibrated with 1X PBS and then centrifuged at 1,000 x g for 2 minutes to remove the storage solution. Next, 1 mL of PBS was added to the Zeba column, and it was centrifuged again at 1,000 x g for 2 minutes, and this step was repeated two more times. The entire volume of the dye-labeled antibodies that had been incubating was purified with the Zeba column to remove unbound IR680 dye by pipetting the entire sample into the column and spinning at 1,000 x g for 2 minutes. The final product was collected into fresh 10 mL tubes.

2.5.2.1.4. Verification of Dye-to-Protein Ratio

To determine the final dye-to-protein (D/P) ratio of the IR680-cetuximab and IR680-trastuzumab, samples were measured using the UV-Vis setting on the NanoDrop. First, the NanoDrop was set to measure at 280 nm and 672 nm and 2 µL samples were placed on the reader and the concentration of dye-conjugated antibodies was recorded. The formula D/P = A672/A280 – (0.04 x A672) was used to calculate the dye-to-protein ratio in Excel. Protein concentration of the conjugate was calculated with the formula: (Protein Concentration (mg) = (A672/A280 – (0.04 x A672)) x (molecular weight of the protein/ molar extinction coefficient of the protein) x Dilution Factor). Dye-conjugated cetuximab and trastuzumab were kept at 4 °C until use.

2.5.2.2. Titration Experiments

2.5.2.2.1. Cell Preparation for Flow Cytometry

Two cell lines were prepared for titration experiments, a canine cell line that was found to be positive for both EGFR1 and EGFR2 from the binding experiments (Nk), and a cell line negative for both receptors (3T3). Cells were dissociated using Gibco™ Versene Solution (Thermo-Scientific; Waltham, MA, USA) for gentle lifting from flasks. Once dissociated, cells were transferred into 15 mL centrifuge tubes and centrifuged at 300 x g for 5 minutes to pellet cells, then the supernatant was carefully aspirated, and cells were washed with 1 mL of ice-cold PBS to remove residual dissociation reagent. After washing, the cell suspension was centrifuged again at 300 x g for 5 minutes, and the supernatant was aspirated completely. Cell concentration was determined using a cell counter, and cells were resuspended in a wash buffer (1x DPBS-no Ca/Mg,

5% FBS or 1% BSA) to a final concentration ranging from 100,000 to 1,000,000 cells per well, depending on the number of cells available on the day of the experiment. Cells were then pipetted into a clear 96-well v-bottom plate, in 100 µL of cold wash buffer per well.

2.5.2.2.2. Live/Dead Blue Staining

To assess cell viability, 0.5 µL of diluted Live/Dead™ Blue viability dye (Thermo-Scientific; Waltham, MA, USA) was added to each designated well, and the plate was incubated on ice for 30 minutes, protected from light. Live/Dead Blue was given to each designated well at a concentration of 0.5 µM/1 million cells and was diluted when necessary for experiments were the number of cells was less than 1 million. A control population was stained with Live/Dead Blue only, while additional conditions combined Live/Dead Blue with varying concentrations of Cetuximab-IR680 to evaluate the effect of antibody binding and viability. After incubation, cells were washed once with 150 µL of cold wash buffer to remove excess dye.

2.5.2.2.3. Apo Tracker Green Staining

To detect apoptotic cells, 400 nM of Apotracker™ Green (also known as Apo-15 peptide) (BioLegend®; 8999 BioLegend Way, San Diego, CA, USA) was added to each designated well following Live/Dead Blue staining in the same designated wells as the Live/Dead Blue. The plate was incubated on ice in the dark for 20 minutes. After incubation, cells were washed once with 150 µL of cold wash buffer to remove excess/unbound dye.

2.5.2.2.4. Fc Blocking

Following the viability stain, Fc receptors were blocked an Fc blocking reagent to account for nonspecific antibody binding. A predetermined volume of Fc block (0.25 µg per 1 million cells) was added to each well before the dye-conjugated antibodies, and the plate was incubated on ice for 10 minutes.

2.5.2.2.5. Antibody Staining and Titration

Labeled antibodies were prepared as a series of titrations (10 µg, 5 µg, 2.5 µg, and 1.25 µg) to optimize staining conditions. The appropriate volume (based on the concentration of the dye antibody stocks) of each antibody concentration was added to designated wells, and the plate was incubated on a rocker, rocking gently, at 4°C for 30 minutes to allow for efficient antibody binding.

2.5.2.2.6. Fixation and Washing

After staining, the plate was centrifuged at 400 x g for 5 minutes at 4°C to pellet cells, and the supernatant was discarded. Cells were fixed by adding 100 µL of 1% paraformaldehyde to each

well, followed by incubation at room temperature for 15 minutes. After fixation, cells were washed with 200 μL of ice-cold PBS to remove residual 1% paraformaldehyde. The plate was centrifuged again at 400 x g for 5 minutes at 4°C, and the supernatant was discarded.

2.5.2.2.7. Final Preparation for Data Collection

To prepare for the cytometer, cells were resuspended in 300 μL of ice-cold PBS per well. The cell suspensions were then filtered into a new u-bottom plates using a plate filter to ensure single-cell suspensions free from clumps or debris. Plates were kept at 4°C and protected from light before being brought to the Cytometer.

2.5.2.2.8. Data Analysis with FCS Express

FCS Express software (DeNovo Software by Dotmatics; Louisville, CO, USA) was used to analyze data collected by the Aurora Cytometer. Gating of populations of cells was done using a stepwise method for accurate identification of the target receptors. Single stained controls were used to correct for spectral overlap between fluorophores, and fluorescent minus one (FMO) condition were used to define gating and help distinguish positive from negative populations of cells. An unstained control was included to assess baseline autofluorescence signals. A time vs. side scatter-height (SSC-H) plot was used to standardize the signal over time. A forward scatter-area (FSC-A) vs. SSC area (SSC-A) was used to identify live cells. An FSC-A vs. FSC height (FSC-H) plot was used to identify and exclude doublets and aggregate cells. FMOs and single-stained controls were used to perform fluorescence-based gating and to specify populations of cells based on marker expression. Stain Index (SI) was calculated in Excel with the equation: (Median fluorescence intensity (MFI) of the positively stained population – MFI of the negatively stained control) / 2 x SD of the negative stained control. The titration with the highest SI were selected for future experiments.

2.5.2.3. Expression Experiments

2.5.2.3.1. Cell Preparation for Flow Cytometry

Canine bladder cancer cell lines were lifted using diluted TripLE for 5-10 minutes. Once dissociated, cells were transferred into three different 15 mL centrifuge tubes – one for each cell line - and centrifuged at 300 x g for 5 minutes to pellet cells. The supernatant was carefully aspirated, cells were washed with 1 mL of cold PBS to remove residual TripLE. After washing, the cell suspensions were centrifuged again at 300 x g for 5 minutes, and the supernatant was aspirated completely. Cell concentration was determined using the cell counter, and cells were

resuspended in a wash buffer (1x DPBS-no Ca/Mg, 5% FBS, 1% BSA) to a final concentration ranging from 100,000 to 500,000 cells per well (depending on the number of cells available on the day of the experiment). Cells were then pipetted into a clear 96-well v-bottom plate, in 100 µL of cold wash buffer per well.

2.5.2.3.2. *Live/Dead Blue Staining*

This step follows the same protocol as described in section 2.5.2.2.2.

2.5.2.3.3. *Apo Tracker Green Staining*

This step follows the same protocol as described in section 2.5.2.2.3.

2.5.2.3.4. *Fc Blocking*

This step follows the same protocol as described section 2.5.2.2.4.

2.5.2.3.5. *Antibody Staining*

This step follows the same protocol as described in section 2.5.2.3.5.

2.5.2.3.6. *Fixation and Washing*

This step follows the same protocol as described in section 2.5.2.2.6.

2.5.2.3.7. *Final Preparation for Data Collection*

This step follows the same protocol as described in section 2.5.2.2.7.

2.5.2.3.8. *Data Analysis with FCS Express*

FCS Express software was used to analyze data collected from the Aurora Cytometer. Gating of populations of cells using a stepwise method for accurate identification of the target receptors and to minimize background and spectral inaccuracies. Single stained controls and FMOs were both used as compensations and controls and for defining gates. A Time vs. SSC-H plot was used to exclude acquisition artifacts, an FSC-A vs. FSC-H plot ensured single-cell gating. Live/Dead Blue viability staining was used to compare exclude the non-viable population from final receptor analysis. Apo-tracker staining was used to exclude apoptotic cells from final analysis. Differences in receptor level expression across canine bladder cancer cell lines were to be determined by gating out populations of cells positive for the IR680-antibody and the percent of positively fluorescent population was going to be compared with a negative population and these percentages were going to be compared across canine cell lines for receptors of interest.

2.5.3. *Lu-177 Clonogenic Assays*

2.5.3.1. *Antibody Control Clonogenic Experiments*

2.5.3.1.1. *Seeding Cells*

Each canine bladder cancer cell line selected (AxA, Sh, and Nk) for the control clonogenic experiments was seeded in 6-well clear plates on the afternoon before the experiment. For the antibody control experiments cells received cetuximab + trastuzumab combined with all concentrations applied in triplicate. About 2-3 hours before cell seeding, 1 mL of media only was pipetted into all wells, and plates were put back into the incubator to allow the media to warm before the addition of cells. Antibody treatment was prepared as 8 serial dilutions (1:2) with 2 mg/100 mL (137 nM) as the highest concentration of each antibody, and the lowest concentration as 0 mg/mL (0 nM). This top concentration was based on the concentration of the drug proposed for the canine clinical trials. Cells were seeded in triplicate for all conditions, at 200 cells/well in 1 mL of their respective media, and added to the 1 mL of media already in the wells. After seeding, plates were removed from the biosafety cabinet and shaken up and down 5x, and side to side 5x on a flat, stable surface (lab bench) to promote equal seeding of cells in each well. Plates were then left to sit on the lab bench for 5 minutes to settle and placed into the incubator overnight.

2.5.3.1.2. *Preparation of Antibodies (Concentration)*

Antibodies were prepared using 30K MWCO spin protein concentrator. Trastuzumab is received in powder form, and tubes containing 0.5-2 mg were weighed and resuspended in 1 mL PBS (1X) and vortexed. Cetuximab and IgG are received in liquid form, and concentration labels from the source vials were used to determine the initial amount of antibody about to be concentrated based on the volume. All antibodies were concentrated by adding the entire volume of an antibody into the bottom of the reservoir of the spin concentrator topped by an additional 1 mL PBS (1X) for the first spin. Antibodies were centrifuged at 3200 x g, for 9-12 minutes, or until the final volume in the reservoir was ~200 μL. After the first spin, the flow through was discarded, and 2 mL more of 1X PBS was dispensed into the sample reservoir and spun again two more times. After the final spin, concentrated antibodies were transferred into fresh, labeled tubes. The volume of the final product was estimated by pipetting, and concentration was measured with the Nanodrop and recorded.

2.5.3.1.3. Antibody Filtration for Sterilization

Antibodies were sterilized using a Whatman Puradisc 4mm PVDF syringe filter (0.2 μM; Tisch, North Bend, OH, USA). Before filtering the antibody, 500 μL of sterile PBS (1X) was slowly passed through the filter using a 12-gauge BD PrecisionGlide™ needle (#305125, regular bevel, 1- 1/2 inch, blue; Vitality Medical; Salt Lake City, UT, USA) attached to a 3 mL syringe (#309657, leur lock tip; Vitality Medical; Salt Lake City, UT, USA) to pre-wet the membrane of the filter. Antibodies were sterilized by drawing up the entire volume of the concentrated antibody and passing it through the syringe into a new sterile 1.5 mL tube labeled with the name of the antibody being filtered. Once filtered, a sample (4 μL) of the sterilized antibody was pipetted into a separate tube to be transported to the Nanodrop for concentration measurement, and to determine any loss of antibody to the filter membrane. Concentrations and volumes (estimated by pipetting) after filtration were measured and recorded. The final product was stored in a 1.5 mL tube, and parafilm was wrapped around the opening of the tube. Filtered, sterilized antibodies were stored at 4°C until dilution plate preparation.

2.5.3.1.4. Dilution Plate Preparation for Unlabeled Control Experiments

Dilution series of unlabeled antibody were prepared in 96-well plates, as a 1:2 serial dilution with 7 concentrations with 0.02 mg/mL as the highest concentration of antibody, and a condition with 0 mg/mL (media only) as a control. All unlabeled antibody dilution series were prepared as a combination of cetuximab + trastuzumab. Stock solutions for the highest concentration of antibody were calculated and prepared based on the Nanodrop recording after PVDF filtration. The dilution series was prepared by transferring 75 μL of the cetuximab stock solution and 75 μL of the trastuzumab stock solution for a combined total of 150 μL of the stock solution into the top wells of the 96-well plate, and 75 μL of media into the lower wells. To achieve a 1:2 dilution 75 μL was transferred from the top well to the next lower well and mixed thoroughly in the media, and this step was repeated until the second to lowest well (7^{th} dilution). The dilution of antibodies was not applied to the lowest wells, and they contained 75 μL of media only.

2.5.3.1.5. Dilution Plate to Cell Addition

The 6-well plates containing cells were removed from the incubator and 50 μL of the dilution series (in the 96-well plate) was transferred to the wells with cells, with triplicate wells for each concentration. Negative control wells with no antibodies received 50 μL of media only. Wells were

labeled according to the concentration of antibody being added. Plates were moved in a Figure 8 motion to distribute the antibody equally in the wells and then placed back into the incubator for one hour. After one hour of incubation, plates were removed from the incubator, wells were washed 2x with sterile PBS (1X), and all wells were replenished with 2 mL of fresh media before being placed into the incubator.

2.5.3.1.6. Incubation Post-Treatment

Plates were allowed to incubate for around a week, depending on the cell line. Every day, the growth of the cells in all wells was observed with an Olympus Inverted Phase Contrast Microscope (SKU: CKX53-BSC; Evident Scientific Inc., Waltham. MA, USA) until it appeared that there were clusters of 50 or more cells, or colonies.

2.5.3.1.7. Fixing and Staining

After about a week, or until it appeared that there were clusters of 50 or more cells in the wells, plates were removed from the incubator and all media was gently aspirated. All wells were washed 2x with PBS (1X) and then fixed with 1 mL of 10% formalin for 20 minutes. Colonies of cells were stained by adding 1-2 mL of a solution of 0.5% crystal violet in PBS (1X) for 30 minutes. After staining, the 10% formalin with the 0.5% crystal violet was removed from the wells followed by washing with MilliQ water. Wells were rinsed with MilliQ water 3 times, or until it appeared that residual stain was removed. Plates were left to dry open faced, over an absorbent surface overnight at room temperature.

2.5.3.1.8. ChemiDoc™ Imaging

Stained cells were imaged using a ChemiDoc™ MP Imaging System (Bio-Rad Laboratories; Hercules, CA, USA). Before imaging, a White Sample Tray for the ChemiDoc™ (Bio-Rad Laboratories; Hercules, CA, USA) was installed on the imaging stage of the transillumator drawer. Plates were placed face up in the center of the White Sample Tray, and the transillumator drawer and door were closed. The 'Application' and 'Application Category' used to capture images were 'Protein Gels' and 'Coomassie Blue,' respectively. The ChemiDoc™ was kept to the default exposure option. Images were then acquired and downloaded for further processing in ImageJ.

2.5.3.1.9. ImageJ Analysis

ChemiDoc™ images were processed using Fiji, an extension of ImageJ software (https://imagej.net/software/fiji/) (119). Image files were opened in ImageJ, and Image Type was changed to 'RGB Color.' Next, the color threshold was adjusted by selecting the thresholding

method chosen for the respective cell line being analyzed. The oval tool was used to carefully draw around the well. 'Analyze Particles' was selected next, and the size (pixel^2) was changed to '5-infinity' before selecting 'OK.' Output from the analysis includes a summary data table with recordings for Slice, Count, Total Area, Average Size, % Area, and Mean. ImageJ analysis was performed individually for each well. All summary data was recorded in Microsoft Excel to be converted to .csv files for analysis in RStudio.

2.5.3.1.10. RStudio Statistical Analysis

Assumptions of normality of residuals and homogeneity of variances were tested before performing linear regression analysis. A Shapiro-Wilk test was performed for all concentrations of antibodies with an online calculator (https://www.statskingdom.com/shapiro-wilk-test-calculator.html) and variances were tested with Bartlett's test in RStudio at the 5% significance level. Triplicates were used to generate standard error values. Significance was measured with Linear Regression analysis in RStudio. If data was nonparametric, transformation either by log or square root were done to satisfy parametric assumptions necessary for linear regression analysis.

2.5.3.2. Antibody Control Study Across Three Time Points

2.5.3.2.1. Cell Seeding

The AxA cell line selected to match the Lu-177 conditions for the radiation experiment that was assessed across three different time points (1 hour, 12 hours, and 24 hours). About 2-3 hours before seeding cells, 1 mL of media was pipetted into six 6-well plates, two for each time point, and placed into the incubator to warm over time. For each time point, one 6-well plate served as a no treatment control, and for the second 6-well plate, the top three wells received 68.5 nM of cetuximab + trastuzumab, and the bottom three wells received IgG. AxA cells were seeded at 200 cells/well in 1 mL of their respective media, and added to the 1 mL of media already present in the wells. After seeding, plates were removed from the biosafety cabinet and shaken up and down 5x, and side to side 5x to ensure equal seeding of cells in the well. After shaking the plates, they were left to sit on a flat surface (a lab bench) for 5 minutes to settle, then placed into the incubator overnight.

2.5.3.2.2. Preparation of Antibodies (Concentration)

Antibodies cetuximab, trastuzumab, and IgG were prepared following the same protocol from section 2.5.3.1.2.

2.5.3.2.3. Antibody Filtration for Sterilization

Antibodies were sterile filtered following the same protocol from section 2.5.3.1.3.

2.5.3.2.4. Antibody to Cell Addition

Sterilized cetuximab, trastuzumab and IgG were diluted with media into separate 1.5 mL tubes at 68.6 nM, accounting for the dilution factor for once the antibody is added to the 2 mL of media already present in the wells with cells. Experimental condition IgG received 50 μL of the IgG stock, and the cetuximab + trastuzumab condition received 25 μL + 25 μL of each respective antibody. No-treatment control wells received 50 μL of fresh media only. Plates with cells were then placed back into the incubator. After each incubation time point (1 hour, 12 hours, and 24 hours), designated plates (two plates for each time-point) were removed from the incubators, washed once with 1X PBS, and wells were replenished with fresh media before being placed back into the incubator.

2.5.3.2.5. Incubation Post-Treatment

Cells were incubated following the same protocol as stated in section 2.5.3.1.6.

2.5.3.2.6. Fixing and Staining

This step follows the same protocol as described in the antibody control section 2.5.3.1.7.

2.5.3.2.7. ChemiDoc™ Imaging

This step follows the same protocol as described in the antibody control section 2.5.3.1.8.

2.5.3.2.8. ImageJ Analysis

This step follows the same protocol as described in the antibody control section 2.5.3.1.9.

2.5.3.2.9. RStudio Analysis

Assumptions of normality of residuals and homogeneity of variances were tested before performing linear regression analysis. A Shapiro-Wilk test was performed for all concentrations of antibodies with an online calculator (https://www.statskingdom.com/shapiro-wilk-test-calculator.html) and variances were tested with Bartlett's test in RStudio both at the 5% significance level. Triplicates were used to generate standard error values and means. Significance was measured with either Kruskal-Wallis and Dunn's test for each time point in RStudio.

2.5.3.3. Cisplatin Control Clonogenic Experiments

2.5.3.3.1. Cell Seeding

The cell lines selected for the control clonogenic experiments were AxA, Sh, and Nk as they were the cell lines chosen for the Lu-177 experimental clonogenic experiments and were seeded in 6-

well plates on the afternoon before the experiment. Cisplatin control experiments served as a positive control for inhibiting cell growth, with the highest dilution of cisplatin at 100 μM (120,121). About 2-3 hours before cell seeding, 1 mL of media only was pipetted into all wells, and plates were put back into the incubator to allow the media to warm before the addition of cells. Cisplatin treatment was prepared as 7 serial dilutions (1:2) with 100 μM as the highest concentration, and a no treatment control. This concentration was based on existing literature (122). Cells were seeded in triplicate for all conditions, at 200 cells/well in 1 mL of their respective media, added to the 1 mL of media already in the wells. After seeding, plates were removed from the biosafety cabinet and shaken up and down 5x, and side to side 5x to ensure equal seeding of cells in the well. After shaking the plates, they were left to sit on a flat surface (a lab bench) for 5 minutes to settle, then placed into the incubator overnight.

2.5.3.3.2. *Cisplatin Preparation*

Cisplatin was received from MedChemExpress® (Monmouth Junction, NJ, USA) and was resuspended with DMF for use *in vitro.* To prepare the stock solution, 3.33 mL of DMF was added to the tube containing Cisplatin to resuspend it to a final concentration of 10 mM. The tube was warmed to 60°C and mixed by sonication for 5 minutes. Once mixed, the stock vial was aliquoted at smaller volumes in cryovials to prevent multiple freeze-thaw cycles and vials were stored at -80°C for up to 6 months.

2.5.3.3.3. *Dilution Plate Preparation with Cisplatin*

Dilution series of Cisplatin were prepared in 96-well plates, as a 1:2 serial dilution with 7 concentrations and 100 μM as the highest concentration, and a condition with 0 μM as a control. Stock solutions for the highest concentration of Cisplatin were calculated and prepared based on the 10 μM resuspension of the original cisplatin stock vial with 3.33 mL DMF and accounted for the dilution factor. The dilution series was prepared by transferring 150 μL of the 100 μM Cisplatin solution into the top wells of the 96-well plate, and 75 μL of fresh media into the lower wells. To achieve a 1:2 dilution 75 μL was transferred from the top well with Cisplatin to the next lower well and mixed thoroughly in the media, and this step was repeated until the second to lowest well (7^{th} dilution). The dilution of Cisplatin was not applied to the lowest wells, and they contained 75 μL of media only.

2.5.3.3.4. Dilution Plate to Cell Addition

This step follows the same protocol as described in the antibody control section 2.5.3.1.5.

2.5.3.3.5. Incubation Post-Treatment

This step follows the same protocol as described in the antibody control section 2.5.3.1.6.

2.5.3.3.6. Fixing and Staining

This step follows the same protocol as described in the antibody control section 2.5.3.1.7.

2.5.3.3.7. ChemiDoc™ Imaging

This step follows the same protocol as described in the antibody control section 2.5.3.1.8.

2.5.3.3.8. ImageJ Analysis

This step follows the same protocol as described in the antibody control section 2.5.3.1.9.

2.5.3.3.9. RStudio Analysis

This step follows the same protocol as described in the antibody control section 2.5.3.1.10.

2.5.3.4. Initial Lu-177 Clonogenic Experiment

2.5.3.4.1. Cell Seeding

For the first Lu-177 Clonogenic experiment, canine bladder cancer cell lines positive for expression of both EGFR1 and EGFR2 were selected. For each cell line, three antibodies were radiolabeled with the isotope: cetuximab + trastuzumab together, IgG, and another condition serving as a no-treatment control. All treatments for the first experiments included triplicates of 200 cells/well with two different concentrations of radiolabeled antibodies.

2.5.3.4.2. Concentration of Antibodies

Antibodies were concentrated and measured using the same method as described in section 2.5.3.1.2.

2.5.3.4.3. Metal-Free Reagent Preparation

All reagents used for Lu-177 radiolabeling were prepared using metal-free water (MFW). MFW was prepared by adding 1-2 g of Chelex-100 resin (Bio-Rad Laboratories; Hercules, CA, USA) to 500 mL of MilliQ water in a 500 mL glass bottle and stored at 4°C overnight. The next day, resin beads were removed from the water with a 0.2 μm disposable filter unit (Nylon; Thermo-Scientific; Waltham, MA, USA). Reagents were additionally filtered with Chelex-100 resin-packed disposable 10 mL polypropylene columns (Thermo-Scientific; Waltham, MA, USA). Before the reagents were filtered through the column, 1-2 mL of 1 M HCl was added and allowed to sit on the resin for 5 minutes. After this waiting period, 10-20 mL MFW was used to wash the HCl out

and flowed through the column until there was no more dripping. Reagents were then poured into the top of the column and allowed to pass through the resin. All Chelex-100 purified reagents were purified in individual columns and dripped into new, fresh tubes.

2.5.3.4.4. Stock Antibody pH Adjustment for p-SCN-Bn-DOTA Conjugation

Antibodies were pH-balanced before conjugation with the p-SCN-Bn-DOTA chelator. Approximately 500 μg of antibody that had previously been concentrated in PBS (1X) was maintained to a pH of 8.5-9 using carbonate buffer (0.1M NaHCO3 and 5mM Na2CO3; Chelex-100 purified) 10 μL at a time, until the desired pH was achieved. pH was measured using MQuant™ pH test strips (pH 2.0-9.0; Millipore Sigma, Burlington, MA, USA).

2.5.3.4.5. p-SCN-Bn-DOTA Conjugation

Pre-prepared lyophilized p-SCN-Bn-DOTA kits (prepared for conjugating 1 mg of antibody) were retrieved from storage at -20°C in a freezer and allowed to warm to room temperature. Kits were resuspended with 500 μL of DMSO and mixed by sonication for 5 minutes. Resuspended p-SCN-Bn-DOTA was added to 1.5 mL tubes with 200 μg pH-balanced cetuximab and trastuzumab at a 2:1 molar excess ratio (chelator: antibody). IgG was conjugated at 400 μg, a concentration two times higher than cetuximab and trastuzumab. Tubes were then allowed to incubate at 37°C while shaking at 500 rpm for 4 hours, covered with aluminum foil to protect the reaction from light.

2.5.3.4.6. Removal of Unconjugated for p-SCN-Bn-DOTA Chelator

Unconjugated p-SCN-Bn-DOTA was removed from the conjugated antibodies by exchanging the buffer to 0.15 M NH4OAc buffer (pH=7) with Pierce™ Protein Concentrators (30K MWCO), first by transferring the entire volume of conjugated antibody into the reservoir of the concentrator. Next, 2 mL of 0.15 M NH4OAc buffer (pH=7) was pipetted into the reservoir of the spin concentrator and concentrators were subsequently centrifuged at 3200 x g for 9-10 minutes. After spinning, this step was repeated two more times, with an additional 2 mL of 0.15 M NH4OAc added to the sample reservoir each time. The concentration of buffer-exchanged DOTA-antibodies was measured with the Nanodrop and recorded. Final stocks were immediately utilized for radiolabeling.

2.5.3.4.7. Enhancing Radiochemical Purity and pH Maintenance of Lu-177

Two aliquots of 4-5 mCi were taken from a stock vial containing Lu-177 and dispensed into two 1.5 mL tubes, one labeled for DOTA-cetuximab + DOTA-trastuzumab combined, and the other for the p-SCN-Bn-DOTA-IgG control. The volume of the aliquot retrieved from the source vial was

recorded. The activity of the aliquots was measured using a dose calibrator (set to 450*10 for Lu-177) and the time of measurement were recorded. To enhance the stability and radiochemical purity of Lu-177, 50 μL of 35 mM Ascorbic acid and 35 mM Gentisic acid solution were pipetted into both tubes. Lu-177 pH was maintained at 4.5 by adding 100 μL 0.2 M Ammonium acetate (pH 4.5).

2.5.3.4.8. Radiolabeling of Antibodies

The entirety of the conjugated DOTA-cetuximab + DOTA-trastuzumab was added to one of the tubes containing the maintained Lu-177, and DOTA-IgG isotype control was added to the other. Tubes were incubated on an Eppendorf heating block (M#5384; Marshall Scientific, Hampton, NH, USA) at 37°C shaking at 500 rpm. Radiochemical yield was checked every 30 minutes during incubation by iTLC using 10 mM EDTA in 0.15 M NH4OAc as a mobile phase. Once 70-90% radiochemical yield was achieved (after about 2-3 hours of incubation), radiolabeled DOTA-antibodies were removed from the heating block for purification.

2.5.3.4.9. Purification of Radiolabeled Antibodies

During the radiolabeling period, two 10 mL disposable polypropylene columns were packed with G-25 Sephadex resin swelled in PBS (1X), one for radiolabeled cetuximab + trastuzumab and the other for radiolabeled IgG and allowed to equilibrate. Purification was performed by adding the total volume of radiolabeled antibodies, with an additional 1 mL of PBS (1X), and collecting 1 mL fractions in 2 mL tubes. Each time a fraction was collected, an additional 1mL of PBS was added to the column for the next fractions. Approximately 8 vials were collected until an initial protein-activity peak and the second, later peak of free Lu-177 were measured. Each fraction's activity was measured using the dose calibrator (set to 450*10) and recorded. The fractions containing the highest level of activity were selected for further analysis with iTLC and Bradford Assay.

2.5.3.4.10. iTLC (instant Thin Layer Chromatography)

The final purity of the radiolabeled Lu-177-DOTA-Ab fraction was determined by iTLC with 10 mM EDTA in 0.15 M NH_4OAc as a mobile phase. Approximately 400 μL of mobile phase was dispensed into two 10 mL microcentrifuge tubes, and tubes were labeled with their respective radiolabeled antibody. A sample of 2 μL of Lu-177-DOTA-Ab from the selected fraction was placed on the bottom of a strip cut from iTLC-SG-Glass microfiber chromatography paper impregnated with silica gel, and strips were placed into the 10 mL tubes with the sample located slightly above the height of the solvent. Once the solvent front appeared to be at the top of the

strip, strips were cut into halves, and pieces were put into 2 mL tubes to be measured on the gamma counter for quantification of purity. Purity was calculated with the equation [(bottom/(top+bottom)]/100%, and results above 80% were considered acceptable for the first cell experiments.

2.5.3.4.11. Bradford Protein Assay

Fractions of Lu-177-DOTA-Ab with >80% purity protein concentration was measured with Bradford Protein Concentration Assays. A Bradford standard was prepared with 7 dilutions with the highest concentration as 500 µg (1:2 ratio) and a 0 mg/mL concentration and 5 µL was pipetted in duplicate down the column of a clear 96-well plate. Samples of 5 µl for both the Lu-177-DOTA-cetuximab + Lu-177-DOTA-trastuzumab and the Lu-177-DOTA-IgG control were also added to the plate containing the duplicate standard ladder. Absorbance was measured and analyzed with SoftMax Pro Software and the linear equation generated by the standard ladder was used to determine the concentration of the samples. Concentrations calculated from the Bradford Protein Assay were used to calculate the specific activity of Lu-177-DOTA-Abs (mCi/mg).

2.5.3.4.12. Sterilization of Radiolabeled Antibodies

Lu-177-DOTA-Abs were sterilized before being applied to cells with 4 mm PVDF membrane syringe filters (0.2 µm) to prevent microbial contamination and maintain aseptic cell culture conditions. All syringe filters were pre-rinsed with 500 µL of PBS to saturate the membrane and minimize loss of sample during filtration. Lu-177-DOTA-Abs were collected into a 3 mL leur lock syringe with 12-gauge BD PrecisionGlide™ needle, and the needle was exchanged with the pre-rinsed filter after the entire volume of sample was collected. Lu-177-DOTA-Abs were subsequently dispensed into new sterile 1.5 mL tubes.

2.5.3.4.13. Post-Sterilization iTLC and Bradford Assays

The methods previously described in Sections 2.5.3.3.10 and 2.5.3.3.11 were used to determine the final purity and concentration of the sterilized Lu-177-DOTA-Abs after filtration.

2.5.3.4.14. Treatment Stock Preparation and Transfer to Clonogenic Assay

Two target molar concentrations were decided for both the cetuximab + trastuzumab and the IgG isotype control conditions before radiolabeling: a high concentration of around 10 nM, and a low concentration of around 2 nM. For each condition, two treatment stock tubes were prepared with sufficient volume to dispense 50 µL into all wells receiving treatment, with additional volume to account for potential pipetting error. Sterile Lu-177-DOTA-Abs were diluted with media in new 2

mL tubes dedicated for treatment stock preparation to achieve the desired target molar concentrations, and tubes were vortexed to ensure homogeneity of the mixture. The 6-well plates with cells were taken from the incubator, and 50 μL from the stock tubes was applied to the wells in triplicate, and the nM concentration of Lu-177-DOTA-cetuximab + Lu-177-DOTA-trastuzumab and Lu-177-DOTA-IgG added to the wells were labeled on the plates. No treatment control wells received 50 μL of media only. All plates were gently shaken to ensure even distribution of Lu-177-DOTA-Abs covered the wells.

2.5.3.4.15. Incubation and Washing

Plates were returned to the incubator for one hour. Following this incubation period, the media was removed from wells, which were then washed twice with 2 mL of PBS (1X) to mimic urination conditions and to wash away any Lu-177-DOTA-Ab that did not bind to cells during the incubation period. All wells then received 2 mL of fresh media after washing. After media replacement, plates were allowed to incubate for one week.

2.5.3.4.16. Fixing and Staining

This step follows the same protocol as described in the antibody control section 2.5.3.1.7.

2.5.3.4.17. ChemiDoc™ Imaging

This step follows the same protocol as described in the antibody control section 2.5.3.1.8.

2.5.3.4.18. ImageJ Analysis

This step follows the same protocol as described in the antibody control section 2.5.3.1.9.

2.5.3.4.19. RStudio Analysis

Assumptions of normality of residuals and homogeneity of variances were tested before performing ANOVA. A Shapiro-Wilk test was performed for all triplicate concentrations with an online calculator (https://www.statskingdom.com/shapiro-wilk-test-calculator.html) and variances were tested with Bartlett's test in RStudio. Triplicates were used to generate standard error values and means. Significance was measured with ANOVA in RStudio, and Tukey's HSD was performed as a post-hoc test. All statistical analyses were performed at the 5% significance level.

2.5.3.5. Further Lu-177 Clonogenic Experiments

An additional Lu-177 Clonogenic Experiments was performed with adjustments to the experimental design and more optimized radiolabeling protocol.

2.5.3.5.1. Cell Seeding

For the next Lu-177 Clonogenic study, one canine bladder cancer cell line positive for expression of both EGFR1 and EGFR2 was selected (AxA). Antibodies were radiolabeled with the isotope, cetuximab + trastuzumab together, IgG, and a no-treatment control without any radiolabeled antibody. All treatments included triplicates of 200 cells/well with one concentration targeted to be 137 nM of radiolabeled antibodies. For these experiments, cells were seeded for three different washing time points, with two 6-well plates seeded for each time point (1 hour, 12 hours, and 24 hours), two plates for each time point – one for each of the radiolabeled antibody conditions (cetuximab + trastuzumab, and IgG) and the second plate served as the no treatment control for both conditions.

2.5.3.5.2. Concentration of Antibodies

This step follows the same protocol as described in the antibody control section 2.5.3.1.2.

2.5.3.5.3. Metal-Free Reagent Preparation

This step follows the same protocol as described in the antibody control section 2.5.3.3.3.

2.5.3.5.4. Antibody pH Adjustment for p-SCN-Bn-DOTA Conjugation

Antibodies were pH-balanced before conjugation with the p-SCN-Bn-DOTA chelator. Approximately 800 μg of both cetuximab and trastuzumab, and 1.6 mg of IgG that were previously concentrated in PBS (1X) was maintained to a pH of 8.5-9 using carbonate buffer (0.1 M NaHCO3 and 5 mM Na2CO3; Chelex-100 purified) 20 μL at a time, until desired pH was achieved. pH was measured using MQuant™ pH test strips (pH 2.0-9.0).

2.5.3.5.5. p-SCN-DOTA Conjugation

Pre-prepared lyophilized p-SCN-Bn-DOTA kits (prepared for conjugating 1 mg of antibody) were retrieved from storage at -20°C in a freezer and allowed to warm to room temperature. Kits were resuspended with 1 mL of DMSO and mixed by sonication for 5 minutes. Resuspended p-SCN-Bn-DOTA was added to 1.5 mL tubes with 800 μg pH-balanced cetuximab and trastuzumab at a 2:1 molar excess ratio (chelator: antibody). IgG was conjugated at 1600 μg, a concentration two times higher than cetuximab and trastuzumab. Tubes were then allowed to incubate at 37°C while shaking at 500 rpm for 4 hours, covered with aluminum foil to protect the reaction from light.

2.5.3.5.6. Removal of Unconjugated p-SCN-Bn-DOTA

Unconjugated p-SCN-Bn-DOTA was removed from the conjugated antibodies by exchanging the buffer to 0.15 M NH4OAc buffer (pH=7) with Pierce™ Protein Concentrators (10K MWCO), first

by transferring the entire volume of conjugated antibody into the reservoir of the concentrator. Next, 2 mL of 0.15 M NH4OAc buffer (pH=7) was pipetted into the reservoir of the spin concentrator and concentrators were subsequently centrifuged at 500 x g for 10-15 minutes. After spinning, this step was repeated two more times, with an additional 2 mL of 0.15 M NH4OAc added to the sample reservoir each time. The concentration of buffer-exchanged DOTA-antibodies was measured with the Nanodrop and recorded. Final stocks were immediately utilized for radiolabeling.

2.5.3.5.7. *Enhancing Radiochemical Purity and pH Maintenance of Lu-177*

Two aliquots of approximately 10 mCi were taken from a stock vial containing Lu-177 and dispensed into two 1.5 mL tubes, one labeled for DOTA-cetuximab + DOTA-trastuzumab combined, and 20 mCi was dispensed into a third 1.5 mL tube for the DOTA-IgG control. The volume of the aliquot retrieved from the source vial was recorded. The activity of the aliquots was measured using a dose calibrator (set to 450*10 for Lu-177) and the time of measurement was recorded. To enhance the stability and radiochemical purity of Lu-177, 100 μL of 35 mM Ascorbic acid and 35 mM Gentisic acid solution were pipetted into both tubes. Lu-177 pH was maintained at 4.5 by adding 200 μL 0.2 M Ammonium acetate (pH 4.5) to both tubes.

2.5.3.5.8. *Radiolabeling of Antibodies*

The entirety of the conjugated DOTA-cetuximab + DOTA-trastuzumab was added to one of the tubes containing the maintained Lu-177, and DOTA-IgG Ab control was added to the other. Tubes were incubated in an Eppendorf heating block at 37°C shaking at 500 rpm. Radiochemical yield was checked every hour during incubation by iTLC using 10 mM EDTA in 0.15 M NH4OAc as a mobile phase. Once 70-90% radiochemical yield was achieved (typically after 3-4 hours of incubation), radiolabeled DOTA-antibodies were removed from the heating block for purification.

2.5.3.5.9. *Purification of Radiolabeled Antibodies*

Purification was performed by adding the total volume of the sample of radiolabeled antibody, with an additional 100-200 μL of PBS (1X), in a 10K MWCO Pierce™ Protein Concentrator (PES, 0.15 mL) followed by centrifugation at 500 x g for 10-15 minutes. This step was repeated three times, and each time the 200 μL of PBS was replaced. After spinning, the sample was pipetted from the reservoir of the spin concentrator and pipetted into a fresh 1.5 mL tube. Activity was measured using the dose calibrator (set to 450*10) and recorded. Next, further analysis with iTLC and Bradford Assay were performed.

2.5.3.5.10. iTLC (instant Thin Layer Chromatography

This step follows the same protocol as described in the antibody control section 2.5.3.4.10.

2.5.3.5.11. Bradford Protein Assay

Fractions of Lu-177-DOTA-Ab with >90% purity protein concentration was measured with Bradford Protein Concentration Assays. A Bradford standard was prepared with 7 dilutions with the highest concentration as 2 mg/mL (1:2 ratio) and a 0 mg/mL concentration and 5 μL was pipetted in duplicate down two columns of a clear 96-well plate. Samples of 5μL for both the Lu-177-DOTA-cetuximab + Lu-177-DOTA-trastuzumab and the Lu-177-DOTA-IgG conditions were also added to the plate containing the standard ladder. Absorbance was measured and analyzed with SoftMax Pro Software and the linear equation generated by the standard ladder was used to determine the concentration of the samples. Concentrations calculated from the Bradford Protein Assay were used to calculate the specific activity of Lu-177-DOTA-Abs (mCi/mg).

2.5.3.5.12. Sterilization of Radiolabeled Antibodies

All Lu-177-Abs were sterilized using the same method as described in section 2.5.3.3.12.

2.5.3.5.13. Post-Sterilization iTLC and Bradford Assays

iTLC procedure was done using the same method as described in section 2.5.3.3.10. Bradford Assays were also performed using the same method as in section 2.5.3.4.11., with the protein ladder that had 2000 μg as the highest concentration.

2.5.3.5.14. Treatment Stock Preparation and Transfer to Clonogenic Assay

Stock vials with a molar concentration of 68.5 nM for both the radiolabeled cetuximab + trastuzumab and the radiolabeled IgG isotype control were prepared. For each condition, two treatment stock tubes were prepared with sufficient volume to dispense 50 μL into all wells receiving treatment, with additional volume included to account for potential pipetting error. Sterile Lu-177-DOTA-Abs were diluted with media in new 2mL tubes dedicated for treatment stock preparation to achieve the desired target molar concentrations, and tubes were vortexed to ensure homogeneity of the mixture. The 6-well plates with cells were retrieved from the incubator, and 50 μL from the stock tubes was applied to the wells in triplicate, and the nM concentration of Lu-177-DOTA-cetuximab + Lu-177-DOTA-trastuzumab and Lu-177-DOTA-IgG added to the wells were labeled. No treatment control wells received 50 μL of media only. All plates were gently shaken to ensure even distribution of Lu-177-DOTA-Abs in the wells.

2.5.3.5.15. Incubation and Washing

Plates were returned to the incubator. There were three different time points for when the media was removed from the wells and washed twice with 2 mL of PBS (1X); a condition washed at 1 hour, another at 12 hours, and another at 24 hours to wash away any Lu-177-DOTA-Ab that did not bind to cells during incubation periods. Control plates were also washed and had media replaced at each designated time points. All wells received 2 mL of fresh media immediately after washing. After media replacement, all plates were allowed to incubate for one week.

2.5.3.5.16. Fixing and Staining

This step follows the same protocol as described in the antibody control section 2.5.3.1.7.

2.5.3.5.17. ChemiDoc™ Imaging

This step follows the same protocol as described in the antibody control section 2.5.3.1.8.

2.5.3.5.18. ImagingJ Analysis

This step follows the same protocol as described in the antibody control section 2.5.3.1.9.

2.5.3.5.19. RStudio Analysis

Assumptions of normality of residuals and homogeneity of variances were tested before performing ANOVA. A Shapiro-Wilk test was performed for all triplicate concentrations with an online calculator (https://www.statskingdom.com/shapiro-wilk-test-calculator.html) and variances were tested with Bartlett's test in RStudio. Triplicates were used to generate standard error values and means. Significance was measured with Kruskal Wallis (for each time point separately) in RStudio, and Dunn's test was used as a post hoc test for pairwise comparison. All statistical analyses were performed at a 5% significance level.

3. RESULTS

3.1. Antibody Radiolabeling Results

There was successful radiolabeling of antibodies cetuximab, trastuzumab, and IgG to isotopes Tc-99m and Lu-177. The specific activity of the Tc-99m labeled antibody was 53.71 μCi/μg on average (range = 13.74 – 141.39), and for Lu-177 was 23.28 μCi/μg on average (range = 15.3 – 28.18). Prior to experiments, the purity of the radioactivity bound to the antibodies was measured via iTLC for the fractions selected from G-25 column purification. For Tc-99m experiments, >95% purity was acceptable and considered to be sufficient for binding experiments. The results for the iTLC are presented in Figure 3 and Table 1 for Tc-99m labeled cetuximab and trastuzumab and Figure 4 and Table 2 for Lu-177 labeled cetuximab, trastuzumab, and IgG.

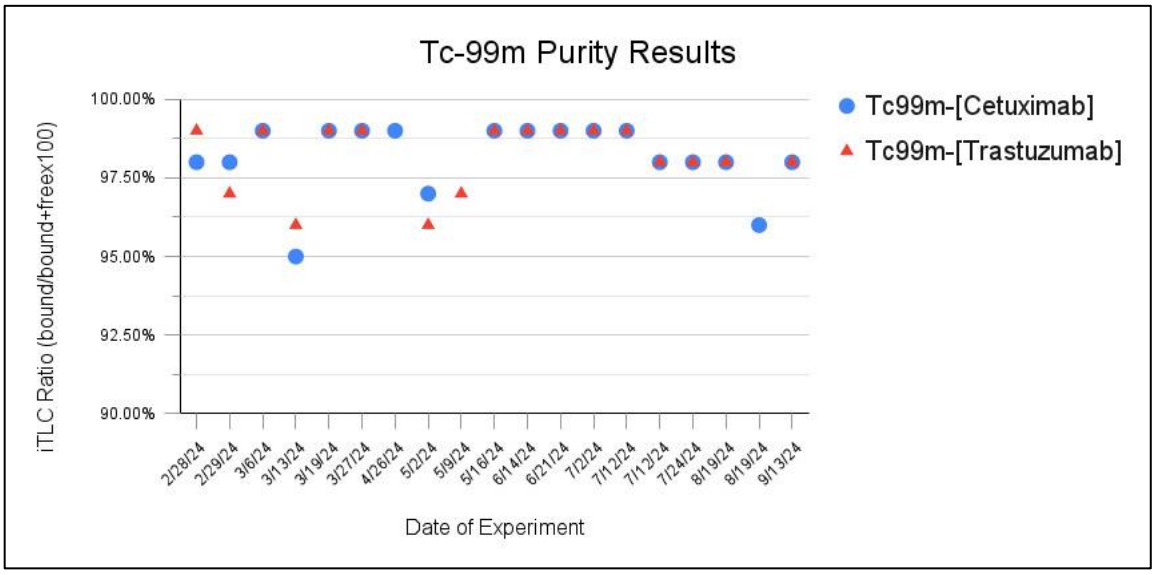

Figure 3. iTLC Results for Tc-99m radiolabeling of cetuximab and trastuzumab. Data are shown as percentages of Tc-99m bound to each antibody divided by the activity of Tc-99m (bound+free), or (bound/bound+free) x 100%. Any value above or equal to 95% (95% of Tc-99m was bound to antibody) was considered as sufficient and was accepted for subsequent experiments.

	Tc99m-[Cetuximab]	**Tc99m-[Trastuzumab]**
Mean	97%	97%
SD	0.04	0.05

Table 1. Summary of iTLC values for Tc-99m labeled cetuximab and trastuzumab.

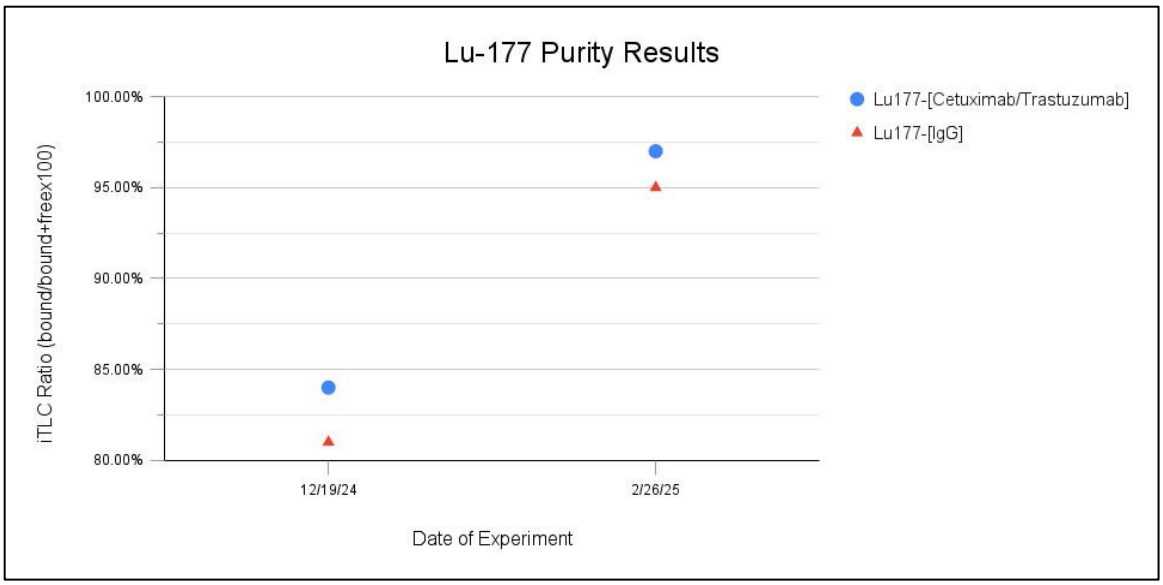

Figure 4. Data are shown as percentages of Lu-177 bound to antibodies divided by the activity of Lu-177 (bound+free), or (bound/bound+free). 100%. Any value above or equal to 80% (at least 80% of Tc-99m was bound to antibody) was considered as sufficiently pure and was accepted for subsequent experiments.

	Lu177-[Cetuximab/Trastuzumab]	**Lu177-[IgG]**
Mean	91%	88%
SD	0.09	0.10

Table 2. Summary of iTLC values for Lu-177 labeled cetuximab + trastuzumab and IgG.

3.2. Validation of Receptor Expression

3.2.1. Specific Binding of Antibodies to Cell Lines and Determining Kd (Binding Affinity)

Tc-99m specific binding experiments with cetuximab and trastuzumab were only performed if iTLC results yielded at least 95% purity and Bradford Protein Concentration measurements confirmed that the radiolabeled products could be diluted while still achieving the concentration necessary for receptor saturation. Once preparation of the dilution series, application of the dilutions to the cells, an incubation period, washing, and the ATPlite assay were complete, individual wells were collected as samples and were measured for radioactivity (CPM) using the gamma counter instrument. Conversion of CPM values to mCi was done using 1.42 million CPM/mCi as the conversion factor – a value determined by calibration of the gamma counter.

Further analysis was performed as described in the methods section using GraphPad Prism. The values are reported in Table 3.

Date of Experiment	Cell Line	Tc-99m-labeled-Antibody	Bmax (nM)	Kd (nM)	Fit R^2
3/19/24	AxA	cetuximab	3.96E-07	10.2	0.98
3/19/24	AxA	trastuzumab	4.98E-07	1.33	0.98
3/19/24	AxA	cetuximab	3.87E-07	11.39	0.99
3/19/24	AxA	trastuzumab	3.69E-07	1.39	0.99
7/24/24	Org	cetuximab	3.34E-08	Unstable	0.94
7/24/24	Org	trastuzumab	7.10E-07	0.8751	0.95
8/16/24	Org	cetuximab	6.75E-08	7.165	0.96
8/16/24	Org	trastuzumab	5.42E-07	2.649	0.92
3/27/24	Org	trastuzumab	6.67E-07	3.291	0.98
3/13/24	Nk	cetuximab	2.34E-08	Unstable	0.96
2/29/24	Nk	trastuzumab	9.65E-07	2.043	0.99
5/9/24	Nk	cetuximab	2.31E-07	Unstable	0.99
7/24/24	Nk	trastuzumab	5.31E-07	1.435	0.99
6/14/24	AxC	cetuximab	-1.07E-10	Unstable	0.97
6/14/24	AxC	trastuzumab	6.80E-08	1.391	0.97
6/14/24	AxC	cetuximab	2.77E+07	Unstable	0.98
6/14/24	AxC	trastuzumab	5.96E-08	0.9381	0.91
7/2/24	Sh	cetuximab	1.68E-07	4.517	0.98
7/2/24	Sh	trastuzumab	1.17E-07	1.902	0.96
9/13/24	Sh	cetuximab	2.05E-07	Unstable	0.99
3/27/24	Sh	trastuzumab	1.17E-07	2.217	0.99

Table 3. Bmax and Kd values for K9UTC cell lines determined by binding experiments and analysis with GraphPad Prism.

Specific binding graphs were generated using One-Site Specific Binding Non-Linear Fit Analysis in GraphPad Prism for all cell lines as shown in Figures 5 to 13.

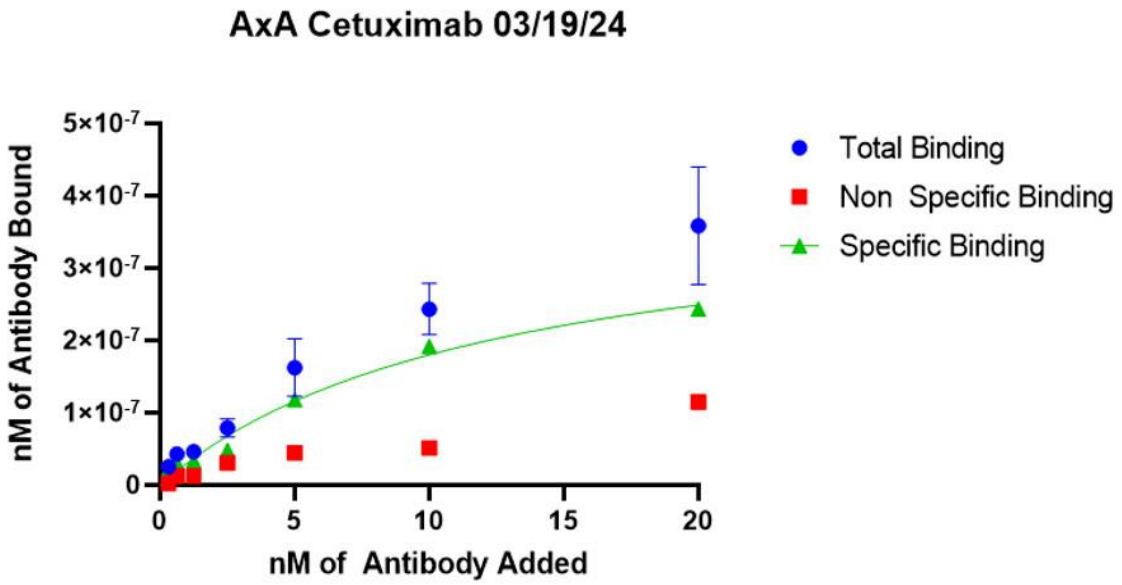

Figure 5. Tc-99m-cetuximab binding results for K9UTC AxA cell line.

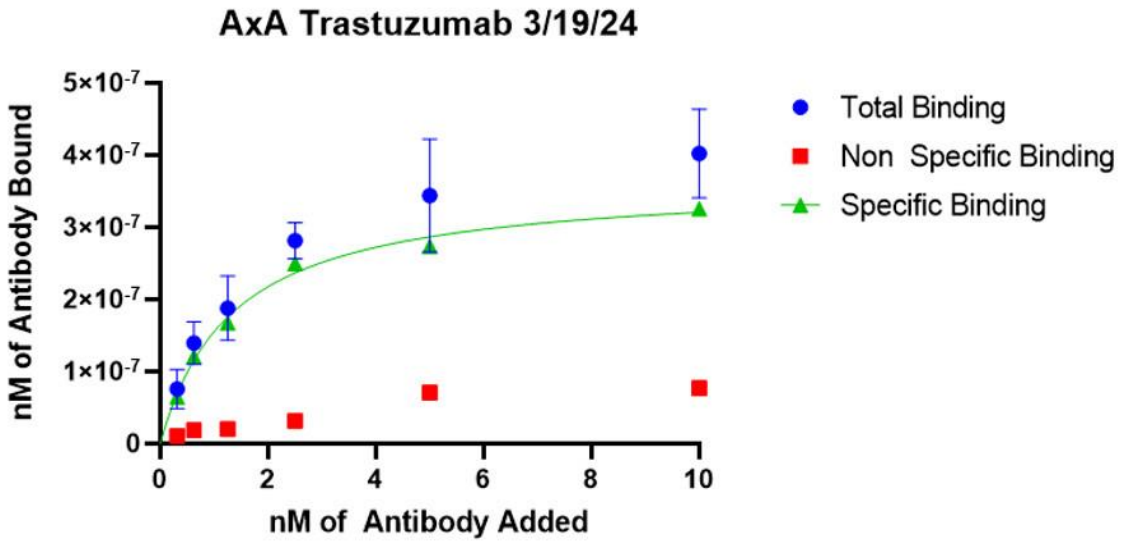

Figure 6. Tc-99m-trastuzumab binding results for K9UTC AxA cell line.

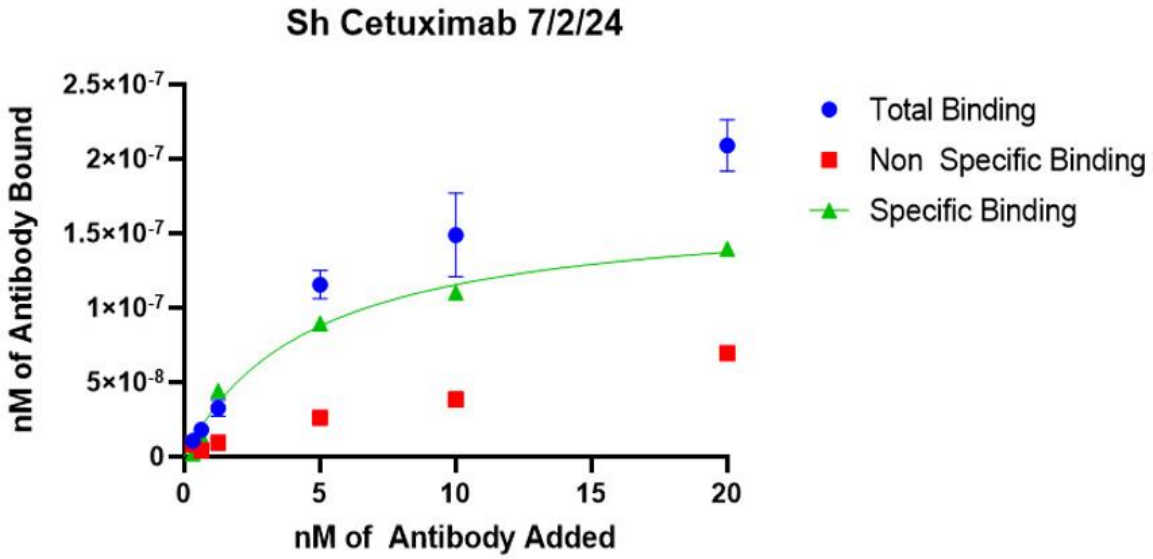

Figure 7. Tc-99m-cetuximab binding results for K9UTC Sh cell line.

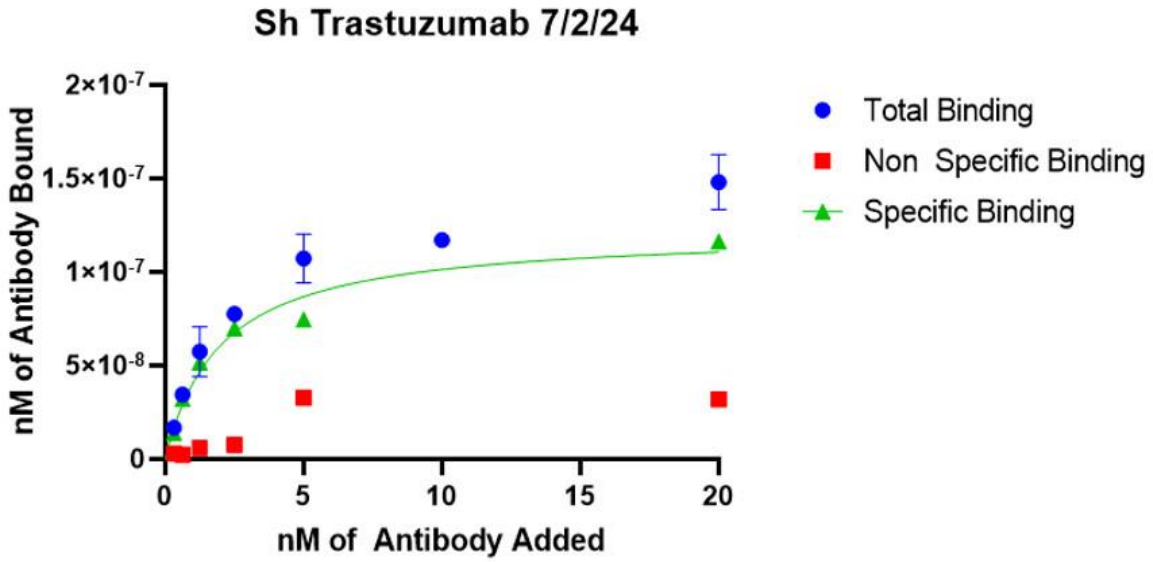

Figure 8. Tc-99m-trastuzumab binding results for K9UTC Sh cell line.

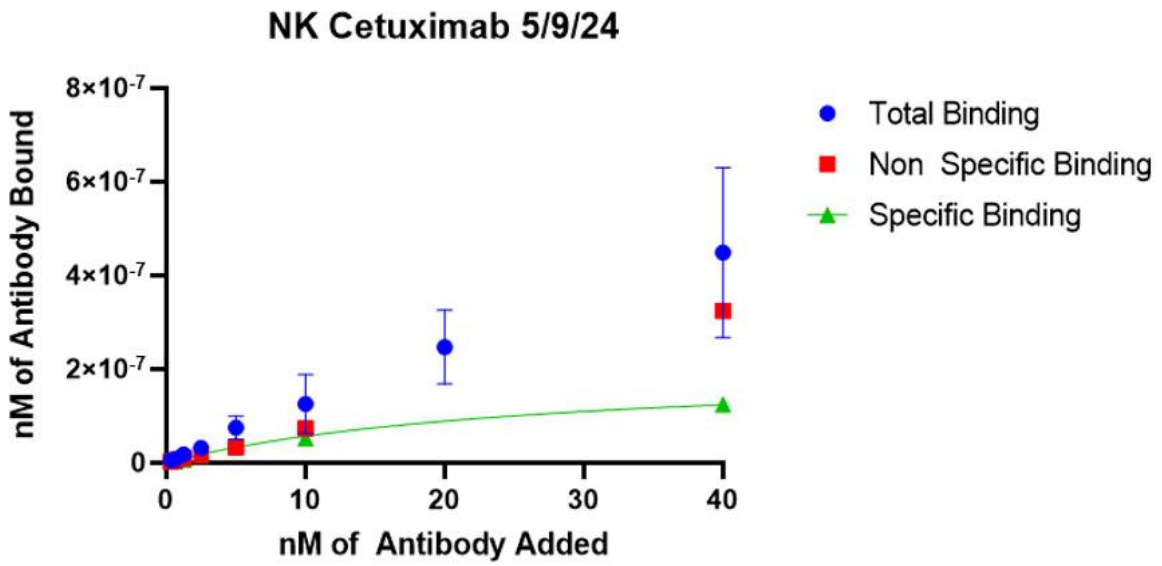

Figure 9. Tc-99m-cetuximab binding results for K9UTC Nk cell line.

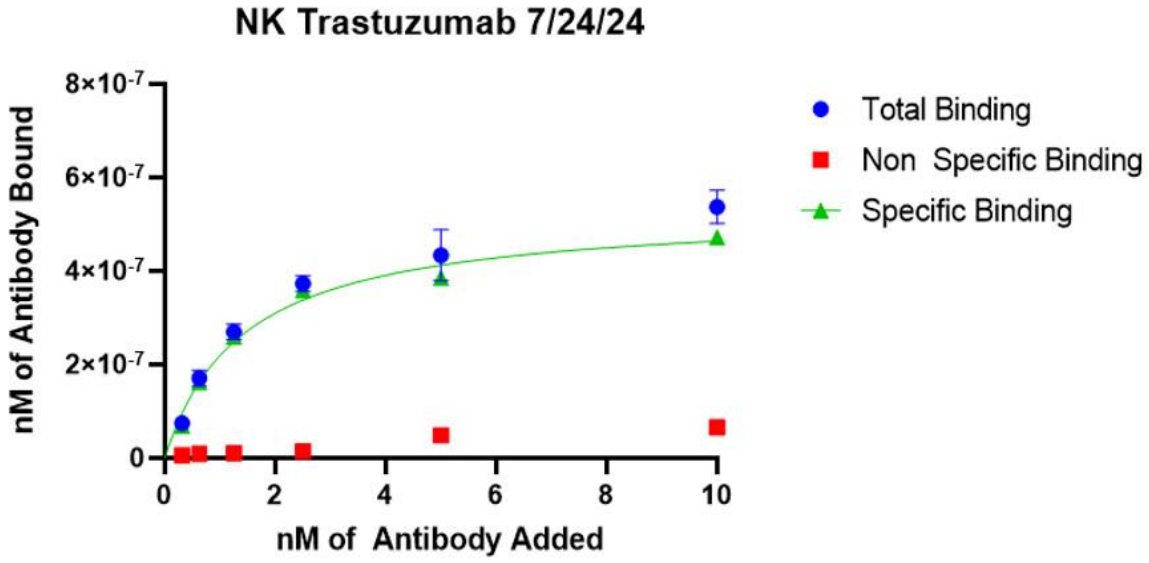

Figure 10. Tc-99m-trastuzumab binding results for K9UTC Nk cell line.

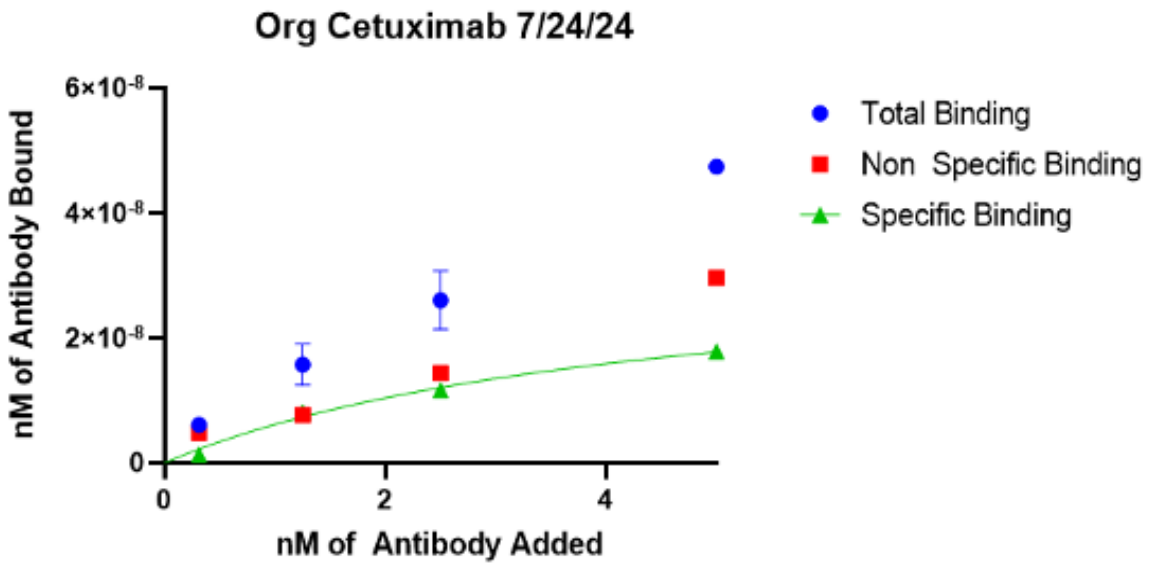

Figure 11. Tc-99m-cetuximab binding results for K9UTC Org cell line.

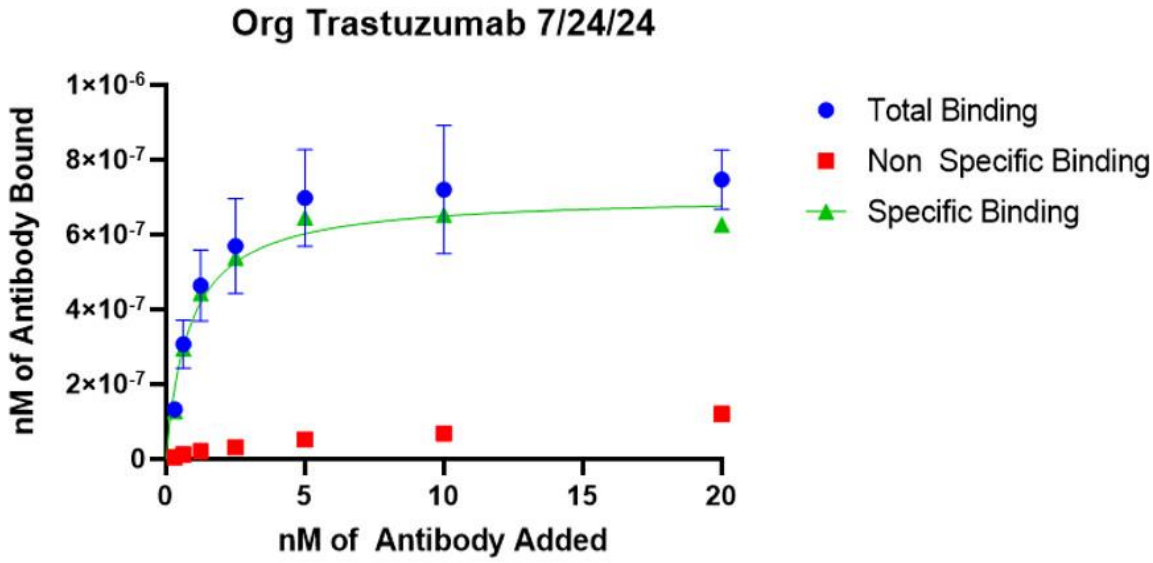

Figure 12. Tc-99m-trastuzumab binding results for K9UTC Org cell line.

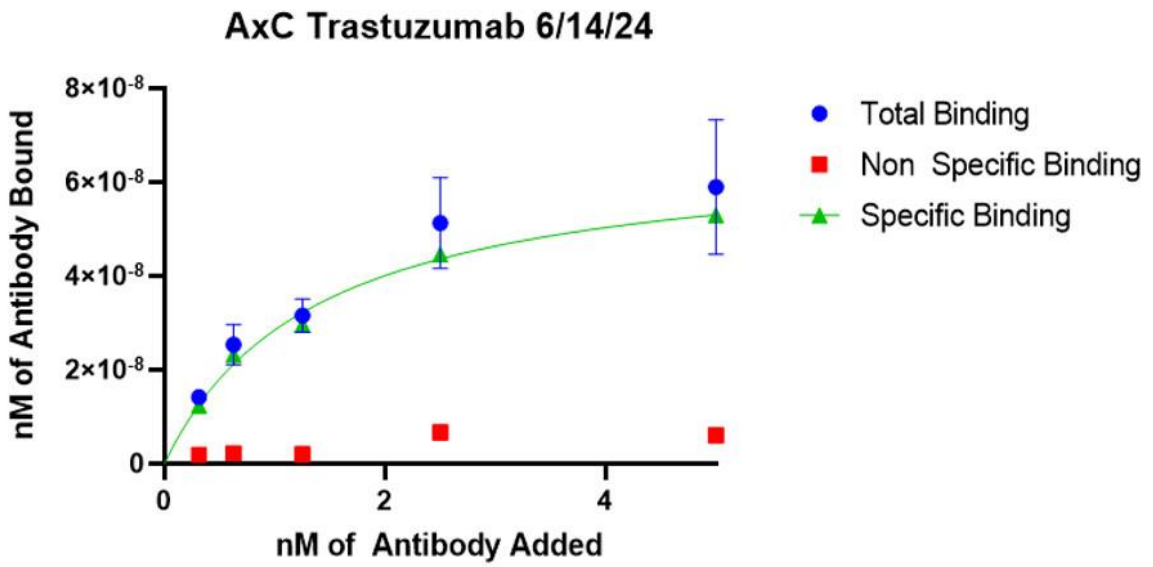

Figure 13. Tc-99m-trastuzumab binding results for K9UTC AxC cell line.

Analysis of the binding data for the AxC cell line showed no detectable binding or affinity of cetuximab with EGFR1. AxC was not used for a negative control, as flow cytometry results during titration experiments suggested that there is some binding of cetuximab to EGFR1, although very minimal. A mouse fibroblast cell line (3T3/NIH) was instead used as the negative control for titration experiments as this cell line was previously determined to be negative for EGFR1 and EGFR2 and does not bind cetuximab or trastuzumab.

3.2.2. Cell Numbers for Specific Binding Assays

The number of cells in each binding experiment were quantified with an ATPlite assay following the incubation with radiolabeled antibodies, and after washes. Photons/second values (Luminescence) were attained using Living Image Software, which were converted to cell numbers with a standard curve. Standard curves were determined by a linear dilution of cells that had been previously prepared, and a linear equation was determined by the photon/second and the number of cells in wells. Values were accepted only when within the standard curve and replicates typically generated a relative standard error (RSE) less than 5%. RSE values below 25% were considered reliable sampling. Cell counts are reported in Table 4.

Date of Experiment	Cell Line	Mean Cell Count	Standard Error	RSE (%)
3/19/24	AxA1	1.33E+05	2.82E+03	2.13
3/19/24	AxA2	1.24E+05	3.50E+03	2.81
7/24/24	Org	1.90E+05	3.30E+03	1.73
8/16/24	Org1	1.36E+05	5.06E+03	3.72
3/27/24	Org	1.22E+05	3.56E+03	2.92
3/13/24	Nk	9.15E+04	3.98E+03	4.35
2/29/24	Nk	1.79E+05	2.58E+03	1.44
5/9/24	Nk	1.02E+05	1.78E+03	1.75
7/24/24	Nk	9.66E+04	1.85E+03	1.92
6/14/24	AxC1	5.45E+04	2.42E+03	4.44
6/14/24	AxC2	7.07E+04	2.59E+03	3.67
3/27/24	Sh	8.98E+04	2.13E+03	2.37
7/2/24	Sh	4.42E+04	1.68E+03	3.79
9/13/24	Sh	3.62E+04	2.49E+03	6.87

Table 4. Cell Number ATPlite analysis.

3.2.3. Estimated Receptor Numbers

The number of receptors and expression of EGFR1 and EGFR2 was estimated using results from Table 4 cell count and Table 3 Bmax and Kd. The EGFR1 and EGFR2 levels estimated per single cell for each cell line can be found in Table 5.

Date of Experiment	Cell Line	Receptor Type	Bmax (nM)	Average Estimated Cell Count	# of Receptors/Cell
3/19/24	AxA	EGFR1	3.96E-07	1.33E+05	1.80E+03
3/19/24	AxA	EGFR2	4.98E-07	1.33E+05	2.26E+03
3/19/24	AxA	EGFR1	3.87E-07	1.24E+05	1.87E+03
3/19/24	AxA	EGFR2	3.69E-07	1.24E+05	1.78E+03
7/24/24	Org	EGFR1	3.34E-08	1.90E+05	1.06E+02
7/24/24	Org	EGFR2	7.10E-07	1.90E+05	2.25E+03
8/16/24	Org	EGFR1	6.75E-08	1.36E+05	2.99E+02
8/16/24	Org	EGFR2	5.42E-07	1.36E+05	2.40E+03
3/27/24	Org	EGFR2	6.67E-07	1.22E+05	3.30E+03
3/13/24	Nk	EGFR1	2.34E-08	9.15E+04	1.54E+02
2/29/24	Nk	EGFR2	9.65E-07	1.79E+05	3.25E+03
5/9/24	Nk	EGFR1	2.31E-07	1.02E+05	1.37E+03
7/24/24	Nk	EGFR2	5.31E-07	9.66E+04	3.31E+03

Table 5. Receptor numbers estimated per cell line per antibody.

Table 5 (cont'd).

6/14/24	AxC	EGFR2	6.80E-08	5.45E+04	7.52E+02
6/14/24	AxC	EGFR2	5.96E-08	7.07E+04	5.08E+02
7/2/24	Sh	EGFR1	1.68E-07	4.42E+04	2.29E+03
7/2/24	Sh	EGFR2	1.17E-07	4.42E+04	1.59E+03
9/13/24	Sh	EGFR1	2.05E-07	3.62E+04	3.41E+03
3/27/24	Sh	EGFR2	1.17E-07	8.98E+04	7.84E+02

The average number of receptors (EGFR1 and EGFR2) was determined for each cell line across all independent experiments for that cell line. The averages, standard error, and relative standard error can be found in Table 6.

Cell Line	**Receptor Type**	**Average Across Receptors/Cell**	**SE**	**RSE (%)**
AxA	EGFR1	1.84E+03	36.88	2
AxA	EGFR2	2.02E+03	2.39E+02	12
Org	EGFR1	2.02E+02	9.67E+01	48
Org	EGFR2	2.65E+03	3.28E+02	12
Nk	EGFR1	7.60E+02	6.06E+02	80
Nk	EGFR2	3.28E+03	3.25E+01	1
AxC	EGFR1	N/A	N/A	N/A
AxC	EGFR2	6.30E+02	1.22E+02	19
Sh	EGFR1	2.85E+03	5.61E+02	20
Sh	EGFR2	1.19E+03	4.03E+02	34

Table 6. Average estimated receptor levels across all K9UTC cell lines.

3.3. Flow Cytometry Experiments

Flow cytometry experiments were attempted on cell lines AxC and Nk for the purpose of confirming low levels of EGFR1 binding where the binding experiments had variable results for binding to specific receptors. These cell lines also exhibited 'Unstable' Kd values across multiple independent binding experiments which could have affected the reliability of binding experiment results due to poor binding affinity of cetuximab to EGFR1. At the time of writing this thesis, there is still a need for more optimal conditions, such as adjustments to the antibody-fluorophore panel, and different viability dyes and apoptosis trackers. Preliminary data suggesting the cetuximab binds to EGFR1 expressed by the AxC cell line can be found in Figure 14. The Mean Fluorescent Intensity (MFI) for the 'cetuximab+' group was 36207.36, and the MFI for the negative population was 577.96.

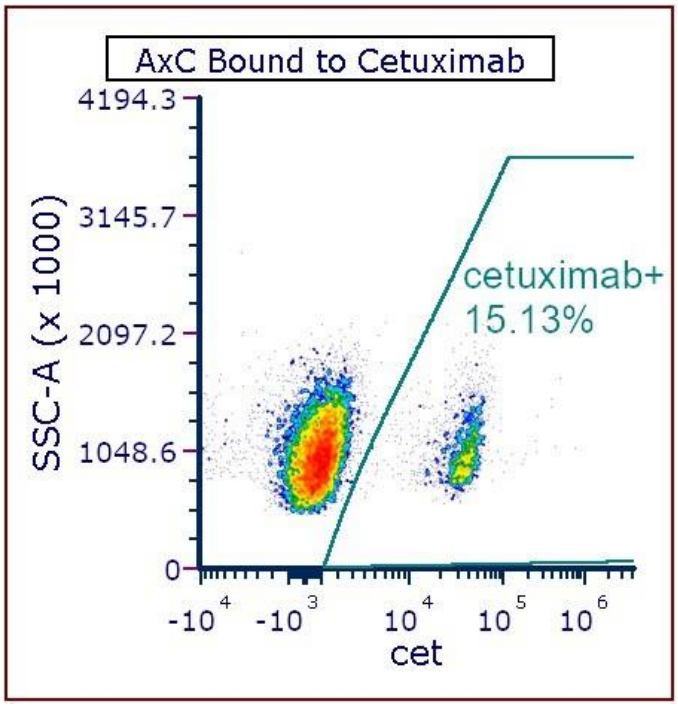

Figure 14. Preliminary evidence that there is some binding of cetuximab to EGFR1 expression by the AxC cell line from titration experiment.

3.4. Efficacy of Targeted Killing with Lu-177

3.4.1. Clonogenic Control Experiments Treated with Antibodies Only

The three canine bladder cancer cell lines selected as candidates for continuation of targeted killing studies were treated with the antibodies in combination with the highest concentration of combined antibodies being 0.02 mg/mL (or 137nM) to mimic the preplanned conditions for the canine clinical trial. Cells treated with a 1:2 dilution of combined antibodies were tested by Shapiro-Wilkes, and Bartlett's test to confirm assumptions were met for parametric analysis by Linear Regression. Each variable output from ImageJ (Count, Total Area, % Area, and Average Size) was analyzed. Count was the variable of most interest and was looked at first after analysis. Table 7 shows a regression summary for the variable Count for the three selected K9UTC cell lines from the antibody control experiments. Table 8 shows a regression summary for other response variables for the three K9UTC cell lines for antibody control experiments. Linear regression relationships of response variables and concentrations of combined cetuximab and trastuzumab can be seen in Figures 15 to 46.

Antibody Control Clonogenic: Regression Summary for Count Variable					
Cell Line	**Experiment**	**R^2**	**Adjusted R^2**	**β-Coefficient**	**p-value**
AxA	1	2.80E-02	-2.32E-02	0.02798	0.496
AxA	2	6.52E-02	2.27E-02	-0.04736	0.229
AxA	3	0.3799	0.3517	-0.15046	0.001**
Nk	1	3.38E-02	-1.01E-02	0.03515	0.390
Nk	3	0.1764	0.139	0.02834	0.041*
Nk	2	2.44E-02	-1.99E-02	-0.08777	0.466
Sh	1	1.72E-04	-4.53E-02	0.003016	0.952
Sh	2	1.04E-02	-3.46E-02	-0.01689	0.635

*Signif. codes: 0 '***' 0.001 '**' 0.01 '*' 0.05 '.' 0.1 ' ' 1*

Table 7. Regression summary for the variable 'Count' for each cell line for antibody control experiment.

Antibody Control Clonogenic: Regression Summary for Variables Total Area, Average Size, and Percent Area							
Cell Line	**Experiment**	**Total Area (p-value)**	**Total Area (β)**	**Average Size (p-value)**	**Average Size (β)**	**Percent Area (p-value)**	**Percent Area (β)**
AxA	1	0.916	0.3228	0.722	-0.01233	0.9939	1.80E-05
AxA	2	0.009**	-4.775	0.008**	-0.07422	0.009**	-0.003757
AxA	3	0.433	-5.873	0.142	0.1629	0.629	-0.002854
Nk	1	0.062	-6.808	0.009**	-0.18281	0.078	-0.00478
Nk	2	0.518	3.208	0.984	-0.001078	0.566	0.002081
Nk	3	0.039*	-7.66	0.731	-0.348	0.1974	-0.003682
Sh	1	0.850	-0.3805	0.882	0.004107	0.839	-0.00033
Sh	2	0.801	-0.8445	0.706	-0.05842	0.812	-0.0006157

*Signif. codes: 0 '***' 0.001 '**' 0.01 '*' 0.05 '.' 0.1 ' ' 1*

Table 8. Regression summary for other response variables for each cell line for antibody control experiments.

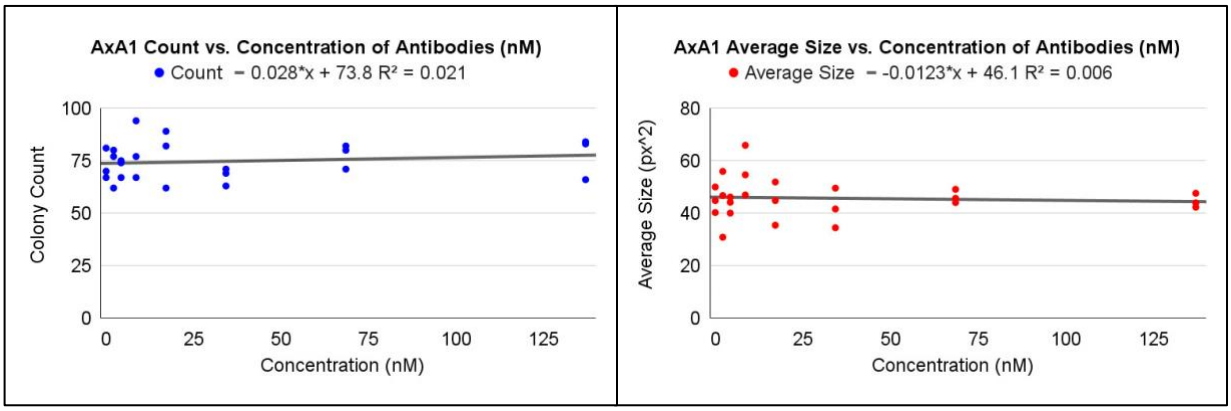

Figures 15 and 16. Antibody control linear regression results for Count and Average Size from the first experiment for the AxA cell line.

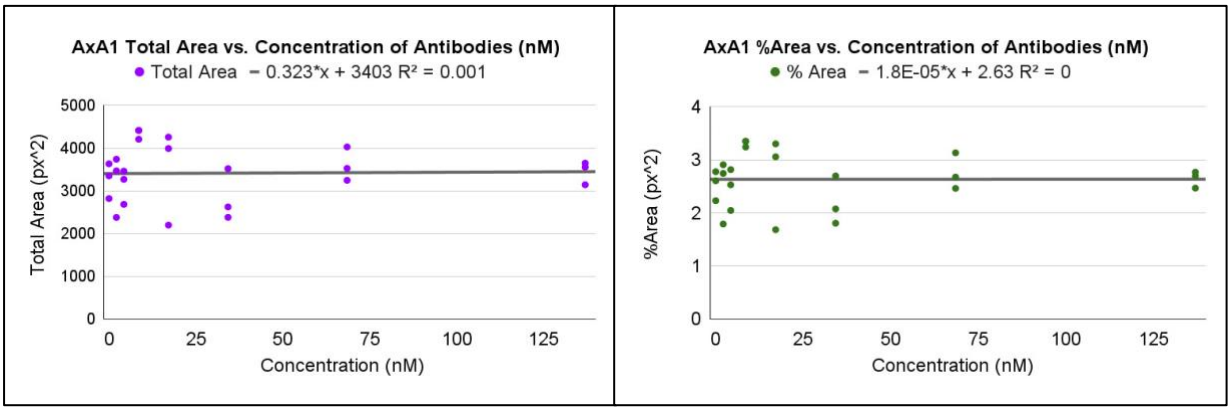

Figures 17 and 18. Antibody control linear regression results for Total Area and % Area from the first experiment for the AxA cell line.

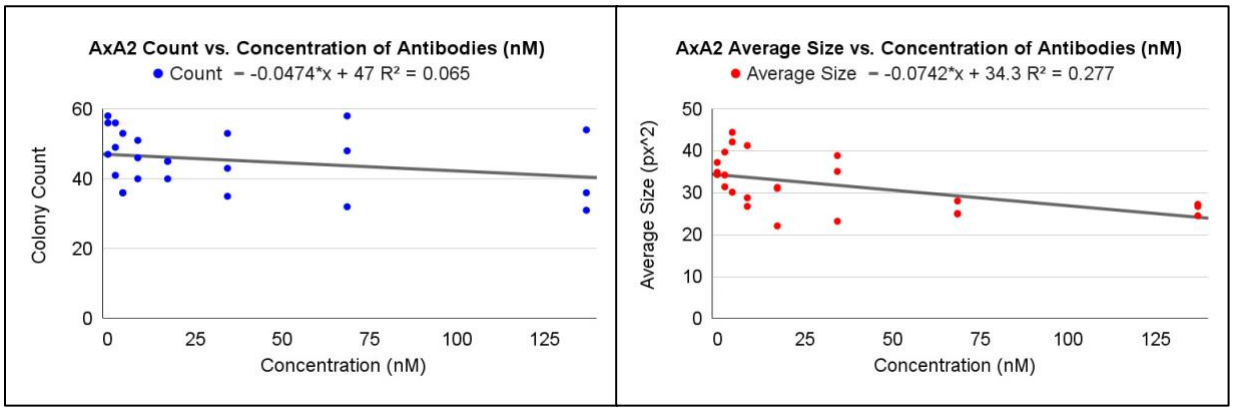

Figures 19 and 20. Antibody control linear regression results for Count and Average Size from the second experiment for the AxA cell line.

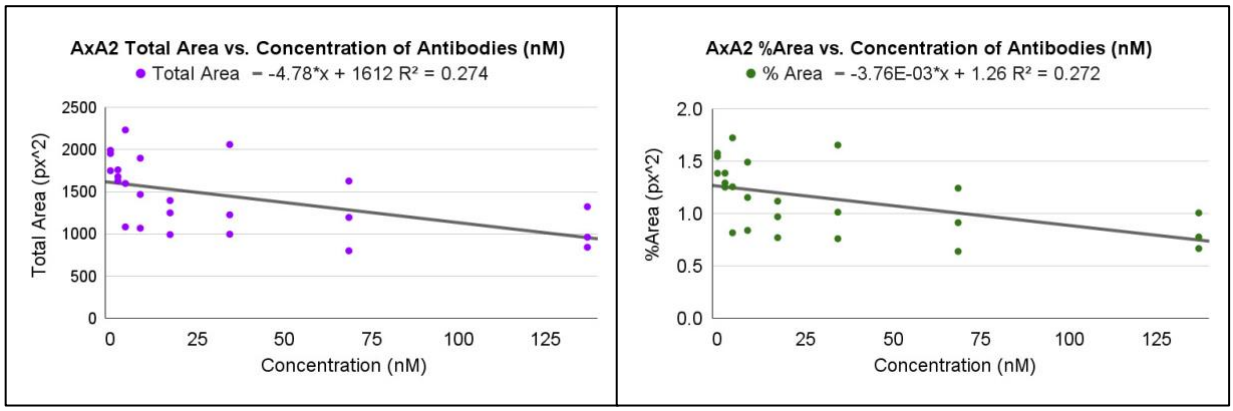

Figures 21 and 22. Antibody control linear regression results for Total Area and % Area from the second experiment for the AxA cell line.

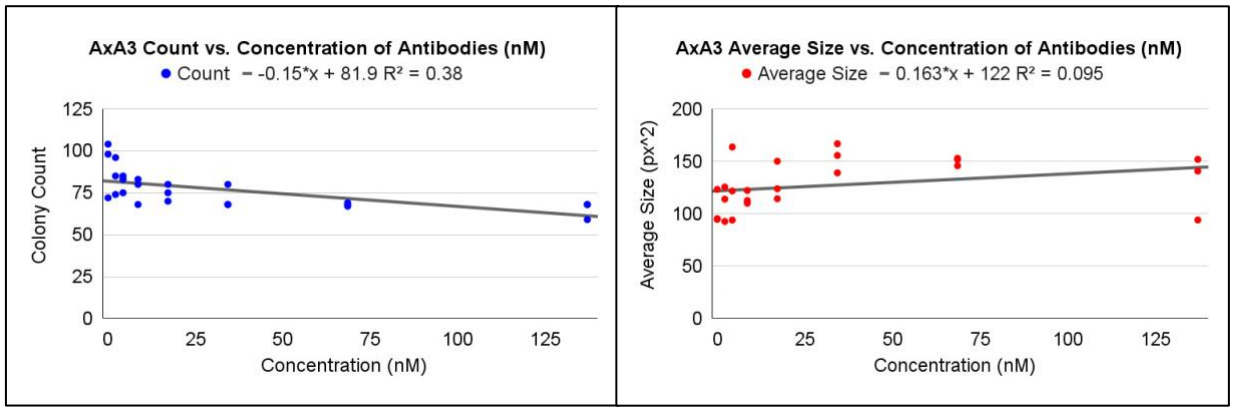

Figures 23 and 24. Antibody control linear regression results for Count and Average Size from the third experiment for the AxA cell line.

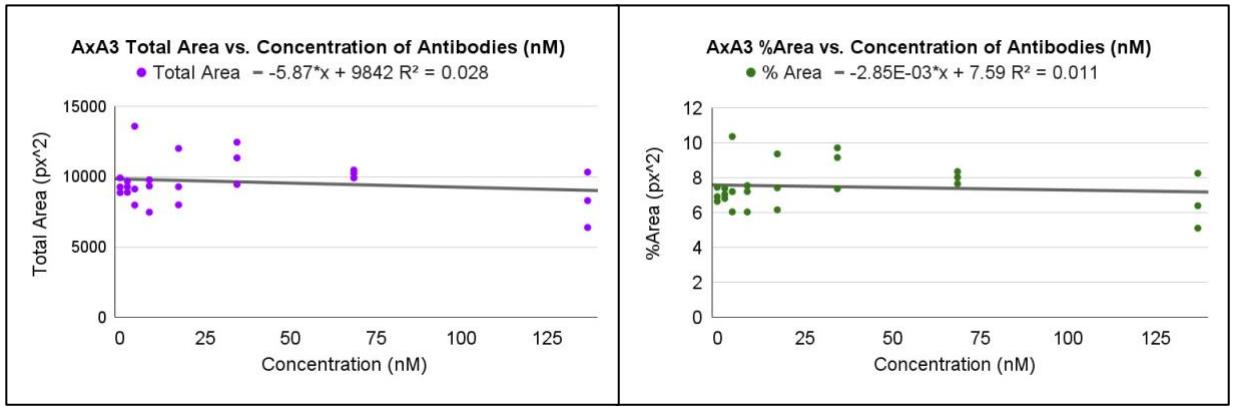

Figures 25 and 26. Antibody control linear regression results for Total Area and % Area from the third experiment for the AxA cell line.

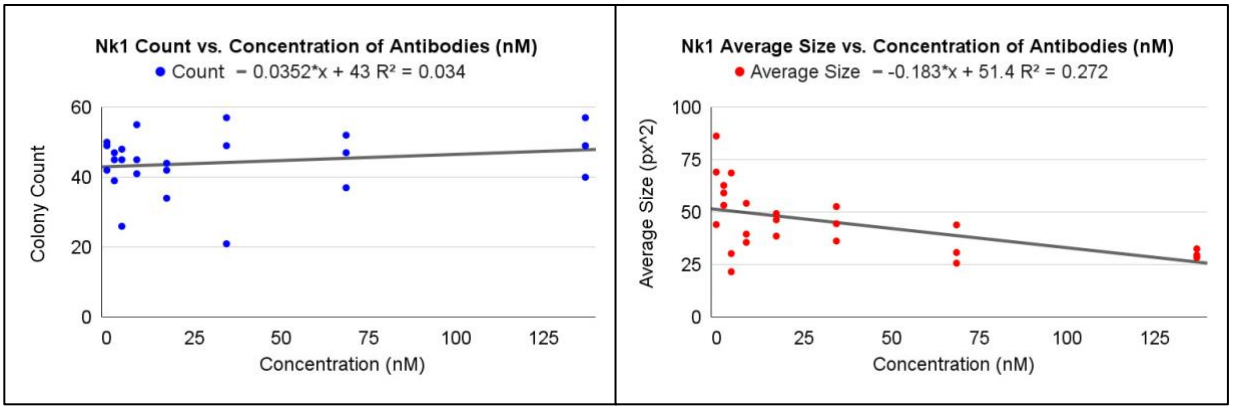

Figures 27 and 28. Antibody control linear regression results for Count and Average Size from the first experiment for the Nk cell line.

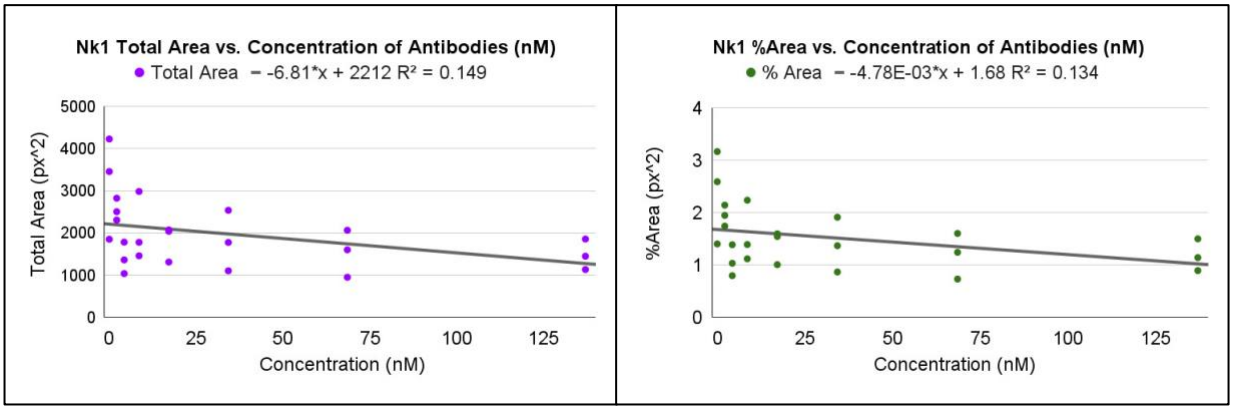

Figures 29 and 30. Antibody control linear regression results for Total Area and % Area from the first experiment for the Nk cell line.

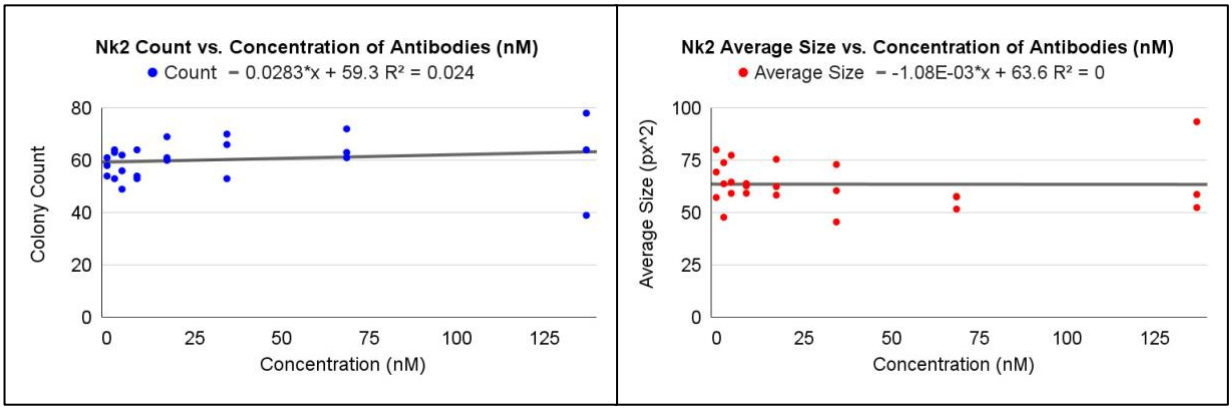

Figures 31 and 32. Antibody control linear regression results for Count and Average Size from the second experiment for the Nk cell line.

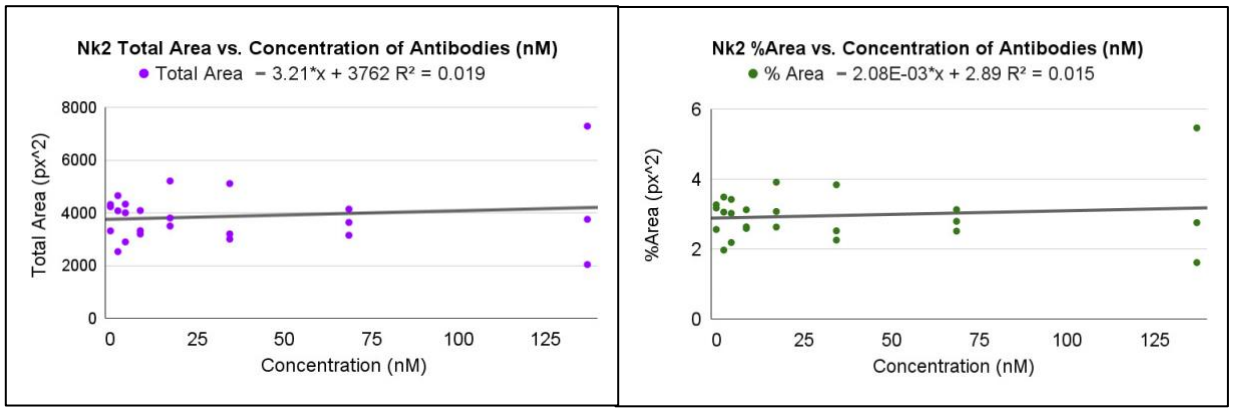

Figures 33 and 34. Antibody control linear regression results for Total Area and % Area from the second experiment for the Nk cell line.

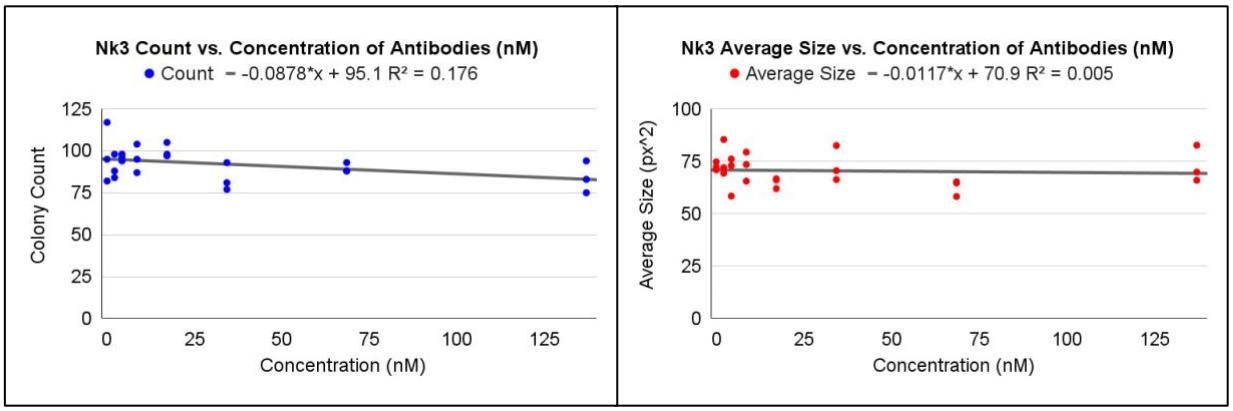

Figures 35 and 36. Antibody control linear regression results for Count and Average Size from the third experiment for the Nk cell line.

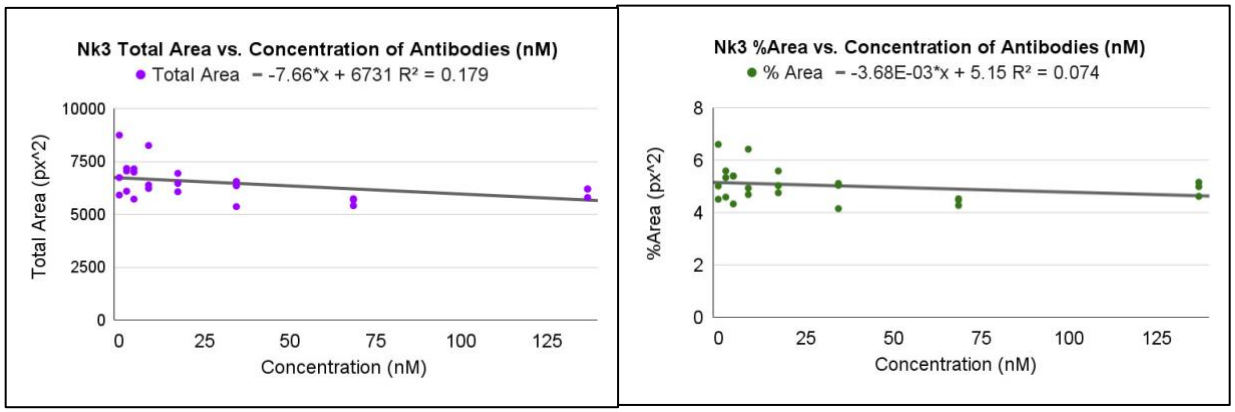

Figures 37 and 38. Antibody control linear regression results for Total Area and % Area from the third experiment for the Nk cell line.

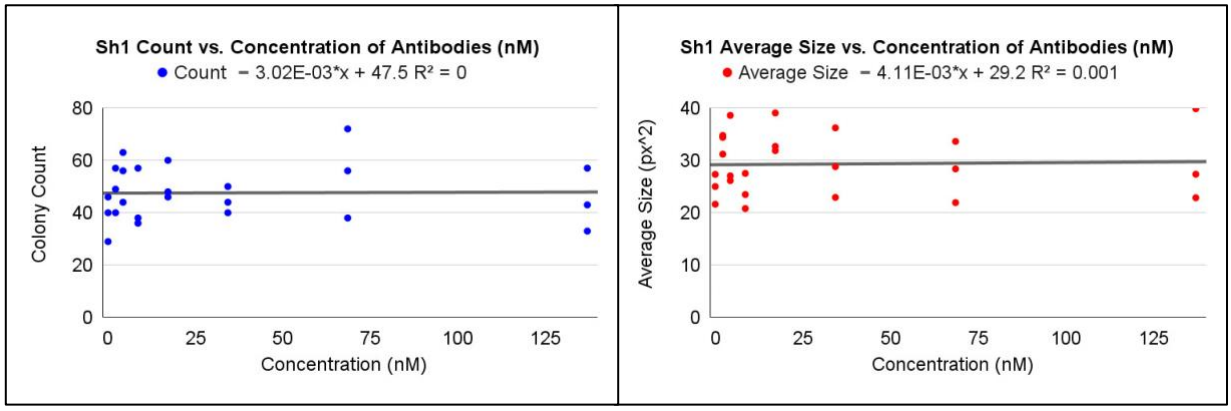

Figures 39 and 40. Antibody control linear regression results for Count and Average Size from the first experiment for the Sh cell line.

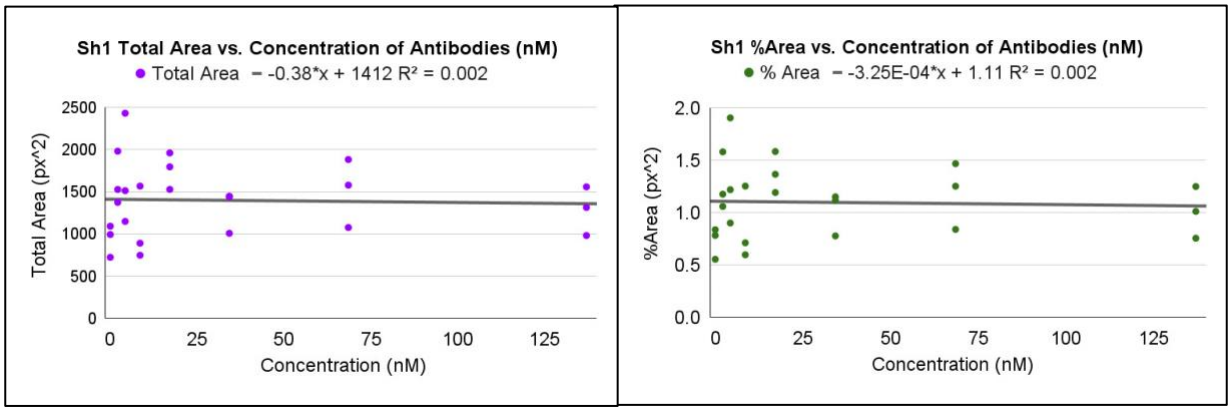

Figures 41 and 42. Antibody control linear regression results for Total Area and % Area from the first experiment for the Sh cell line.

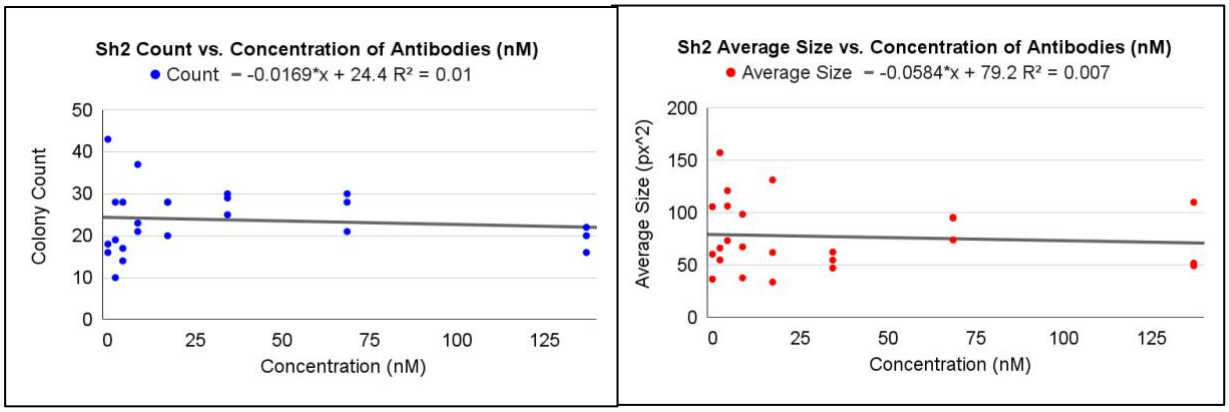

Figures 43 and 44. Antibody control linear regression results for Count and Average Size from the second experiment for the Sh cell line.

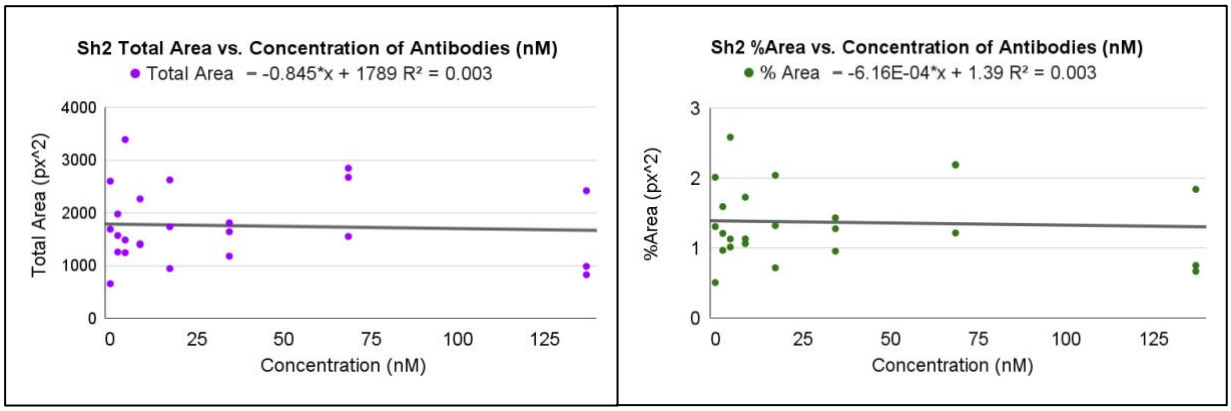

Figures 45 and 46. Antibody control linear regression results for Total Area and % Area from the second experiment for the Sh cell line.

An antibody control experiment was also performed on the AxA cell lines at 68.5 nM for cetuximab + trastuzumab, and IgG across three different time points (1 hour. 12 hours, and 24 hours) to match the conditions of the second Lu-177 experiment. These experiments were analyzed with One-Way ANOVA in R-Studio for each time point, and results can be seen in Table 9.

Time Point	Variable	Df	Sum Sq	Mean Sq	F value	p-value	Significant? (p < 0.05)
1 hour	**Count**	2	177.0	88.5	0.782	0.486	No
	Total Area	2	43661908	21830954	1.341	0.309	No
12 hours	**Count**	2	290.2	145.1	2.189	0.168	No
	Total Area	2	118314490	59157245	3.701	0.0672	No
24 hours	**Count**	2	13.5	6.8	0.078	0.926	No
	Total Area	2	703428	351714	0.021	0.979	No

Table 9. Summary of ANOVA for the Ab only control experiments across three time points.

3.4.2. Clonogenic Experiments Treated with Cisplatin

The three canine bladder cancer cell lines selected for continuation to targeted radiation studies were treated with chemotherapy (cisplatin) to serve as a positive control for comparison to efficacy of radiolabeled antibodies (originally intended for comparison with an alpha-emitting isotope, but due to supply issues, Lu-177, a beta-emitting isotope was used instead). Cells treated with a 1:2 dilution of cisplatin with the highest concentration being 100 μM were analyzed with Linear

Regression. Each variable output from ImageJ was analyzed, with Count being the variable of most interest. Total Area, and % Area had to be log transformed for the AxA experiment, Total Area, Average Size, and % Area had to be log transformed for the Nk experiment, and Total Area and % Area were log- transformed to satisfy the homogeneity of variance assumption required for parametric linear regression analysis. Table 10 shows the regression summary for all cisplatin experiments, and Figures 47 to 58 show the linear regression relationships of Count, Total Area, % Area, and Average Size, vs. concentrations of cisplatin.

Cisplatin Control Clonogenic: Regression Summary					
Count					
Cell Line	**R^2**	**Adjusted R^2**	**β-Coefficient**	**p-value**	**Significance**
AxA	0.830	0.822	-0.641	6.47E-10	yes
Nk	0.871	0.865	-1.006	3.08E-11	yes
Sh	0.856	0.849	-1.029	1.03E-10	yes
Average Size					
Cell Line	**R^2**	**Adjusted R^2**	**β-Coefficient**	**p-value**	**Significance**
AxA	0.892	0.887	-1.337	4.09E-12	yes
Nk	0.866	0.860	-0.008	4.40E-11	yes
Sh	0.641	0.624	-0.578	2.64E-06	yes
Total Area					
Cell Line	**R^2**	**Adjusted R^2**	**β-Coefficient**	**p-value**	**Significance**
AxA	0.956	0.954	-0.015	2.20E-16	yes
Nk	0.831	0.823	-0.935	6.09E-10	yes
Sh	0.954	0.952	-0.017	3.04E-16	yes
Percent Area					
Cell Line	**R^2**	**Adjusted R^2**	**β-Coefficient**	**p-value**	**Significance**
AxA	0.955	0.953	-0.014	2.70E-16	yes
Nk	0.831	0.823	-0.026	5.86E-10	yes
Sh	0.953	0.951	-0.017	4.10E-16	yes

*Signif. codes: 0 '***' 0.001 '**' 0.01 '*' 0.05 '.' 0.1 ' ' 1*

Table 10. Regression model summary for each cell line for Cisplatin experiments.

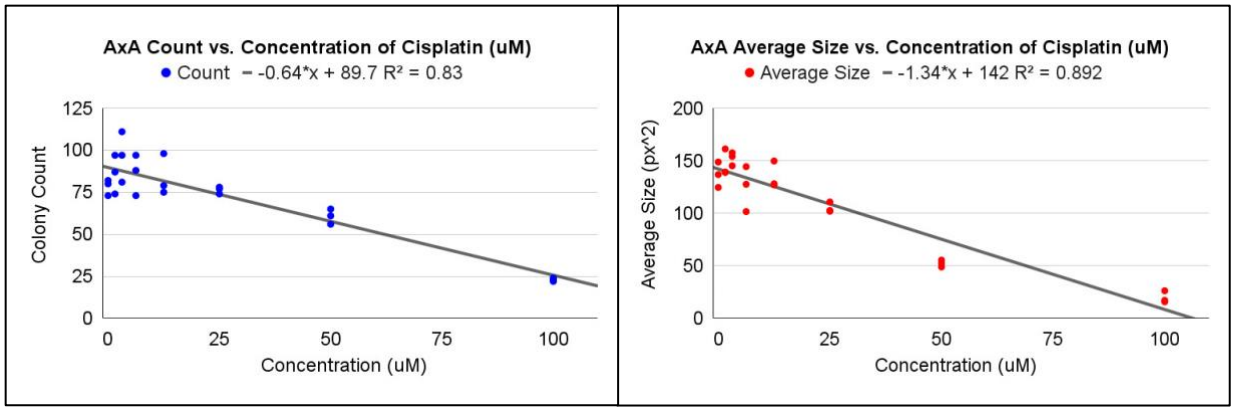

Figures 47 and 48. Cisplatin linear regression results for Count and Average Size for the AxA cell line.

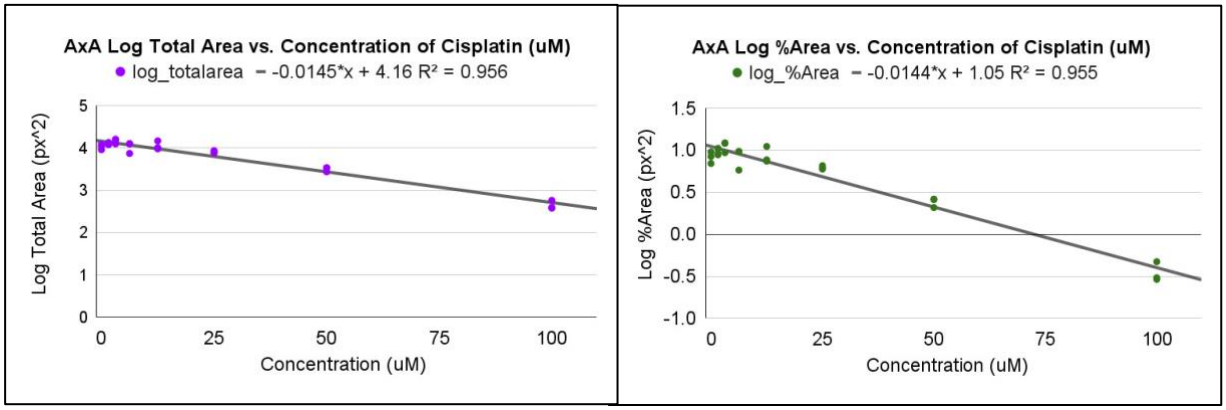

Figures 49 and 50. Cisplatin linear regression results for Total Area and % Area for the AxA Cell line.

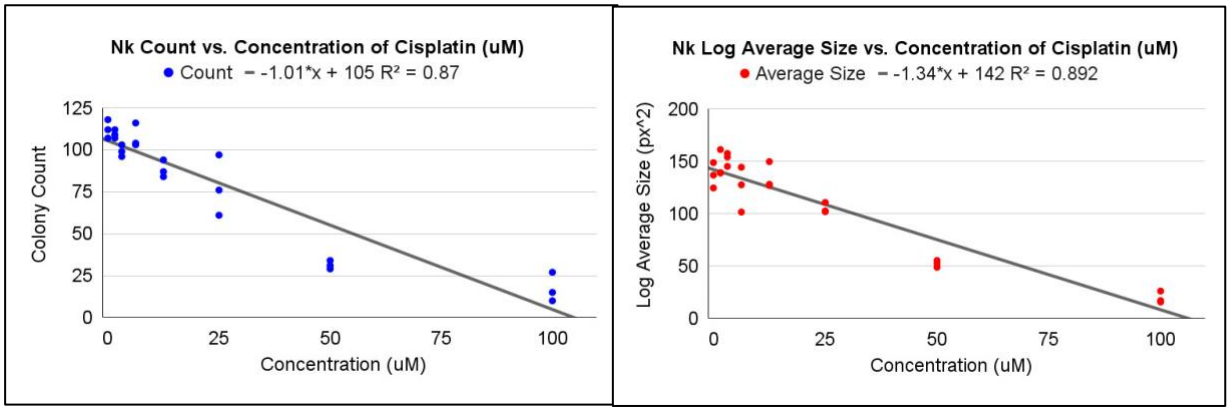

Figures 51 and 52. Cisplatin linear regression results for Count and Average Size for the Nk cell line.

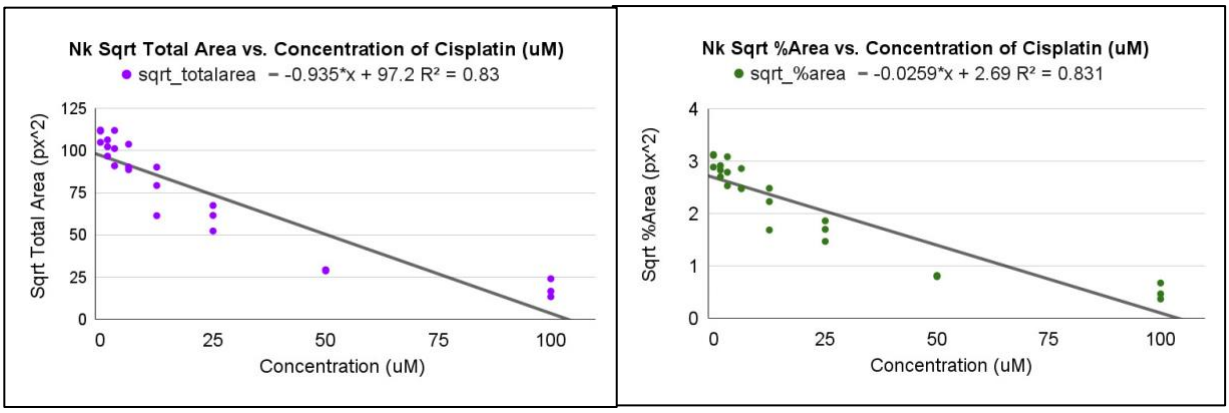

Figures 53 and 54. Cisplatin linear regression results for Total Area and % Area for the Nk Cell line.

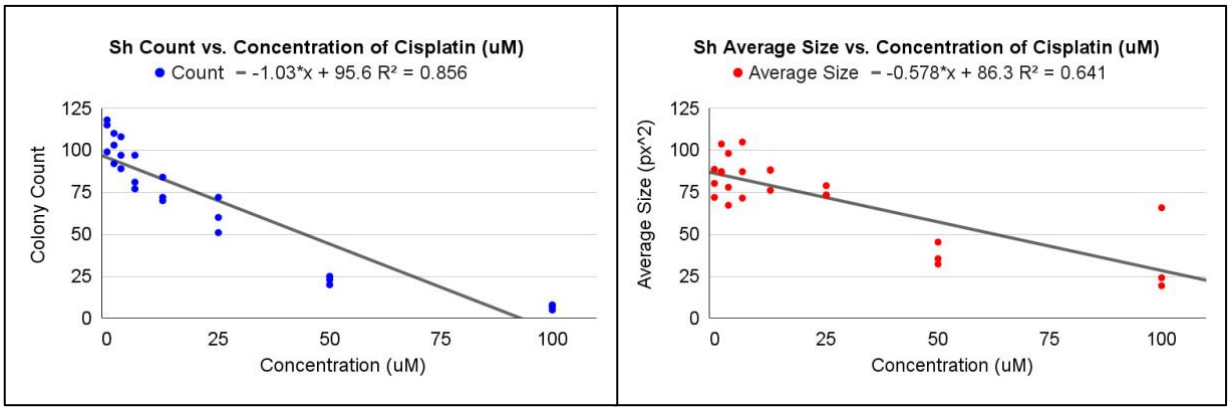

Figures 55 and 56. Cisplatin linear regression results for Count and Average Size for the Sh cell line.

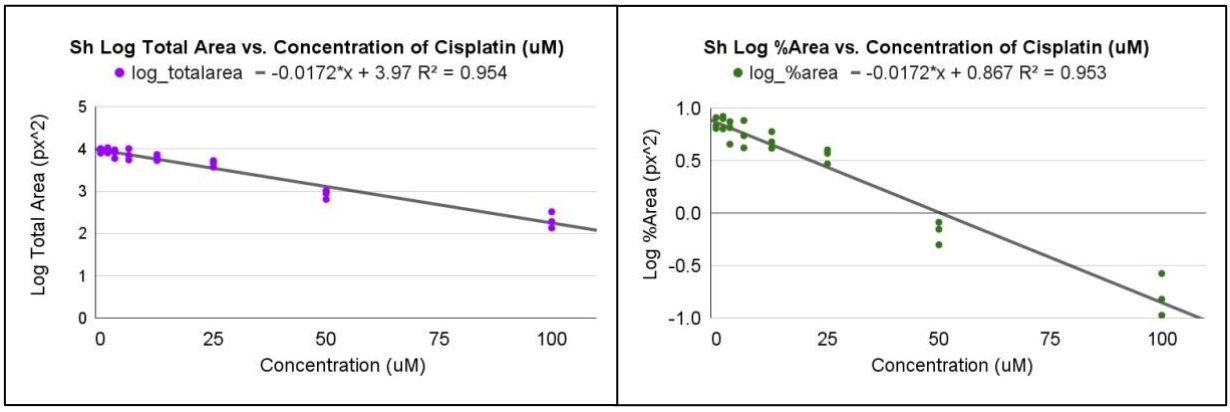

Figures 57 and 58. Cisplatin linear regression results for Total Area and % Area for the Sh Cell line.

3.4.3. *Clonogenic Experiments Treated with Lu-177 Labeled Antibodies*

Due to limited access to Lu-177, only one of the three cell lines that were selected as candidates for further experimentation, AxA, was assessed due to this cell line's similar EGFR1 and EGFR2 expression levels. The AxA cell line was treated with Lu-177 radiolabeled cetuximab + trastuzumab combined, and Lu-177 radiolabeled IgG with DOTA as the chelator. Due to limited access to Lu-177, the first experiment performed with the lower concentrations of radiolabeled antibodies' method was not optimal, and due to the control plates being stored in a separate incubator than experimental plates, the results were mostly likely confounded. The amount of added radioactivity also should have been equivalent across the IgG and cetuximab + trastuzumab conditions, as well as the specific activities. The high concentration of Lu-177 labeled antibodies (7 nM cetuximab + trastuzumab and 8 nM IgG) and low concentration (0.5 nM for both) were compared with the 0 nM control condition. A radiolabeling summary for the first experiment can be seen in Table 11 for the cetuximab + trastuzumab (CT) and IgG conditions. Data analyzed by One-Way ANOVA for the response variable 'Count' for Lu-177-labeled cetuximab + trastuzumab, and Lu-177-labeled IgG for the first experiment can be found in Tables 12 and 13.

Antibody	**Concentration (ug/mL)**	**Fraction (uCi/mL)**	**Specific Activity (uCi/ug)**	**iTLC Purity**
CT	11.44	175	15.30	84%
IgG	10.06	225	22.36	81%

Table 11. Summary of Lu-177 radiolabeling result for first Lu-177 experiment.

ANOVA Table for the Effect of Different nM Concentrations of Lu-177-Cetuximab + Trastuzumab (CT) on Colony Count					
Count	Df	Sum Sq	Mean Sq	F value	Pr(>F)
Concentration CT (nM)	2	338.7	169.33	2.051	**0.21**
Residuals	6	495.3	82.56		

Table 12. ANOVA table for the effect of different nM concentrations of Lu-177 labeled cetuximab + trastuzumab on colony count.

ANOVA Table for the Effect of Different nM Concentrations of Lu-177-IgG on Colony Count					
Count	Df	Sum Sq	Mean Sq	F value	Pr(>F)
Concentration IgG (nM)	2	106.9	53.44	0.857	**0.47**
Residuals	6	374	62.33		

Table 13. ANOVA table for the effect of different nM concentrations of Lu-177 labeled IgG on colony count.

For the second Lu-177 experiment that followed a more optimized radiolabeling protocol, a higher concentration of radiolabeled antibodies was achieved (68.5 nM applied to cells for both the CT and IgG conditions), as well as more equivalent specific activities and treatment conditions. A summary of the radiolabeling results for both the Lu-177-CT and Lu-177-IgG conditions can be seen in Table 14 for the second Lu-177 experiment. The AxA cell line was used again and treated with Lu-177 radiolabeled CT and Lu-177 radiolabeled IgG with DOTA as the chelator, with an 8.5-fold increase in concentration compared to the initial Lu-177 experiment. There was also the addition of different time points, and treatments were allowed to incubate with cells for 1, 12, and 24 hours. Data was analyzed in RStudio at each time-point using Kruskal Wallis, with Dunn's test for post-hoc analysis. Descriptive statistics can be seen in Table 15 and a summary of the statistical analysis and post-hoc tests can be found in Tables 16 and 17. Box plots visualize the distribution of cell count and total area measurements across different treatment groups (Lu177-CT, Lu177-IgG, Control) at various time points. Box plots are representing the central tendency and spread of the data, the median, interquartile range (IQR), and outliers. The response variables 'Count' and 'Total Area' were included in analysis. These graphs (created using Biorender) can be found in Figures 59 to 64.

Antibody	Concentration (ug/mL)	Fraction (uCi/mL)	Specific Activity (uCi/ug)	iTLC Purity
C/T	2211	62300	28.18	97%
IgG	2381.6	65000	27.29	95%

Table 14. Summary of Lu-177 radiolabeling result for the second Lu-177 experiment.

Count					
1 Hour	***Minimum***	***25th percentile***	***Median***	***75th percentile***	***Maximum***
Lu-177-CT (68.5 nM)	98	98	104	105	105
Lu-177-IgG (68.5 nM)	106	106	109	115	115
Control	99	105.75	109	116.5	124
12 Hours	***Minimum***	***25th percentile***	***Median***	***75th percentile***	***12 Hours***
Lu-177-CT (68.5 nM)	78	78	79	89	89
Lu-177-IgG (68.5 nM)	64	64	94	95	95
Control	86	89	93.5	98.25	105
24 Hours	***Minimum***	***25th percentile***	***Median***	***75th percentile***	***Maximum***
Lu-177-CT (68.5 nM)	61	61	62	72	72
Lu-177-IgG (68.5 nM)	63	63	69	71	71
Control	100	100.75	107	114.75	120
Total Area					
1 Hour	***Minimum***	***25th percentile***	***Median***	***75th percentile***	***Maximum***
Lu-177-CT (68.5 nM)	16500	16500	18621	21469	21469
Lu-177-IgG (68.5 nM)	17692	17692	17692	25416	25416
Control	16800	17086.5	21458	25637.5	27373
12 Hours	***Minimum***	***25th percentile***	***Median***	***75th percentile***	***Maximum***
Lu-177-CT (68.5 nM)	9057	9057	9572	9892	9892
Lu-177-IgG (68.5 nM)	7289	7289	8813	10107	10107
Control	19562	19692.5	22249	23055.25	24619
24 Hours	***Minimum***	***25th percentile***	***Median***	***75th percentile***	***Maximum***
Lu-177-CT (68.5 nM)	3744	3744	5390	6466	6466
Lu-177-IgG (68.5 nM)	3696	3696	3905	5562	5562
Control	15426	18354.75	23116.5	25099	25219

Table 15. Descriptive statistics for Kruskal Wallis analysis for Count and Total Area.

Time Point	Variable	Kruskal-Wallis (H) Statistic	df	p-value	Significant? (p < 0.05)
1 hour	Count	4.603	2	0.1001	No
	Total Area	0.733	2	0.693	No
12 hours	Count	3.766	2	0.1521	No
	Total Area	8.423	2	**0.0148**	**Yes**
24 hours	Count	8.423	2	**0.0148**	**Yes**
	Total Area	8.423	2	**0.0148**	**Yes**

Table 16. Kruskal-Wallis test results.

12 Hour Total Area		
Comparison	**Adjusted p-value**	**Significant? (p < 0.05)**
Control vs. Lu-177 CT	0.0155	Yes
Control vs. Lu-177 IgG	0.0054	Yes
Lu-177 CT vs. Lu-177 IgG	0.367	No
24 Hour Count		
Comparison	**Adjusted p-value**	**Significant? (p < 0.05)**
Control vs. Lu-177 CT	0.0054	Yes
Control vs. Lu-177 IgG	0.0155	Yes
Lu-177 CT vs. Lu-177 IgG	0.367	No
24 Hour Total Area		
Comparison	**Adjusted p-value**	**Significant? (p < 0.05)**
Control vs. Lu-177 CT	0.0155	Yes
Control vs. Lu-177 IgG	0.0054	Yes
Lu-177 CT vs. Lu-177 IgG	0.367	No

Table 17. Dunn's Test results.

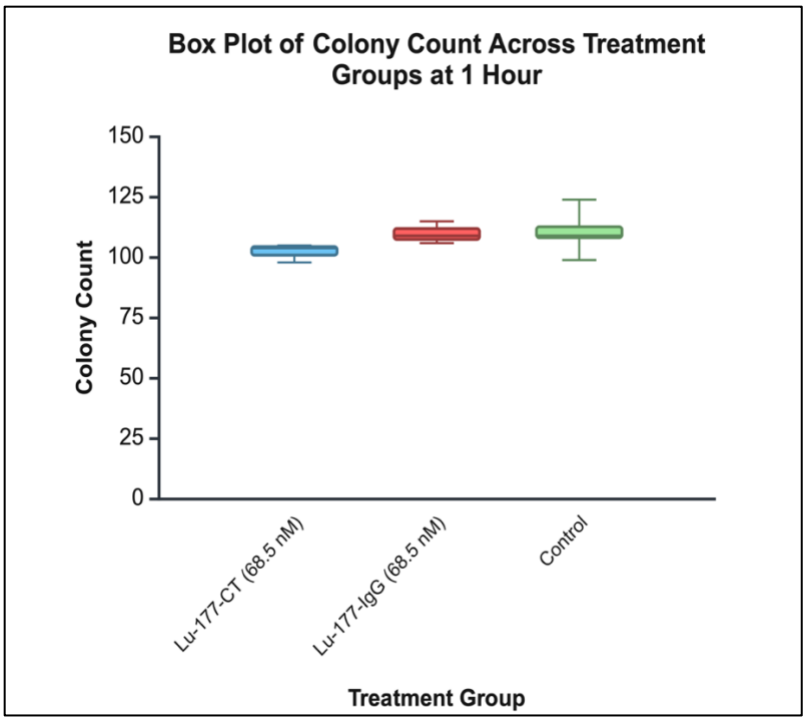

Figure 59. Box plot of colony count after 1 hour incubation per treatment.

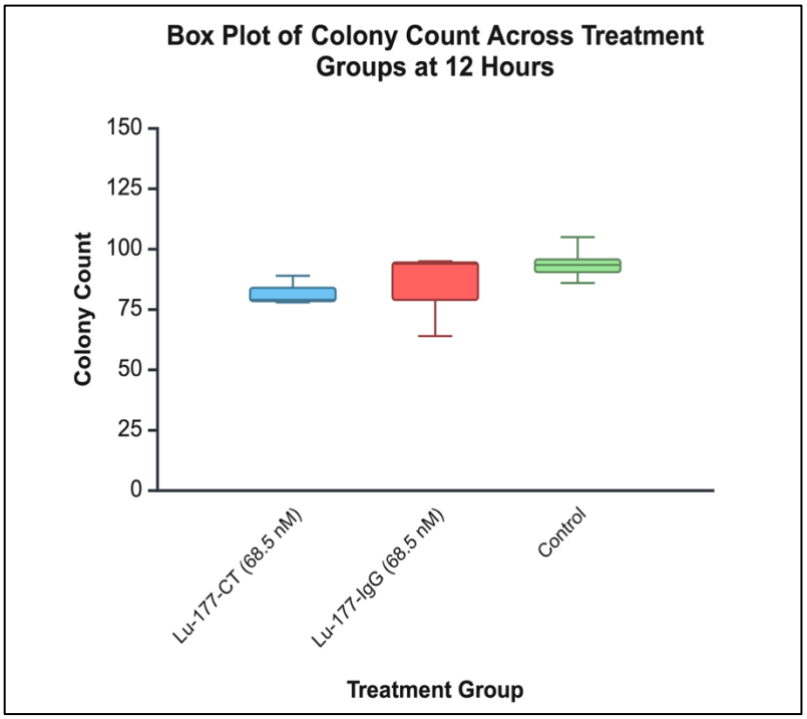

Figure 60. Box plot of colony count after 12 hours of incubation per treatment.

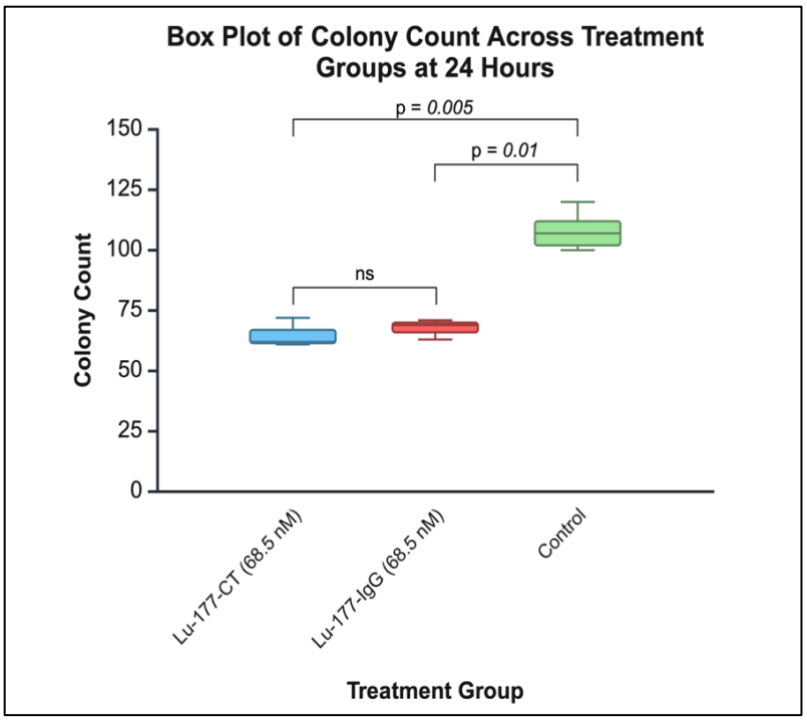

Figure 61. Box plot of colony count after 24 hours of incubation per treatment.

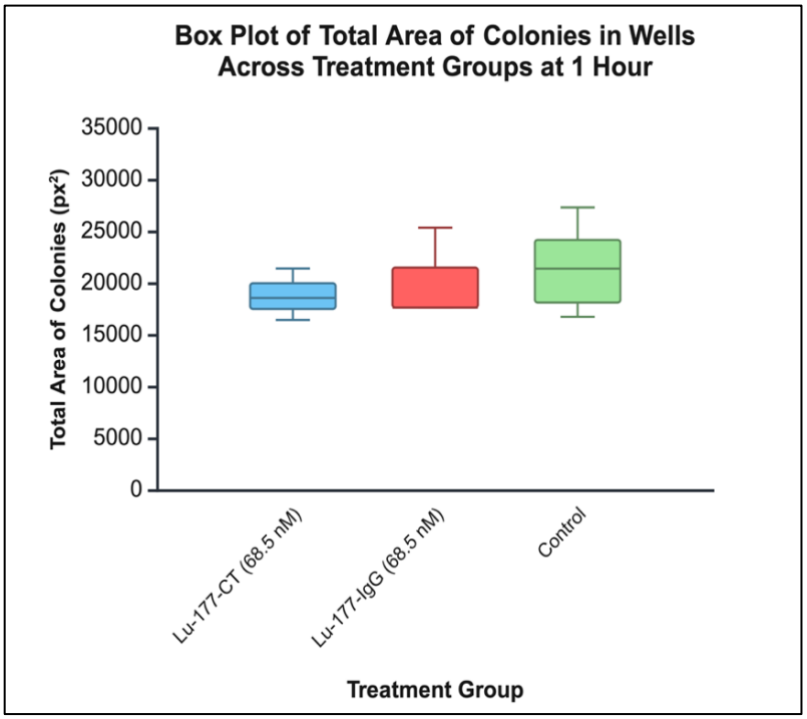

Figure 62. Box plot of total area of colonies after 1 hour of incubation per treatment.

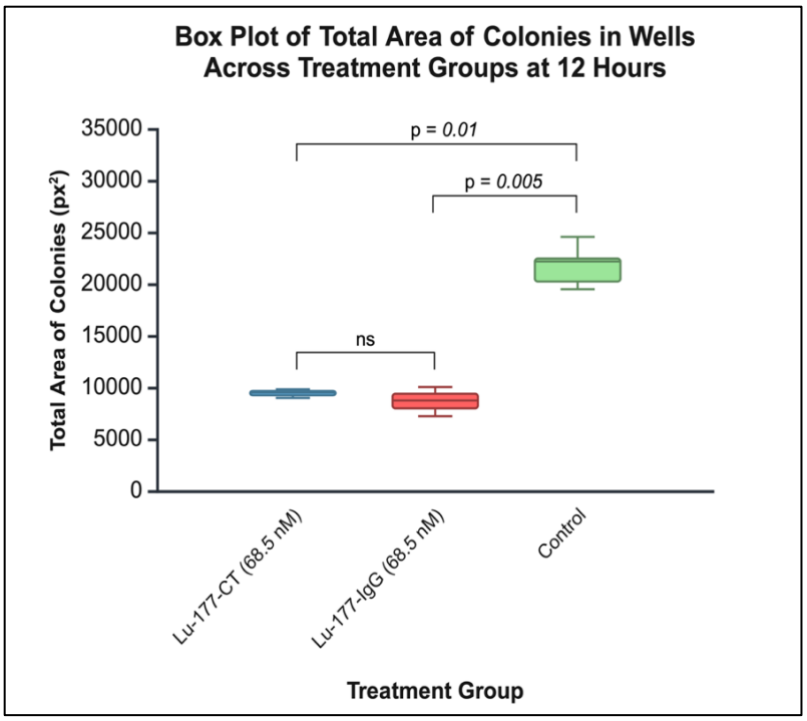

Figure 63. Box plot of total area of colonies after 12 hours of incubation per treatment.

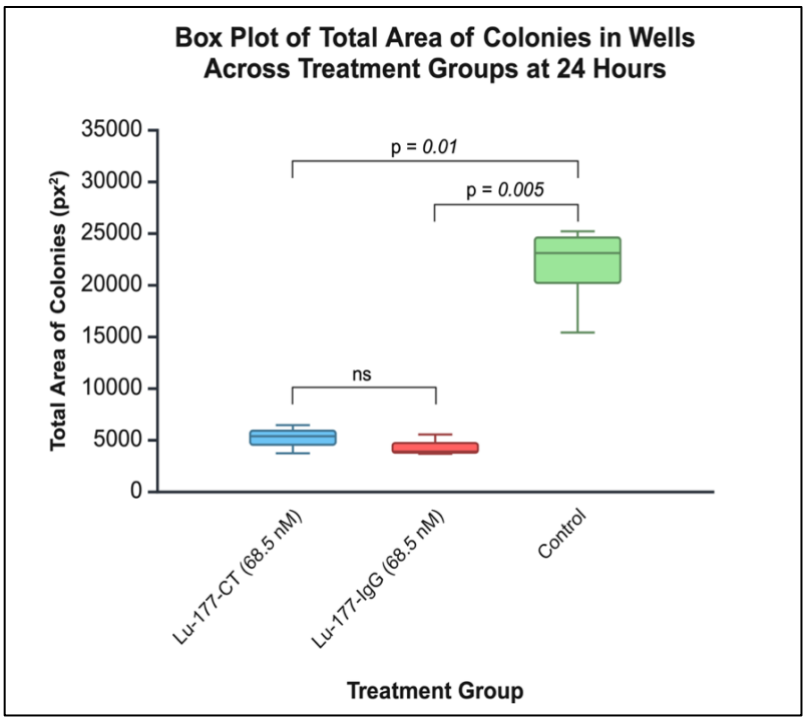

Figure 64. Box plot of total area of colonies after 24 hours of incubation per treatment.

4. DISCUSSION

4.1. Radiolabeling Antibodies and Estimates of Quantifications of Receptors

4.1.1. Radiolabeling with Tc-99m

FDA-approved monoclonal antibodies cetuximab and trastuzumab were used to assess binding affinity and binding saturation values of canine bladder cancer cell lines established from tumors from four different pet dogs (115). Antibodies were radiolabeled with Tc-99m to track specific binding to EGFR1 and EGFR2 receptors expressed by each cell line, and to determine the binding affinities of the receptor/ligand interactions. To ensure optimal experimental conditions and accurate results, Tc-99m was confirmed to be pure and stably bound to each antibody before applying it to the cells for binding experiments. Purity was determined by iTLC, where the percentage of radiation bound to antibody was calculated using the equation Tc-99m bound antibody / (Tc-99m bound antibody + free Tc-99m) x 100%. iTLC results at or above 95% were pure enough for cell experiments, and percentages less than that were rejected for further use. Across 19 independent binding experiments performed for this thesis, 97% +/- 0.04 and 97% +/- 0.05 were the average +/- STDEV values for the iTLC percentages of Tc-99m bound to cetuximab and trastuzumab respectively. The low variability across different days shows that the Tc-99m radiolabeling procedure is consistent and effective.

4.1.2. Radiolabeling with Lu-177 Required Optimization

Cetuximab and trastuzumab, targeting EGFR1 and EGFR2, were radiolabeled with Lutecium-177 (Lu-177) and applied *in vitro* through colony formation assays to evaluate the isotope's potential for targeted cancer therapy by assessing colony growth inhibition of canine bladder cancer cell lines from single cells. Both antibodies were co-administered to mimic the proposed real-life dual-treatment that would be given to pet dogs during trials. IgG, an isotype matched control antibody that does not bind the specific antigens of interest, was also radiolabeled with Lu-177. This control was to differentiate whether the effect of radiolabeled cetuximab + trastuzumab was due to specific receptor targeting rather than off-target radiation. An alpha-emitting isotope was originally proposed as the first choice for these experiments, as opposed to Lu-177 labeled antibodies (beta-emitting), but due to difficulty sourcing an alpha-emitting isotope, Lu-177 was used as a more practical option due to its convenient cost, availability, and clinical relevance. The Lu-177 radiolabeling process is a developable, technique-driven process, hence the differences in purity

yield across the first and second experiments. Protocol optimization, practice, and gained experience proved to be effective in improving results.

Two experiments done on two different days assessed the effectiveness of the Lu-177 labeled antibodies. For the first experiment, two different concentrations of Lu-177, a 7 nM and 8 nM concentration, and 0.5 nM and 0.5 nM concentration of labeled CT and IgG antibodies, respectively, were tested to determine if there were differences in growth inhibition after one hour of incubation. For the second study, cells were treated with a higher concentration of Lu-177-Abs than the highest concentration of the first experiment, and the radiation treatment was washed off cells after three different time points to determine if (1) a higher dose of radiation was necessary for more optimal colony formation inhibition and (2) if the amount of time that the treatment is exposed to cells affected colony inhibition. Prior to applying radiolabeled antibodies to cells, purity (%) was assessed by iTLC to confirm that Lu-177 was appropriately bound to each antibody. Percent purity was calculated with the equation: Lu-177 bound antibody / (Lu-177 bound antibody + free Lu-177) x 100%. Results above 80% were considered pure enough for the first experiment. The reason for this lower purity was due to it being the first Lu-177 radiolabeling performed for these studies, and how more experience was needed for better results. Since this was a new radioactive material in the lab, the process required optimization, and practice to achieve higher purity in the later experiment. Due to limited opportunities for experimental trials with Lu-177, the first experiment was conducted with lower purity to gain experience. iTLC purity values for the initial experiment were 84% for Lu-177-cetuximab + trastuzumab and 81% for Lu-177-IgG.

For the second experiment performed with the optimized protocol, a scale-down test was done for practice prior to the radiolabeling on the day of the cell experiment. Results from the optimized protocol yielded 97% purity for two attempts of cetuximab + trastuzumab labeling, and 95% for one attempt of IgG labeling. These improved results show that optimization of the radiolabeling protocol and more practice was needed for better results, and that better purity was reproducible after adjustments to the first protocol were made and once experience was gained.

4.1.3. Experimental Kd (Estimated Binding Affinities)

The dissociation constant (Kd) quantifies the binding affinity of a ligand for its receptor at equilibrium. A lower nM Kd value indicates higher binding affinity, as it reflects the ratio of the antibody dissociation rate to antibody association rate, and therefore the smaller the Kd, the greater the binding affinity of the ligand for its target antigen(123). This study used specific binding

experiments with Tc-99m to determine the Kd of cetuximab and trastuzumab to EGFR1 and EGFR2 receptors expressed by canine bladder cancer cell lines. The binding assays done for this thesis were conducted at 37°C to mimic physiological conditions of future *in vivo* studies, where the targeted radiotherapeutic would be at body temperature. The Tc-99m specific binding protocol allowed for the quantification of the Kd of antibodies for their receptors of interest across all K9UTC cell lines. For three of the cell lines (Org, Nk, and AxC), Kd of cetuximab for EGFR1 was found to be unstable across multiple independent experiments, which could indicate that cetuximab does not consistently or stably bind EGFR1. However, for cell lines where stable binding was observed, the Kd (mean+/-STDEV) for Tc-99m-cetuximab binding to EGFR1 was 7.63 +/- 3.69 nM and for Tc-99m-trastuzumab binding to EGFR2, 1.89 +/- 0.48 nM. A Kd < 10 nM is generally considered as high affinity binding (123). Results suggest that both targeting antibodies, on average, have high affinity for their respective receptors under the experimental conditions, with Tc-99m-trastuzumab having a stronger interaction with EGFR2 compared to Tc-99m-cetuximab with EGFR1.

A reason for the difference in affinity between cetuximab binding to EGFR1 and trastuzumab binding to EGFR2 could be variation in canine and human epitope regions. Existing literature indicates that the human and canine cetuximab epitope differs by 4 amino acids: Lys443 is replaced by Arg, Ser468 by Asn, Gly471 by Asp, and Asn473 by Lys in canines. In terms of the trastuzumab binding site, the human and canine epitope region differs by only 1 amino acid – Pro557 to Ser in canines (124). These differences suggest that cetuximab's reduced cross-species binding may result from epitope divergence, and that trastuzumab maintains higher affinity due to greater epitope conservation between species. The affinity data from these experiments agrees with this notion and demonstrate that cetuximab and trastuzumab have the ability stably bind to canine EGFR1 and EGFR2 receptors, albeit with reduced affinity in some cell lines regarding cetuximab and supports the possibility of using them as targeting molecules for radiotherapy in a canine clinical setting.

4.1.4. Binding (Bmax) Results for Each Canine Bladder Cancer Cell Line

The Bmax values from binding experiments showed variation in EGFR1 and EGFR2 receptor expression across the canine bladder cancer cell lines. For the AxA cells, receptor expression was moderate and similar for both cetuximab binding EGFR1 (average = 1.84×10^3, n=2) and trastuzumab binding EGFR2 (average = 2.02×10^3, n=3). For AxC, cetuximab binding was too

low to determine a reliable receptor number by Tc-99m binding experiments. Trastuzumab binding was detected (average = 6.30×10^2, n=2), at lower levels than AxA cells. Differences in receptor expression between these two cell lines, despite their shared origin, emphasizes tumor heterogeneity. For the Org cells, trastuzumab binding (average = 2.65×10^3, n=3) was higher than cetuximab (average = 2.02×10^2, n=2). For Nk cells, trastuzumab binding EGFR2 was the highest of all cell lines (average = 3.28×10^3, n=2), and cetuximab binding EGFR1 showed weak and inconsistent receptor expression (average = 7.60×10^2, n=2). Sh cells showed the highest levels of cetuximab binding (average = 2.85×10^3, n=2), while trastuzumab binding was lower (average = 1.19×10^3, n=2.

Variability in Bmax values across independent experiments for some cell lines likely reflected the unstable binding affinity mentioned earlier, which make it more challenging to accurately quantify the cetuximab-EGFR1 interaction and receptor expression. Bmax values are not reliably reported for cell lines where the Kd for cetuximab binding to EGFR1 was undetected by the Tc-99m binding experiments (Org, Nk, and AxC). This could be due to low receptor densities, resulting in similar levels of binding in the blocked and total-binding conditions in the assays, and thus a low signal to noise ratio. Saturation binding experiments tend to be contaminated with "noise," from interactions with non-specific binding sites (125), and when this noise is measured at a comparable signal to low specific binding signal due to low receptor density, calculation of Bmax and Kd are likely unreliable. Furthermore, high affinity is required for a high signal to noise ratio when there are low receptor densities, however in the case of cell lines Org, Nk, and AxC, undetected binding affinity of cetuximab could be the result of divergence of canine and human binding epitope of EGFR1 by four amino acids (124). Accurate measurement of Bmax and binding affinity Kd may be unattainable below a certain number of receptors with radioligand binding experiments, when there is poor binding affinity for these receptors, or without further optimization to the experiment (124–126). Other methods, like flow cytometry experiments, and/or using a cananized version of cetuximab (can225IgG) that has better binding affinity to EGFR1 expressed by canine cell lines, may yield more accurate results (117).

Furthermore, tumor cell characteristics *in vitro* are known to evolve over time. Although certain cancer hallmarks may remain stable, extended passaging can lead to notable phenotypic drift, including changes in antigen expression(127,128). This may have implications for EGFR1 related studies, as shown in a study of NCI-H125 non-small cell lung carcinoma cells, where EGFR

surface expression remarkably declined with increasing passage numbers(129). In this thesis, all canine bladder cancer cell lines were delivered to the lab at later passages (p); AxA (p38), Sh (p31), Org (p36), Nk (p69), and AxC (p25). Higher passage numbers for the tested cell lines raises the possibility that long-term culture may have contributed to reduced EGFR1 surface expression or altered receptor binding accessibility. Although the impact of passage number influencing cetuximab binding these cell lines has not yet been directly tested, these factors may explain the undetectable binding and affinities observed in the Org, Nk, and AxC cell lines in addition to the lack of complete epitope conservation between species for the EGFR1 receptor.

In terms of results of appropriate affinity and expression, differences in Bmax do indeed emphasize the substantial heterogeneity in receptor expression across different bladder cancer cell lines. The comparison between AxA and AxC is particularly interesting, where despite their shared tumor origin, there are distinctly different receptor expression and affinity profiles and tumor heterogeneity. This heterogeneity observed in K9UTC cell lines parallels the variability found in human bladder cancer and supports the notion of applying both antibodies in combination to increase the recruitment of radiotherapeutic-bound targeting agents to cancer cells (118).

4.1.5. Comparison of Binding Studies with Flow Cytometry

Due to high variability in some cell lines and receptors, where receptor expression was suggested to be minimal or none, it is likely that binding experiments might not have been the optimal method to reliably detect lower levels of specific binding and receptor expression due to low signal to noise ratio (125,126). When receptor expression is minimal, the bound dose of Tc-99m might be weaker and harder to distinguish from nonspecific binding conditions. To address this limitation, flow cytometry offers a single-cell approach, enabling a more detailed confirmation of binding levels. This method allows for distinguishing between populations that might otherwise go undetected in the binding experiments that assess cells in bulk. Previous literature supports the findings from binding experiments regarding EGFR1 expression of the AxA, Sh, and Org cell lines with flow cytometry (116). Radioligand binding experiments agreed with results yielded by Nagaya *et al.*, with Org exhibiting minimal expression, AxA showing low expression, and Sh with intermediate to high expression of EGFR1. Due to time constraints, flow cytometry experiments were not able to be optimized or replicated before the completion of this thesis. Data for the AxC cell line from the titration experiment that suggested that it could not be used as a negative control and led to the belief that the results from the binding experiments do not reliably detect low levels

of binding, as discussed in the previous section. Although there was insufficient time to perform additional flow cytometry experiments before the completion of this thesis, further investigation is warranted. This should include analysis of receptor expression in the remaining cell lines, with an additional focus on EGFR2 expression, to more comprehensively assess the potential for targeted therapies in canine models.

4.2. Colony Formation Assay Sterility Optimization

Ensuring sterility while also maintaining protein integrity of the antibodies during filtration was critical for experimental consistency and successful data acquisition. During initial experiments, unexpected contamination was observed in antibody-only treated wells, which prompted investigation into potential sources. A mini-experiment was conducted to assess possible sources of contamination with materials used during cell experiments; old and new DMEM/F12 media, PBS alone, a 1:1 mixture of media and PBS, antibodies resuspended in PBS, and bath water from the incubator where cells were stored. Contamination was isolated to the wells with the antibodies and indicated that they were the source of contamination and required sterilization before use. Sterilization by filtration required optimization. Initially, 25 mm nylon filters were the available option, but these were unsuitable for sterilizing concentrated antibody stocks due to the low volume of the stocks (200 to 300 µL). An alternative approach, treating media with antibodies, filtering the media with the 25 mm nylon filters, and then applying it to cells, was considered. However, this method prevented post-filtration concentration measurement with the Nanodrop or with Bradford Protein Assay due to the presence of additional proteins and color of the media. To address these limitations, smaller filters capable of passing low-volume antibody stocks while allowing for concentration measurement post-filtration were needed. One paper guided the decision to select 4 mm PVDF membrane filters, which proved to be effective (130). These filters allowed for filtration of the entire 200 to 300 µL volume of the antibody stocks in PBS with minimal loss of volume and protein. After filtering the entire volume of antibody stocks in PBS, an aliquot could be measured with the Nanodrop to determine concentration, which enabled accurate preparation for cell treatments at the experimental concentrations. With these new filters, contamination never reoccurred.

4.3. Using Cetuximab and Trastuzumab for Dual-Targeting of EGFR1 and EGFR2 for Radiotherapy

Muscle invasive bladder cancers in both dogs and humans show heterogeneity in EGFR1 and EGFR2 overexpression (118,131). EGFR1 and EGFR2 overexpression is observed in 70% and 60% of canine urothelial carcinoma cases, respectively, for dogs (80,132), and in humans EGFR1 overexpression is seen in 74%, and EGFR2 overexpression in about 40% of urothelial cancers (118) compared to negligible expression in healthy urothelium in both species (80,118). The use of a combination of cetuximab and trastuzumab could have more efficient targeting effects by covering a broader range of tumor cells with varying receptor expression levels. The first part of this study, where the receptor numbers were quantified across various canine bladder cancer cell lines supports the concept of tumor heterogeneity of these receptors, both across individual dogs and within the same tumor from the same dog. Quantification of the receptor levels across different cell lines was necessary for determining if cell lines qualified for targeted radiation studies. Understanding differences in receptor level expression also allows for assessment of potential responses to the targeted radiation therapy, or dosimetry to tumors, which would be important for developing more personalized treatment options for individual canine and human patients in the future. To limit toxicity to healthy bladder tissue and to ensure that targeted radiation therapies to deliver proper dosimetry levels to tumors, it is important that targeted receptors are overexpressed in tumor cells relative to healthy cells, though this distinction has been observed in both canine and human bladder cells(80,133).

4.4. Effect of Unradiolabeled Antibodies

Experiments with unlabeled antibodies were conducted to determine whether the combined unlabeled antibodies had any therapeutic effect sans radiation therapy and aimed to assess whether significant dose-dependent effects could be observed. Increasing concentrations of cetuximab + trastuzumab did not consistently inhibit colony formation across the different cell lines under the tested conditions. When effects were observed, they were some of the times and very modest. Regression analysis of the Count variable in antibody-only assays demonstrated inconsistent statistical significance across experiments. Significant effects were observed in one out of three experiments for the AxA and Nk cell lines (the Sh cell line did not have any significant effects in any experiments) after one hour of incubation. Regression analysis for the other response variables like total area, average size, and percent area also revealed inconsistent statistical significance

across independent experiments for the AxA and Nk cell lines (and again, no significance was observed for the Sh cell line in any experiments) after one hour of incubation. Further experiments conducted on the AxA cell line with antibodies alone across three incubation time points (1 hour, 12 hours, and 24 hours) at 68.5nM of cetuximab and trastuzumab combined also did not inhibit colony formation. These studies served as confirmation that cetuximab and trastuzumab themselves are not responsible for any killing or growth inhibition effects in the targeted radiation studies for these cell lines, and that any effects observed during radiolabeled experiments are because of radiation emission.

Cetuximab and trastuzumab both target receptor tyrosine kinases (RTKs) EGFR1 and EGFR2, which are transmembrane proteins involved in key cellular signaling pathways that promote cancer (for example, PI3K/AKT, RAS/MAPK/ERK, JAK/STAT) (134,135). RTKs consist of an extracellular ligand binding domain, a single transmembrane helix, and an intracellular tyrosine kinase domain that initiate downstream signaling upon phosphorylation (135). The cetuximab and trastuzumab bind to the external binding domain of their receptors with higher affinity than natural ligands, preventing activation events that lead to homodimerization or heterodimerization with other EGFR family members (136,137). The absence of treatment effects *in vitro* suggest that additional mechanisms may be involved allowing these canine bladder cancer cell lines to persist despite treatment with these antibodies. It is possible that downstream signaling remained active independent of the upstream active blockade by antibody treatment. This could be due to resistance mechanisms that have been well documented in cancers, like gain-of function mutations, constitutive receptor activation, or ligand-independent autophosphorylation (134,135,138). Both cetuximab and trastuzumab are FDA-approved for the treatment of various human cancers, however, despite their effectiveness in clinical cases, resistance to these therapies have been reported (139,140). In canines, Lapatinib has proven to be an effective RTK dual inhibitor by selectively targeting EGR1 and EGFR2 tyrosine kinases (131). Lapatinib is a small molecule tyrosine kinase inhibitor, and its mechanism differs from that of cetuximab and trastuzumab, as it functions intracellularly by competing with ATP for the ATP-binding domain, preventing phosphorylation and subsequent downstream effects that lead to cancer progression (141). Resistance to Lapatinib has been reported and is suggested to be a result of constitutive activation of MAPK and PI3K/AKT/mTOR signaling pathways (142).

Overall, these resistance mechanisms emphasize the complexity of targeting RTKs for cancer therapy and suggest that the canine bladder cancer cell lines used in this study may possess similar resistance mechanisms, although further testing is necessary to confirm these suspicions. Therefore, it may be important to consider both extracellular and intracellular targeting for future therapeutic strategies to amplify the effectiveness of targeting EGFR1 and EGFR2 receptors, and to consider that resistance mechanisms may still persevere in some cases.

4.5. Cisplatin Control Results

For comparison, cisplatin, a platinum-based chemotherapeutic agent with proven efficacy in treating both human and canine muscle invasive bladder cancer (121) served as a positive control for assessing the impact on clonogenic survival in comparison with targeted radiotherapy. The AxA, Nk, and Sh cell lines all showed a dose-dependent effect to increasing concentrations of cisplatin across multiple independent experiments. These results were originally intended to be compared with treatment from a targeted alpha-emitting isotope (Pb-214/Bi-214), to assess whether there was a comparable effect to chemotherapy. Due to supply issues, experiments using alpha-particle therapy were not completed before the writing of this thesis due to supply issues and the inability to acquire an alpha-emitting isotope for experimentation. With a more targeted approach, it is expected that alpha-particle therapy will be a more specific option for killing cancer cells than chemotherapeutic agents and could eventually improve treatment options for canine and human patients with bladder cancer. In the future, alpha-particle therapy will be compared with cisplatin results. The Lu-177 therapy, although it exhibited some killing effect on the tested cell lines over later time-points, did not appear to be as effective as cisplatin, although these results were expected and will be discussed in a later section.

4.6. Targeted Radiation Therapy for Bladder Cancer: Alpha vs. Beta Emitting Isotopes

Targeted radiation therapies have promising potential for treatment of bladder cancer in both human and canine patients. Although external beam radiation therapy (EBRT) is not commonly used as a first line of defense in human bladder cancer patients, it has some benefits as it can alleviate some of the negative symptoms related to the disease but has the potential for added toxicity(143), it is routinely used in canine patients where it has shown success in combination with other therapies(144–146). Targeted radiation approaches would be a more accurately delivered option that would reduce off-target toxicity to healthy tissues that are a concern of traditional radiation therapies (147,148). Seeing that radiation therapy is already accepted and

effectively administered to canine patients, it is reasonable to expect that improved outcomes would come from a targeted approach(144–146). In both canine and human patients receiving this therapy, the radiopharmaceutical would be installed intravesically, significantly reducing the probability of systemic toxicity (149). In a pilot study assessing Bi-213 (an alpha emitter) labeled cetuximab targeting EGFR1 in human patients with bladder cancer, intravesical administration yielded no adverse effects or toxicity to the bladder wall and showed therapeutic efficacy (150). The potential of intravesical targeted radiation as a safe and effective approach for advancing bladder cancer therapy is promising for both species.

Beta-emitting targeted cancer therapies with Lu-177 have already been approved for use in human patients, including LUTATHERA® for gastroenteropancreatic neuroendocrine tumors, and PLUVICTO® that targets specific biomarkers expressed by prostate tumors (151,152). Lu-177 targeted therapies are still in the early stages of development for use in veterinary oncology, though there is a growing interest in adapting these treatments for use in animals. Lu-177 emits a medium-energy beta particle and low-energy gamma photon as it decays and has a relatively longer half-life of 6.6 days (153). Its beta emission covers a longer range (average range = 0.23 mm in cells and tissues (154)) and has the potential to travel through multiple cancer cells, making it a good choice for treatment of tumor masses (153). The linear energy transfer (LET), or the average energy deposited by ionizing radiation per unit distance traveled, of beta emitters is lower than alpha emitters but can still induce single or double-stranded DNA breaks that may lead to apoptosis of targeted cells (151). The longer range and availability of Lu-177, as well as its clinical track record and affordability, made it a practical choice for this study's *in vitro* experiments.

Alpha-emitting isotopes, such as Pb-214/Bi-214 were the original choice for targeted radiotherapy for this thesis. Pb-214/Bi-214 have a relatively short half-life of 26.8/19.9 minutes and are the source of alpha particle emission that can cause significant and localized damage to targeted cancer cells. Alpha particles deposit high energy over short distances (~71 μm in cells and tissues (155)), causing significant and localized DNA damage that results in irreversible double stranded DNA breaks, making them highly effective at killing individual tumor cells while minimizing penetration into healthy surrounding cells (93). However, their potency can also present significant risks, and if an alpha emitting isotope is delivered to healthy tissues, even in small amounts, it could cause significant off-target toxicity damage to healthy cells due to its high LET (93). Therefore, precise targeting is essential for safe application. Pb-214/Bi-214 are increasingly being

explored for targeted radiation therapy, and offer potential advantages in killing tumor cells, however, these isotopes have not yet been approved for clinical application. Despite their potential, Pb-214/Bi-214 were unavailable for experimentation in this thesis project due to supply chain issues.

Although the use of alpha therapy was not possible for this study, it remains a promising direction for future studies. If successfully directed to cancer cells, alpha emitters could induce cancer cell death in a shorter amount of time and with more drastic effects than beta emitters. However, their toxicity and rapid decay necessitate careful delivery to avoid unintended harm to healthy cells and tissues. Future studies should investigate the potential of targeted alpha therapy for bladder cancer treatment, however, for this study Lu-177 provides an accessible option for assessing targeted beta radiotherapy *in vitro*.

4.7. Effect of Lu-177 Radiolabeled Antibodies

The cell line AxA had similar, intermediate expression of both EGFR1 and EGFR2 and was chosen for assessment of dual-targeting and results that did not favor either receptor's expression. Due to limited access to Lu-177, and protocol optimization, it was not feasible to administer the experimental treatment across all characterized cell lines.

The first experiment with the two lower concentrations of radiolabeled antibodies did not yield any significant results between experimental and control conditions. Additionally, results may have been confounded by control plates being stored in a different incubator than experimental plates, lower purity, and different specific activities between the cetuximab + trastuzumab (CT) and IgG conditions which could have affected colony formation outside of experimental conditions. Results from this experiment were not considered as reliable, and a second experiment was performed later with more stringent conditions for more reliable results.

The second Lu-177 experiment was conducted with a higher antibody concentration and radiation dose and incorporated an additional factor assessing effects across different treatment time-points, to acknowledge the slower decay rate of Lu-177, and to allow more time for decay events to occur to observe a therapeutic effect. Radiolabeling for the second experiment yielded higher purity, and specific activities across the CT and IgG condition were similar. The count and total area variables were analyzed to assess the colonies' proliferative abilities after receiving the radiotherapy. There were no significant differences observed after 1 hour of incubation across all conditions, likely due to the slower decay rate of the Lu-177 isotope. For the count variable, significant differences were

observed at the 24-hour time point (*p=0.01*). Post-hoc analysis showed that the Lu-177-cetuximab + trastuzumab (Lu-177-CT) condition had a lower colony count compared to the no treatment control condition with no antibodies or radiation (*p=0.005*) and the Lu-177-IgG condition did as well (*p=0.01*) when compared to the no treatment control condition. There was no significant difference in colony count between Lu-177-IgG and Lu-177-CT at any of the incubation time points.

There were also differences in the total area of the colonies covering wells between the Lu-177-CT and Lu-177-IgG conditions compared with the no treatment control condition, at 12 hours (*p=0.01*), and 24 hours (*p=0.01*), respectively. At the 12-hour time-point, post-hoc analysis showed that colonies from the Lu-177-CT condition had a significantly lower total area of colonies covering wells compared to the no treatment control condition (*p=0.01*) and significantly lower total area of colonies in the Lu-177-IgG condition compared to the no treatment control (*p=0.005*). The 24-hour post-hoc analysis for 'total area' showed that Lu-177-CT was significantly less than the control condition (*p=0.01*) at this time-point, and Lu-177-IgG too when compared to the no treatment control condition (*p=0.005*). There was no significant difference between Lu-177-IgG and Lu-177-CT for 'total area' at 12 and 24 hours. Results indicated that there is a time-dependent effect of Lu-177 for both the number of colonies and the total area of the colonies covering the wells, and this was expected due to the longer half-life of Lu-177. No significant differences were observed between the Lu-177-CT and Lu-177-IgG conditions at any time point. An additional binding experiment with Tc-99m-IgG for the AxA cell line was done to assess if IgG was binding nonspecifically at levels like cetuximab + trastuzumab binding and confirmed that IgG does not have any detectable binding to the AxA cell line suggesting that non-significant results across time points were not due to IgG nonspecifically binding to cells at higher levels than expected.

It is likely that the similar results across the Lu-177-CT and Lu-177-IgG conditions was due to the nature of the beta-particle therapy and experimental design. Lu-177 is well-suited for treating tumor masses, due to the beta emission's longer path length and modest energy deposition. These effects are beneficial for affecting more than one cell at a time. In these *in vitro* experiments, the intention was to apply a higher dose of radiation to see if cells were sensitive to Lu-177 emission in general. It is probable that the reduction in proliferation and lack of complete cell death overtime points reflects the therapeutic effects of Lu-177, rather than specific binding interactions. Treatment conditions were applied to a monolayer of single cells, and the concentration of added

radioligand was higher than the known amount needed to saturate 30,000 cells. Though it is possible that Lu-177-CT was being delivered and bound to the EGFR1 and EGFR2 receptors expressed on cells by the targeting agents (CT), there was likely more of the unbound dose present in the media and the extended path length of beta emission may have limited the specificity of its therapeutic effect to only the directly bound cells after washing. Nearby cells were likely affected by Lu-177 radiation emission bound to other cells, so the therapeutic effect may not have been restricted to CT-bound receptors. This could explain the reduced observable differences across the CT and IgG conditions. A limitation to this study is that the binding kinetics of these antibodies for these receptors expressed by the AxA cell line is unknown, and therefore it cannot be said when or if the radioligands became unbound to their receptors. Future investigation should include an assessment of how long the targeting molecules take residence at their receptors in addition to measuring the dose present in media that is being washed away.

It is expected that an alpha-emitting isotope would have a more distinct treatment effect between CT and IgG conditions due to its shorter and more powerful length of emission, which would make it more effective towards the cells where it is bound. Further investigation utilizing an alpha emitting isotope at appropriate concentrations for receptor saturation is warranted to better distinguish the effectiveness of targeted therapy in this experimental design when comparing it to the nonspecifically bound IgG control.

4.8. Canines Bladder Cancer as a Model for Radiotherapeutic Development

The shift from traditional murine models to naturally-occurring canine bladder cancer would provide an opportunity to investigate the proposed targeted therapeutic in a model that more accurately mimics the complexities of human bladder cancer, while also addressing the health needs of pet dogs who would benefit from more specific treatment. This study demonstrates variability in receptor expression among different canine bladder cancer cell lines, like what has been observed in human MIBC. The heterogeneity observed in EGFR1 and EGFR2 expression across different canine bladder cancer cell lines suggests that treatment responses may also vary and emphasizes the need for further investigation of the targeted radiotherapeutic with more of the K9UTC cell lines. Experimentation with an alpha-emitting isotope would also help to raise the impact of this therapy and improve its effectiveness in targeting tumor cells with an increased therapeutic effect, and to better differentiate between targeted and control conditions in *in vitro* experiments. The Lu-177 experiments were focused on a single canine bladder cancer cell line,

and additional research involving a wider variety of cell lines with different expression of EGFR1 and EGFR2 will be critical for confirming the broader applicability of this therapeutic approach. The use of Tc-99m-labeled cetuximab and trastuzumab for imaging prior to employing the targeted radiotherapeutic *in vivo* would be a practical step for identifying tumors with sufficient receptor expression for recruitment of targeted therapeutic isotopes. Pre-screening will also ensure that tumor cells would adequately bind radiotherapy and that dogs tolerate the antibodies treatment prior to administering a targeted radiotherapeutic, enhancing the likelihood of a successful outcome.

In conclusion, this project supports the importance of using accurate preclinical models for developing targeted radiotherapies. Overall, the findings from this project contribute to a broader understanding of receptor-targeted therapy in canine UTC, and the value of the dog as an accurate translational model. While further studies are needed to understand the full clinical relevance of applying targeted radiation therapy as treatment for canine UTC, the results presented in this thesis could provide a basis for continued investigation into novel targeted radiotherapeutics in veterinary that may eventually be translated to human medicine.

REFERENCES

1. Bray F, Ferlay J, Soerjomataram I, Siegel RL, Torre LA, Jemal A. Global cancer statistics 2018: GLOBOCAN estimates of incidence and mortality worldwide for 36 cancers in 185 countries. CA Cancer J Clin. 2018 Nov;68(6):394–424.

2. Saginala K, Barsouk A, Aluru JS, Rawla P, Padala SA, Barsouk A. Epidemiology of Bladder Cancer. Vol. 8, Medical sciences (Basel, Switzerland). NLM (Medline); 2020.

3. Jubber I, Ong S, Bukavina L, Black PC, Compérat E, Kamat AM, et al. Epidemiology of Bladder Cancer in 2023: A Systematic Review of Risk Factors. Vol. 84, European Urology. Elsevier B.V.; 2023. p. 176–90.

4. Shermadou ES, Rahman S, Stephen ;, Leslie W. Anatomy, Abdomen and Pelvis: Bladder. 2025.

5. What Is Bladder Cancer? - NCI. 2023 Feb 16 [cited 2025 Jan 27]; Available from: https://www.cancer.gov/types/bladder

6. American Cancer Society. Can Bladder Cancer Be Found Early? Questions to Ask About Bladder Cancer [Internet]. 2024 Mar. Available from: www.cancer.org/cancer/types/bladder-cancer/causes-risks-prevention/risk-

7. Cancer Research UK. Non muscle invasive bladder cancer staging | Cancer Research UK. 2023 Mar 7 [cited 2024 May 9]; Available from: https://www.cancerresearchuk.org/about-cancer/bladder-cancer/types-stages-grades/non-muscle-invasive

8. Babjuk M, Böhle A, Burger M, Capoun O, Cohen D, Compérat EM, et al. EAU Guidelines on Non–Muscle-invasive Urothelial Carcinoma of the Bladder: Update 2016. Eur Urol. 2017 Mar 1;71(3):447–61.

9. Nice. National Collaborating Centre for Cancer Bladder cancer Bladder cancer: diagnosis and management NICE Guideline 2 Bladder cancer: diagnosis and management Contents. 2015.

10. Guo X, Liu M, Hou H, Liu S, Zhang X, Zhang Y, et al. Impact of prostate cancer radiotherapy on the biological behavior and specific mortality of subsequent bladder cancer. Int J Clin Oncol. 2019 Aug 1;24(8):957–65.

11. Koutros S, Kogevinas M, Friesen MC, Stewart PA, Baris D, Karagas MR, et al. Diesel exhaust and bladder cancer risk by pathologic stage and grade subtypes. Environ Int. 2020 Feb;135:105346.

12. Yang F, Liu G, Wei J, Dong Y, Zhang X, Zheng Y. Relationship between Bladder Cancer, Nutritional Supply, and Treatment Strategies: A Comprehensive Review. Vol. 15, Nutrients. Multidisciplinary Digital Publishing Institute (MDPI); 2023.

13. Sommer BC, Dhawan D, Ratliff TL, Knapp DW. Naturally-Occurring Canine Invasive Urothelial Carcinoma: A Model for Emerging Therapies. Vol. 4, Bladder Cancer. IOS Press; 2018. p. 149–59.

14. Knapp DW, Glickman NW, Denicola DB, Bonney PL, Lin TL, Glickman LT. Naturally-occurring canine transitional cell carcinoma of the urinary bladder A relevant model of human invasive bladder cancer. Vol. 5, Urologic Oncology. 2000.

15. Knapp DW, Ramos-Vara JA, Moore GE, Dhawan D, Bonney PL, Young KE. Urinary bladder cancer in dogs, a naturally occurring model for cancer biology and drug development. ILAR J. 2014;55(1):100–18.

16. Fulkerson CM, Knapp DW. Management of transitional cell carcinoma of the urinary bladder in dogs: A review. Vol. 205, Veterinary Journal. Bailliere Tindall Ltd; 2015. p. 217–25.

17. Vilar FO, De Araújo LAP, Lima SVC. Total bladder replacement with de-epithelialized ileum. Experimental study in dogs. Vol. 30, International Braz J Urol Official Journal of the Brazilian Society of Urology. 2004.

18. Glickman LT, Raghavan M, Knapp DW, Bonney PL, Dawson MH. Herbicide exposure and the risk of transitional cell carcinoma in Scottish Terriers. J Am Vet Med Assoc. 2004 May 15;224.

19. Glickman LT, Schofer FS, McKee LJ, Reif JS, Goldschmidt MH. Epidemiologic study of insecticide exposures, obesity, and risk of bladder cancer in household dogs. J Toxicol Environ Health. 1989 Dec 1;28(4):407–14.

20. Zhang Z, Khederzadeh S, Li Y. Deciphering the puzzles of dog domestication. Zool Res. 2020;41(2):97–104.

21. Schiffman JD, Breen M. Comparative oncology: What dogs and other species can teach us about humans with cancer. Vol. 370, Philosophical Transactions of the Royal Society B: Biological Sciences. Royal Society of London; 2015.

22. Gray MM, Granka JM, Bustamante CD, Sutter NB, Boyko AR, Zhu L, et al. Linkage disequilibrium and demographic history of wild and domestic canids. Genetics. 2009 Apr;181(4):1493–505.

23. Vonholdt BM, Pollinger JP, Lohmueller KE, Han E, Parker HG, Quignon P, et al. Genome-wide SNP and haplotype analyses reveal a rich history underlying dog domestication. Nature. 2010 Apr 8;464(7290):898–902.

24. Dobson JM. Breed-Predispositions to Cancer in Pedigree Dogs. ISRN Vet Sci. 2013 Jan 17;2013:1–23.

25. Dewhirst MW, Page RL. Editorial: Emerging Translational Opportunities in Comparative Oncology with Companion Canine Cancers. Vol. 10, Frontiers in Oncology. Frontiers Media S.A.; 2020.

26. Garden OA, Volk SW, Mason NJ, Perry JA. Companion animals in comparative oncology: One Medicine in action. Vol. 240, Veterinary Journal. Bailliere Tindall Ltd; 2018. p. 6–13.

27. Ramsey SA, Xu T, Goodall C, Rhodes AC, Kashyap A, He J, et al. Cross-species analysis of the canine and human bladder cancer transcriptome and exome. Genes Chromosomes Cancer. 2017 Apr 1;56(4):328–43.

28. Walsh NC, Kenney LL, Jangalwe S, Aryee KE, Greiner DL, Brehm MA, et al. Humanized Mouse Models of Clinical Disease. Vol. 12, Annual Review of Pathology: Mechanisms of Disease. Annual Reviews Inc.; 2017. p. 187–215.

29. Connolly KA, Fitzgerald B, Damo M, Joshi NS. Novel Mouse Models for Cancer Immunology. Vol. 6, Annual Review of Cancer Biology. Annual Reviews Inc.; 2022. p. 269–91.

30. Zschaler J, Schlorke D, Arnhold J. Differences in Innate Immune Response between Man and Mouse. Vol. 34, Critical Reviews ™ in Immunology. 2014.

31. Ai M, Curran MA. Immune checkpoint combinations from mouse to man. Vol. 64, Cancer Immunology, Immunotherapy. Springer Science and Business Media Deutschland GmbH; 2015. p. 885–92.

32. Shultz LD, Brehm MA, Victor Garcia-Martinez J, Greiner DL. Humanized mice for immune system investigation: Progress, promise and challenges. Vol. 12, Nature Reviews Immunology. 2012. p. 786–98.

33. Hatogai K, Sweis RF. The Tumor Microenvironment of Bladder Cancer. In: Advances in Experimental Medicine and Biology. Springer; 2020. p. 275–90.

34. Bouchlaka MN, Murphy WJ. Impact of aging in cancer immunotherapy: The importance of using accurate preclinical models. Oncoimmunology. 2013;2(12).

35. Park JS, Withers SS, Modiano JF, Kent MS, Chen M, Luna JI, et al. Canine cancer immunotherapy studies: Linking mouse and human. Vol. 4, Journal for ImmunoTherapy of Cancer. BioMed Central Ltd.; 2016.

36. Holzapfel BM, Wagner F, Thibaudeau L, Levesque JP, Hutmacher DW. Concise review: Humanized models of tumor immunology in the 21st century: Convergence of cancer research and tissue engineering. Stem Cells. 2015 Jun 1;33(6):1696–704.

37. Ciociola AA, Cohen LB, Kulkarni P. How drugs are developed and approved by the FDA: Current process and future directions. Vol. 109, American Journal of Gastroenterology. Nature Publishing Group; 2014. p. 620–3.

38. Kobayashi T, Owczarek TB, McKiernan JM, Abate-Shen C. Modelling bladder cancer in mice: Opportunities and challenges. Vol. 15, Nature Reviews Cancer. Nature Publishing Group; 2015. p. 42–54.

39. De Visser KE, Eichten A, Coussens LM. Paradoxical roles of the immune system during cancer development. Vol. 6, Nature Reviews Cancer. 2006. p. 24–37.

40. Ozaki K, Sukata T, Uwagawa SVS, Seki T, Kawasaki H, Yoshitake A, et al. High Susceptibility of p53 (+/-) Knockout Mice in W-Butyl-W-(4-hydroxybutyl)nitrosamine Urinary Bladder Carcinogenesis and Lack of Frequent Mutation in Residual Allele [Internet]. Vol. 58, CANCER RESEARCH. 1998. Available from: http://aacrjournals.org/cancerres/article-pdf/58/17/3806/2467310/cr0580173806.pdf

41. Hamed S, Ne Larue H, Ne Hovington H, Girard J, Jeannotte L, Latulippe E, et al. Accelerated Induction of Bladder Cancer in Patched Heterozygous Mutant Mice [Internet]. Vol. 64, CANCER RESEARCH. 1938. Available from: http://aacrjournals.org/cancerres/article-pdf/64/6/1938/2523830/zch00604001938.pdf

42. Mitra AP, Pagliarulo V, Yang D, Waldman FM, Datar RH, Skinner DG, et al. Generation of a concise gene panel for outcome prediction in urinary bladder cancer. Journal of Clinical Oncology. 2009 Aug 20;27(24):3929–37.

43. Kim JH, Tuziak T, Hu L, Wang Z, Bondaruk J, Kim MS, et al. Alterations in transcription clusters underlie development of bladder cancer along papillary and nonpapillary pathways. Laboratory Investigation. 2005 Apr;85(4):532–49.

44. Riester M, Taylor JM, Feifer A, Koppie T, Rosenberg JE, Downey RJ, et al. Combination of a novel gene expression signature with a clinical nomogram improves the prediction of survival in high-risk bladder cancer. Clinical Cancer Research. 2012 Mar 1;18(5):1323–33.

45. Blaveri E, Brewer JL, Roydasgupta R, Fridlyand J, Devries S, Koppie T, et al. Bladder cancer stage and outcome by array-based comparative genomic hybridization. Clinical Cancer Research. 2005 Oct 1;11(19 I):7012–22.

46. Sanchez-Carbayo M, Socci ND, Lozano JJ, Li W, Charytonowicz E, Belbin TJ, et al. Gene discovery in bladder cancer progression using cDNA microarrays. American Journal of Pathology. 2003 Aug 1;163(2):505–16.

47. Dyrskjøt L, Thykjaer T, Kruhøffer M, Jensen JL, Marcussen N, Hamilton-Dutoit S, et al. Identifying distinct classes of bladder carcinoma using microarrays. Nat Genet. 2003 Jan 1;33(1):90–6.

48. Lindgren D, Frigyesi A, Gudjonsson S, Sjödahl G, Hallden C, Chebil G, et al. Combined gene expression and genomic profiling define two intrinsic molecular subtypes of urothelial carcinoma and gene signatures for molecular grading and outcome. Cancer Res. 2010 May 1;70(9):3463–72.

49. Zieger K, Marcussen N, Borre M, Ørntoft TF, Dyrskjøt L. Consistent genomic alterations in carcinoma in situ of the urinary bladder confirm the presence of two major pathways in bladder cancer development. Int J Cancer. 2009 Nov 1;125(9):2095–103.

50. Hurst CD, Platt FM, Taylor CF, Knowles MA. Novel tumor subgroups of urothelial carcinoma of the bladder defined by integrated genomic analysis. Clinical Cancer Research. 2012 Nov 1;18(21):5865–77.

51. Lindgren D, Sjödahl G, Lauss M, Staaf J, Chebil G, Lövgren K, et al. Integrated genomic and gene expression profiling identifies two major genomic circuits in urothelial carcinoma. PLoS One. 2012 Jun 7;7(6).

52. Sjödahl G, Lauss M, Lövgren K, Chebil G, Gudjonsson S, Veerla S, et al. A molecular taxonomy for urothelial carcinoma. Clinical Cancer Research. 2012 Jun 15;18(12):3377–86.

53. Gui Y, Guo G, Huang Y, Hu X, Tang A, Gao S, et al. Frequent mutations of chromatin remodeling genes in transitional cell carcinoma of the bladder. Nat Genet. 2011 Sep;43(9):875–8.

54. Ruan JL, Hsu JW, Browning RJ, Stride E, Yildiz YO, Vojnovic B, et al. Mouse Models of Muscle-invasive Bladder Cancer: Key Considerations for Clinical Translation Based on Molecular Subtypes. Vol. 2, European Urology Oncology. Elsevier B.V.; 2019. p. 239–47.

55. McKenna C, Poirier VJ, Oblak ML, Nykamp S, Mutsaers AJ. Reason for euthanasia in dogs with urothelial carcinoma treated with chemotherapy or radiation therapy or both: A retrospective observational study. J Vet Intern Med. 2024 Mar 5;38(2):1127–34.

56. Ahmad I, Sansom OJ, Leung HY. Exploring molecular genetics of bladder cancer: Lessons learned from mouse models. Vol. 5, DMM Disease Models and Mechanisms. 2012. p. 323–32.

57. Dow S. A Role for Dogs in Advancing Cancer Immunotherapy Research. Vol. 10, Frontiers in Immunology. Frontiers Media S.A.; 2020.

58. Withrow SJ, Khanna C. Bridging the gap between experimental animals and humans in osteosarcoma. In: Cancer Treatment and Research. 2009. p. 439–46.

59. Khanna C, Lindblad-Toh K, Vail D, London C, Bergman P, Barber L, et al. How to stay out of a BIND [Internet]. 2006. Available from: http://www.nature.com/naturebiotechnology

60. Tominaga M, Horiuchi Y, Kadosawa T. Flow Cytometric Analysis of Peripheral Blood and Tumor-Infiltrating Regulatory T Cells in Dogs with Oral Malignant Melanoma. Journal of Veterinary Diagnostic Investigation. 2010 May 1;

61. Goulart MR, Pluhar GE, Ohlfest JR. Identification of myeloid derived suppressor cells in dogs with naturally occurring cancer. PLoS One. 2012 Mar 13;7(3).

62. Murakami E, Shionoya T, Komenoi S, Suzuki Y, Sakane F. Cloning and characterization of novel testis-Specific diacylglycerol kinase η splice variants 3 and 4. PLoS One. 2016 Sep 1;11(9).

63. Chow L, Wheat W, Ramirez D, Impastato R, Dow S. Direct comparison of canine and human immune responses using transcriptomic and functional analyses. Sci Rep. 2024 Dec 1;14(1).

64. Bergman PJ, Camps-Palau MA, McKnight JA, Leibman NF, Craft DM, Leung C, et al. Development of a xenogeneic DNA vaccine program for canine malignant melanoma at the Animal Medical Center. Vaccine. 2006 May 22;24(21):4582–5.

65. Shapiro SG, Raghunath S, Williams C, Motsinger-Reif AA, Cullen JM, Liu T, et al. Canine urothelial carcinoma: genomically aberrant and comparatively relevant. Chromosome Research. 2015 Jun 15;23(2):311–31.

66. Meuten DJ, Meuten TLK. Tumors of the Urinary System. In: Tumors in Domestic Animals. Wiley; 2016. p. 632–88.

67. Learn About Bladder Cancer In Dogs | PetCure Oncology.

68. Shinagare AB, Ramaiya NH, Jagannathan JP, Fennessy FM, Taplin ME, Van den Abbeele AD. Metastatic Pattern of Bladder Cancer: Correlation with the Characteristics of the Primary Tumor. American Journal of Roentgenology. 2011 Jan;196(1):117–22.

69. Weinstein JN, Akbani R, Broom BM, Wang W, Verhaak RGW, McConkey D, et al. Comprehensive molecular characterization of urothelial bladder carcinoma. Nature. 2014;507(7492):315–22.

70. Decker B, Parker HG, Dhawan D, Kwon EM, Karlins E, Davis BW, et al. Homologous Mutation to Human BRAF V600E Is Common in Naturally Occurring Canine Bladder Cancer—Evidence for a Relevant Model System and Urine-Based Diagnostic Test. Molecular Cancer Research. 2015 Jun 1;13(6):993–1002.

71. Zhi Y, Ji H, Pan J, He P, Zhou X, Zhang H, et al. Downregulated XPA promotes carcinogenesis of bladder cancer via impairment of DNA repair. Tumor Biology. 2017 Feb 1;39(2):101042831769167.

72. Cekanova M, Uddin MdJ, Bartges JW, Callens A, Legendre AM, Rathore K, et al. Molecular Imaging of Cyclooxygenase-2 in Canine Transitional Cell Carcinomas *In Vitro* and *In Vivo*. Cancer Prevention Research. 2013 May 1;6(5):466–76.

73. Ristimäki A, Nieminen O, Saukkonen K, Hotakainen K, Nordling S, Haglund C. Expression of Cyclooxygenase-2 in Human Transitional Cell Carcinoma of the Urinary Bladder. Am J Pathol. 2001 Mar;158(3):849–53.

74. Wadhwa P, Goswami AK, Joshi K, Sharma SK. Cyclooxygenase-2 expression increases with the stage and grade in transitional cell carcinoma of the urinary bladder. Int Urol Nephrol. 2005 Mar;37(1):47–53.

75. Shariat SF, Karakiewicz PI, Godoy G, Karam JA, Ashfaq R, Fradet Y, et al. Survivin as a Prognostic Marker for Urothelial Carcinoma of the Bladder: A Multicenter External Validation Study. Clinical Cancer Research. 2009 Nov 15;15(22):7012–9.

76. Eissa S, Motawi T, Badr S, Zaghlool A, Maher A. Evaluation of Urinary Human Telomerase Reverse Transcriptase mRNA and Scatter Factor Protein as Urine Markers for Diagnosis of Bladder Cancer. Clin Lab. 2013;59(03+04/2013).

77. Millanta F, Impellizeri J, McSherry L, Rocchigiani G, Aurisicchio L, Lubas G. Overexpression of HER-2 via immunohistochemistry in canine urinary bladder transitional cell carcinoma - A marker of malignancy and possible therapeutic target. Vet Comp Oncol. 2018 Jun 4;16(2):297–300.

78. Chaux A, Cohen JS, Schultz L, Albadine R, Jadallah S, Murphy KM, et al. High epidermal growth factor receptor immunohistochemical expression in urothelial carcinoma of the bladder is not associated with EGFR mutations in exons 19 and 21: a study using formalin-fixed, paraffin-embedded archival tissues. Hum Pathol. 2012 Oct;43(10):1590–5.

79. Dhawan D, Paoloni M, Shukradas S, Choudhury DR, Craig BA, Ramos-Vara JA, et al. Comparative Gene Expression Analyses Identify Luminal and Basal Subtypes of Canine Invasive Urothelial Carcinoma That Mimic Patterns in Human Invasive Bladder Cancer. PLoS One. 2015 Sep 9;10(9):e0136688.

80. HANAZONO K, FUKUMOTO S, KAWAMURA Y, ENDO Y, KADOSAWA T, IWANO H, et al. Epidermal growth factor receptor expression in canine transitional cell carcinoma. Journal of Veterinary Medical Science. 2015;77(1):1–6.

81. Patronek GJ, Waters DJ, Glickman LT. Comparative Longevity of Pet Dogs and Humans: Implications for Gerontology Research. J Gerontol A Biol Sci Med Sci. 1997 May 1;52A(3):B171–8.

82. Dunst J. Textbook of Bladder Cancer Book Review. Int J Radiat Oncol Biol Phys. 2006 Sep;66(1):313.

83. Lei AQ, Cheng L, Pan C xian. Current treatment of metastatic bladder cancer and future directions. Expert Rev Anticancer Ther. 2011 Dec 10;11(12):1851–62.

84. Arnold EJ, Childress MO, Fourez LM, Tan KM, Stewart JC, Bonney PL, et al. Clinical Trial of Vinblastine in Dogs with Transitional Cell Carcinoma of the Urinary Bladder. J Vet Intern Med. 2011 Nov 13;25(6):1385–90.

85. Blumenreich MS, Yagoda A, Natale RB, Watson RC. Phase II trial of vinblastine sulfate for metastatic urothelial tract tumors. Cancer. 1982 Aug 1;50(3):435–8.

86. de Brito Galvao JF, Kisseberth WC, Murahari S, Sutayatram S, Chew DJ, Inpanbutr N. Effects of gemcitabine and gemcitabine in combination with carboplatin on five canine transitional cell carcinoma cell lines. Am J Vet Res. 2012 Aug;73(8):1262–72.

87. Weiner AB, Desai AS, Meeks JJ. Tumor Location May Predict Adverse Pathology and Survival Following Definitive Treatment for Bladder Cancer: A National Cohort Study. Eur Urol Oncol. 2019 May;2(3):304–10.

88. Hayes HM. Canine Bladder Cancer: epidemiologic features. Am J Epidemiol [Internet]. 1976 Dec;104(6):673–7. Available from: https://academic.oup.com/aje/article-lookup/doi/10.1093/oxfordjournals.aje.a112346

89. Hay M, Thomas DW, Craighead JL, Economides C, Rosenthal J. Clinical development success rates for investigational drugs. Nat Biotechnol. 2014 Jan 9;32(1):40–51.

90. Mullard A. The high, and redundant, cost of failure in cancer drug development. Nat Rev Drug Discov. 2023 Sep 4;22(9):688–688.

91. Thamm DH. Canine Cancer: Strategies in Experimental Therapeutics. Front Oncol. 2019 Nov 15;9.

92. Paoloni M, Khanna C. Translation of new cancer treatments from pet dogs to humans. Nat Rev Cancer. 2008 Feb;8(2):147–56.

93. Jadvar H. Targeted Radionuclide Therapy: An Evolution Toward Precision Cancer Treatment. American Journal of Roentgenology [Internet]. 2017 Aug;209(2):277–88. Available from: https://www.ajronline.org/doi/10.2214/AJR.17.18264

94. Zukotynski K, Jadvar H, Capala J, Fahey F. Targeted Radionuclide Therapy: Practical Applications and Future Prospects. Biomark Cancer. 2016 Jan 18;8s2:BIC.S31804.

95. Vermeulen K, Vandamme M, Bormans G, Cleeren F. Design and Challenges of Radiopharmaceuticals. Semin Nucl Med. 2019 Sep;49(5):339–56.

96. Kostelnik TI, Orvig C. Radioactive Main Group and Rare Earth Metals for Imaging and Therapy. Chem Rev. 2019 Jan 23;119(2):902–56.

97. Price EW, Orvig C. Matching chelators to radiometals for radiopharmaceuticals. Chem Soc Rev. 2014;43(1):260–90.

98. Song H, Sgouros G. Alpha and Beta Radiation for Theragnostics. PET Clin [Internet]. 2024 Jul;19(3):307–23. Available from: https://linkinghub.elsevier.com/retrieve/pii/S155685982400021X

99. Aggarwal RR, Luch Sam S, Koshkin VS, Small EJ, Feng FY, de Kouchkovsky I, et al. Immunogenic priming with 177Lu-PSMA-617 plus pembrolizumab in metastatic castration resistant prostate cancer (mCRPC): A phase 1b study. Journal of Clinical Oncology. 2021 May 20;39(15_suppl):5053–5053.

100. Parker C, Nilsson S, Heinrich D, Helle SI, O'Sullivan JM, Fosså SD, et al. Alpha Emitter Radium-223 and Survival in Metastatic Prostate Cancer. New England Journal of Medicine. 2013 Jul 18;369(3):213–23.

101. Delpassand ES, Tworowska I, Esfandiari R, Torgue J, Hurt J, Shafie A, et al. Targeted α-Emitter Therapy with 212Pb-DOTAMTATE for the Treatment of Metastatic SSTR-Expressing Neuroendocrine Tumors: First-in-Humans Dose-Escalation Clinical Trial. Journal of Nuclear Medicine. 2022 Sep;63(9):1326–33.

102. Kratochwil C, Bruchertseifer F, Giesel FL, Weis M, Verburg FA, Mottaghy F, et al. 225Ac-PSMA-617 for PSMA-Targeted α-Radiation Therapy of Metastatic Castration-Resistant Prostate Cancer. Journal of Nuclear Medicine. 2016 Dec;57(12):1941–4.

103. Sathekge M, Bruchertseifer F, Vorster M, Lawal IO, Knoesen O, Mahapane J, et al. mCRPC Patients Receiving 225Ac-PSMA-617 Therapy in the Post–Androgen Deprivation Therapy Setting: Response to Treatment and Survival Analysis. Journal of Nuclear Medicine. 2022 Oct;63(10):1496–502.

104. Eychenne R, Chérel M, Haddad F, Guérard F, Gestin JF. Overview of the Most Promising Radionuclides for Targeted Alpha Therapy: The "Hopeful Eight." Pharmaceutics. 2021 Jun 18;13(6):906.

105. Esteban-Villarrubia J, Torres-Jiménez J, Bueno-Bravo C, García-Mondaray R, Subiela JD, Gajate P. Current and Future Landscape of Perioperative Treatment for Muscle-Invasive Bladder Cancer. Cancers (Basel). 2023 Jan 17;15(3):566.

106. Mooso BA, Vinall RL, Mudryj M, Yap SA, deVere White RW, Ghosh PM. The Role of EGFR Family Inhibitors in Muscle Invasive Bladder Cancer: A Review of Clinical Data and Molecular Evidence. Journal of Urology. 2015 Jan;193(1):19–29.

107. Knapp DW, Dhawan D, Ramos-Vara JA, Ratliff TL, Cresswell GM, Utturkar S, et al. Naturally-Occurring Invasive Urothelial Carcinoma in Dogs, a Unique Model to Drive Advances in Managing Muscle Invasive Bladder Cancer in Humans. Front Oncol. 2020 Jan 21;9.

108. Pouget JP, Georgakilas AG, Ravanat JL. Targeted and Off-Target (Bystander and Abscopal) Effects of Radiation Therapy: Redox Mechanisms and Risk/Benefit Analysis. Antioxid Redox Signal. 2018 Nov 20;29(15):1447–87.

109. Gardner HL, Fenger JM, London CA. Dogs as a Model for Cancer. Annu Rev Anim Biosci. 2016 Feb 15;4(1):199–222.

110. Knapp DW. What causes TCC in dogs? [Internet]. Available from: https://pubmed.ncbi.nlm.nih.gov/36439482/

111. Effer B, Perez I, Ulloa D, Mayer C, Muñoz F, Bustos D, et al. Therapeutic Targets of Monoclonal Antibodies Used in the Treatment of Cancer: Current and Emerging. Biomedicines. 2023 Jul 24;11(7):2086.

112. Spindler S. National Cancer Institute. 2024 [cited 2024 Oct 10]. Lutathera Shows Promise as a Part of Initial Therapy for Some Neuroendocrine Tumors. Available from: https://www.cancer.gov/news-events/cancer-currents-blog/2024/lutathera-neuroendocrine-tumor-initial-treatment

113. Ahmadzadehfar H, Seifert R, Afshar-Oromieh A, Kratochwil C, Rahbar K. Prostate Cancer Theranostics With 177Lu-PSMA. Semin Nucl Med [Internet]. 2024 Jul;54(4):581–90. Available from: https://linkinghub.elsevier.com/retrieve/pii/S0001299824000242

114. Bergkvist GT, Yool DA. Epidermal growth factor receptor as a therapeutic target in veterinary oncology. Vet Comp Oncol. 2011 Jun 16;9(2):81–94.

115. Dhawan D, Ramos-Vara JA, Stewart JC, Zheng R, Knapp DW. Canine invasive transitional cell carcinoma cell lines: In vitro tools to complement a relevant animal model of invasive urinary bladder cancer. Urologic Oncology: Seminars and Original Investigations. 2009 May;27(3):284–92.

116. Nagaya T, Okuyama S, Ogata F, Maruoka Y, Knapp DW, Karagiannis SN, et al. Near infrared photoimmunotherapy targeting bladder cancer with a canine anti-epidermal growth factor receptor (EGFR) antibody [Internet]. Vol. 9, Oncotarget. 2018. Available from: www.oncotarget.comwww.oncotarget.com

117. Singer J, Fazekas J, Wang W, Weichselbaumer M, Matz M, Mader A, et al. Generation of a canine anti-EGFR (ErbB-1) antibody for passive immunotherapy in dog cancer patients. Mol Cancer Ther. 2014;13(7):1777–90.

118. Siddiqui MR, Railkar R, Sanford T, Crooks DR, Eckhaus MA, Haines D, et al. Targeting Epidermal Growth Factor Receptor (EGFR) and Human Epidermal Growth Factor Receptor 2 (HER2) Expressing Bladder Cancer Using Combination Photoimmunotherapy (PIT). Sci Rep. 2019 Feb 14;9(1):2084.

119. Schindelin J, Arganda-Carreras I, Frise E, Kaynig V, Longair M, Pietzsch T, et al. Fiji: an open-source platform for biological-image analysis. Nat Methods. 2012 Jul 28;9(7):676–82.

120. Elbadawy M, Usui T, Mori T, Tsunedomi R, Hazama S, Nabeta R, et al. Establishment of a novel experimental model for muscle-invasive bladder cancer using a dog bladder cancer organoid culture. Cancer Sci. 2019 Sep 23;110(9):2806–21.

121. Knapp DW, Glickman NW, Widmer WR, Denicola DB, Adams LG, Kuczek T, et al. Cisplatin versus cisplatin combined with piroxicam in a canine model of human invasive urinary bladder cancer. 2000.

122. Elbadawy M, Usui T, Mori T, Tsunedomi R, Hazama S, Nabeta R, et al. Establishment of a novel experimental model for muscle-invasive bladder cancer using a dog bladder cancer organoid culture. Cancer Sci. 2019 Sep 23;110(9):2806–21.

123. Wilson BD, Soh HT. Re-Evaluating the Conventional Wisdom about Binding Assays. Trends Biochem Sci. 2020 Aug;45(8):639–49.

124. Singer J, Weichselbaumer M, Stockner T, Mechtcheriakova D, Sobanov Y, Bajna E, et al. Comparative oncology: ErbB-1 and ErbB-2 homologues in canine cancer are susceptible to cetuximab and trastuzumab targeting. Mol Immunol. 2012 Apr;50(4):200–9.

125. Kerwin RW, Pilowsky LS. European Journal of Nuclear Medicine Traditional receptor theory and its application to neuroreceptor measurements in functional imaging. Vol. 22, European Journal of Nuclear Medicine. Springer-Verlag; 1995.

126. Abi-Dargham A, Martinez D, Mawlawi O, Simpson N, Hwang DR, Slifstein M, et al. Measurement of Striatal and Extrastriatal Dopamine D1 Receptor Binding Potential With [11C]NNC 112 in Humans: Validation and Reproducibility. Journal of Cerebral Blood Flow & Metabolism. 2000 Feb 1;20(2):225–43.

127. Mouriaux F, Zaniolo K, Bergeron MA, Weidmann C, De La Fouchardière A, Fournier F, et al. Effects of Long-term Serial Passaging on the Characteristics and Properties of Cell Lines Derived From Uveal Melanoma Primary Tumors. Investigative Opthalmology & Visual Science. 2016 Oct 10;57(13):5288.

128. Mentink A, Isebia KT, Kraan J, Terstappen LWMM, Stevens M. Measuring antigen expression of cancer cell lines and circulating tumour cells. Sci Rep. 2023 Apr 13;13(1):6051.

129. Blanco R, Cedeño M, González N, Rodríguez R, Sánchez J, Rengifo E. Phenotypic heterogeneity in the NCI-H125 cell line affects biological activity using the epidermal growth factor receptor as target / Fenotipska heterogenost u staničnoj liniji NCI-H125 utječe na biološku aktivnost na receptore za epidermalni faktor rasta. Acta Pharmaceutica. 2012 Dec 1;62(4):581–91.

130. Mahler HC, Huber F, Kishore RSK, Reindl J, Rückert P, Müller R. Adsorption Behavior of a Surfactant and a Monoclonal Antibody to Sterilizing-Grade Filters. J Pharm Sci. 2010 Jun;99(6):2620–7.

131. Maeda S, Sakai K, Kaji K, Iio A, Nakazawa M, Motegi T, et al. Lapatinib as first-line treatment for muscle-invasive urothelial carcinoma in dogs. Sci Rep. 2022 Jan 13;12(1):4.

132. Tsuboi M, Sakai K, Maeda S, Chambers JK, Yonezawa T, Matsuki N, et al. Assessment of HER2 Expression in Canine Urothelial Carcinoma of the Urinary Bladder. Vet Pathol. 2019 May 6;56(3):369–76.

133. Li W, Wang Y, Tan S, Rao Q, Zhu T, Huang G, et al. Overexpression of Epidermal Growth Factor Receptor (EGFR) and HER-2 in Bladder Carcinoma and Its Association with Patients' Clinical Features. Medical Science Monitor. 2018 Oct 8;24:7178–85.

134. Yang Y, Li S, Wang Y, Zhao Y, Li Q. Protein tyrosine kinase inhibitor resistance in malignant tumors: molecular mechanisms and future perspective. Signal Transduct Target Ther. 2022 Sep 17;7(1):329.

135. Kumar R, Goel H, Solanki R, Rawat L, Tabasum S, Tanwar P, et al. Recent developments in receptor tyrosine kinase inhibitors: A promising mainstay in targeted cancer therapy. Med Drug Discov. 2024 Sep;23:100195.

136. Wang N, Wang K, Song F, Liu Y. Cetuximab in combination with chemoradiotherapy for nasopharyngeal carcinoma: A meta-analysis. Indian J Cancer. 2018;55(2):196.

137. Swain SM, Shastry M, Hamilton E. Targeting HER2-positive breast cancer: advances and future directions. Nat Rev Drug Discov. 2023 Feb 7;22(2):101–26.

138. Du Z, Lovly CM. Mechanisms of receptor tyrosine kinase activation in cancer. Mol Cancer. 2018 Dec 19;17(1):58.

139. Pohlmann PR, Mayer IA, Mernaugh R. Resistance to Trastuzumab in Breast Cancer. Clinical Cancer Research. 2009 Dec 15;15(24):7479–91.

140. Bray SM, Lee J, Kim ST, Hur JY, Ebert PJ, Calley JN, et al. Genomic characterization of intrinsic and acquired resistance to cetuximab in colorectal cancer patients. Sci Rep. 2019 Oct 25;9(1):15365.

141. Tsang RY, Sadeghi S, Finn RS. Lapatinib, a Dual-Targeted Small Molecule Inhibitor of EGFR and HER2, in HER2-Amplified Breast Cancer: From Bench to Bedside. Clin Med Insights Ther. 2011 Jan 13;3.

142. McDermott M, O'Brien N, McDonald K, Crown J, O'Donovan N, Slamon D. P1-12-06: The Role of MAPK and PI3K/AKT/mTOR Signaling in Innate Lapatinib Resistance. Cancer Res. 2011 Dec 15;71(24_Supplement):P1-12-06-P1-12–06.

143. Ashley S, Choudhury A, Hoskin P, Song Y, Maitre P. Radiotherapy in metastatic bladder cancer. World J Urol. 2024 Jan 20;42(1):47.

144. Clerc-Renaud B, Gieger TL, LaRue SM, Nolan MW. Treatment of genitourinary carcinoma in dogs using nonsteroidal anti-inflammatory drugs, mitoxantrone, and radiation therapy: A retrospective study. J Vet Intern Med. 2021 Mar 26;35(2):1052–61.

145. Nolan MW, Kogan L, Griffin LR, Custis JT, Harmon JF, Biller BJ, et al. Intensity-Modulated and Image-Guided Radiation Therapy for Treatment of Genitourinary Carcinomas in Dogs. J Vet Intern Med. 2012 Jul 25;26(4):987–95.

146. Poirier VJ, Forrest LJ, Adams WM, Vail DM. Piroxicam, Mitoxantrone, and Coarse Fraction Radiotherapy for the Treatment of Transitional Cell Carcinoma of the Bladder in 10 Dogs: A Pilot Study. J Am Anim Hosp Assoc. 2004 Mar 1;40(2):131–6.

147. Zhang S, Wang X, Gao X, Chen X, Li L, Li G, et al. Radiopharmaceuticals and their applications in medicine. Signal Transduct Target Ther. 2025 Jan 3;10(1):1.

148. Chargari C, Rassy E, Helissey C, Achkar S, Francois S, Deutsch E. Impact of radiation therapy on healthy tissues. In 2023. P. 69–98.

149. Tyagi P, Hafron J, Kaufman J, Chancellor M. Enhancing Therapeutic Efficacy and Safety of Immune Checkpoint Inhibition for Bladder Cancer: A Comparative Analysis of Injectable vs. Intravesical Administration. Int J Mol Sci. 2024 May 1;25(9):4945.

150. Autenrieth ME, Seidl C, Bruchertseifer F, Horn T, Kurtz F, Feuerecker B, et al. Treatment of carcinoma in situ of the urinary bladder with an alpha-emitter immunoconjugate targeting the epidermal growth factor receptor: a pilot study. Eur J Nucl Med Mol Imaging. 2018 Jul 11;45(8):1364–71.

151. Paluri RK, Killeen RB. Neuroendocrine Tumor Lu-177-Dotatate Therapy. StatPearls [Internet]. 2024 Feb 12 [cited 2025 Mar 9]; Available from: https://www.ncbi.nlm.nih.gov/books/NBK587368/

152. Iravani A, Violet J, Azad A, Hofman MS. Lutetium-177 prostate-specific membrane antigen (PSMA) theranostics: practical nuances and intricacies. Prostate Cancer Prostatic Dis. 2020 Mar 8;23(1):38–52.

153. Dash A, Pillai MRA, Knapp FF. Production of 177Lu for Targeted Radionuclide Therapy: Available Options. Nucl Med Mol Imaging. 2015 Jun 17;49(2):85–107.

154. Hosono M, Ikebuchi H, Nakamura Y, Nakamura N, Yamada T, Yanagida S, et al. Manual on the proper use of lutetium-177-labeled somatostatin analogue (Lu-177-DOTA-TATE) injectable in radionuclide therapy (2nd ed.). Ann Nucl Med. 2018 Apr 15;32(3):217–35.

155. Hofmann W, Li WB, Friedland W, Miller BW, Madas B, Bardiès M, et al. Internal microdosimetry of alpha-emitting radionuclides. Radiat Environ Biophys. 2020 Mar 21;59(1):29–62.